

# We are IntechOpen, the world's leading publisher of Open Access books Built by scientists, for scientists

6,900

Open access books available

186,000

International authors and editors

200M

Downloads

Our authors are among the

154

Countries delivered to

TOP 1%

most cited scientists

12.2%

Contributors from top 500 universities



WEB OF SCIENCE™

Selection of our books indexed in the Book Citation Index  
in Web of Science™ Core Collection (BKCI)

Interested in publishing with us?  
Contact [book.department@intechopen.com](mailto:book.department@intechopen.com)

Numbers displayed above are based on latest data collected.  
For more information visit [www.intechopen.com](http://www.intechopen.com)



# High Power Tunable Tm<sup>3+</sup>-fiber Lasers and Its Application in Pumping Cr<sup>2+</sup>:ZnSe Lasers

Yulong Tang and Jianqiu Xu

*Shanghai Institute of Optics and Fine Mechanics*

*Chinese Academy of Science, Shanghai 201800,*

*China*

## 1. Introduction

### 1.1 Research background

Interest in the Tm<sup>3+</sup>-doped fiber laser originates from its emission band in the range of 1400-2700nm lying between the bands of Er<sup>3+</sup> and Nd<sup>3+</sup> ions. Since the advent of double-cladding configuration of fiber and the recent technological development of high-power laser diodes, output power (performance) of Tm<sup>3+</sup>-doped fiber lasers has scaled exponentially. Up to date, the maximum output achieved in Tm<sup>3+</sup>-doped fiber lasers has been comparable with that from Yb<sup>3+</sup>-doped fiber lasers. Laser beam in the 2~3μm wavelength range has wide applications. First, it is a good candidate in laser microsurgery due to high absorption of water in this spectral region thus can provide high-quality laser tissue cutting and welding. In addition, this wavelength-range laser has potential applications in environment monitoring, LIDAR, optical-parametric-oscillation (OPO) pump sources, and so on [1-4].

For obtaining laser emission in the mid-infrared wavelength region, the Tm<sup>3+</sup>-doped fiber is an excellent candidate due to several unique advantages it possesses. First, the Tm<sup>3+</sup>-doped fiber has a strong absorption spectrum that has good overlap with the emission band of commercially available AlGaAs laser diodes, which have been significantly developed and are being developed with an unprecedented speed. Second, the specific energy-level structure of Tm<sup>3+</sup> ions provides the Tm<sup>3+</sup>-doped fiber laser a special advantageous energy-transfer process-the  $^3H_4+^3H_6 \rightarrow ^3F_4+^3F_4$  cross relaxation process. In this process, two excited-state ions can be obtained with depletion of just one absorbed pump photon. With an appropriately high doping level, the cross relaxation process can offer a quantum efficiency close to two, which greatly improves the efficiency of the Tm<sup>3+</sup>-doped fiber laser. Thirdly, the Tm<sup>3+</sup>-doped fiber has a very broad emission band, spanning over more than 400 nm. This feature offers the Tm<sup>3+</sup>-doped fiber laser an especially high-degree wavelength tunability, which is very useful in applications such as spectroscopy, atmospheric sensing and so on.

### 1.2 Host material of Tm<sup>3+</sup>-doped fiber

For laser ions, the combination of the energy gaps between the excited level and the one just below it and the maximum phonon energy (MPE) plays an important role in the nonradiative relaxation rate, which in turn has a significant influence on the laser efficiency originated from the excited states. For Tm<sup>3+</sup> ions, different host materials show a great

Source: Frontiers in Guided Wave Optics and Optoelectronics, Book edited by: Bishnu Pal, ISBN 978-953-7619-82-4, pp. 674, February 2010, INTECH, Croatia, downloaded from SCIYO.COM

difference in the MPE value. Two most common host materials used for  $\text{Tm}^{3+}$  fibers are silica and fluoride glass. Their MPE differs about several times, being  $1100 \text{ cm}^{-1}$  (silicate) and  $550 \text{ cm}^{-1}$  (fluorides), respectively [5]. Large MPE of the silicate glass fiber limits its infrared transparency range less than  $2.2 \mu\text{m}$  and improves its multiphonon relaxation rates. Therefore, fluoride fibers are preferred as the host material for  $\text{Tm}^{3+}$  ions to achieve comparatively longer-wavelength emission.

In  $\text{Tm}^{3+}$ -doped fiber lasers, the  ${}^3\text{F}_4 \rightarrow {}^3\text{H}_6$  transition is usually exploited to achieve the  $\sim 2 \mu\text{m}$  high-power laser output. This transition can produce a very wide emission band, providing a broad tuning range for lasers and a wide optical bandwidth for amplifiers. However, the relaxation of the  ${}^3\text{F}_4$  level is predominantly nonradiative. The measured lifetime of the  ${}^3\text{F}_4$  level for  $\text{Tm}^{3+}$  doped silica fiber is just  $0.2 \text{ ms}$  [6] showing a high nonradiative rate thus low quantum efficiency. Therefore,  $\text{Tm}^{3+}$ -doped fiber lasers usually have high laser thresholds. On the contrary,  $\text{Tm}^{3+}$ -doped fluoride fiber lasers have comparatively lower thresholds due to a low MPE. The high nonradiative rate, however, does not impair laser slope efficiency, because stimulated emission will dominate nonradiative relaxation once the laser has been risen above threshold. Due to high damage threshold and the very effective modified chemical vapor deposition (MCVD) technique for fiber fabrication,  $\text{Tm}^{3+}$  silica fibers are usually chosen to construct high-power  $2\text{-}\mu\text{m}$  fiber lasers.

### 1.3 Fiber design for cladding pumping

$\text{Tm}^{3+}$ -doped fibers can be either core pumped or cladding pumped. In the past, the fiber laser was usually core pumped. The fiber core areas are generally  $< 100 \mu\text{m}^2$ , which limit the power scalability because this method depend on expensive high-beam-quality pump sources. Since the invention of double cladding fiber configuration with a larger cladding area  $> 10000 \mu\text{m}^2$ , together with a high numerical aperture (NA) of  $0.3\text{-}0.55$ , output power of  $\text{Tm}^{3+}$ -doped fiber lasers can be greatly improved by use of high-power diode-arrays as pumping sources.

In the design of fibers for cladding pumping, the core of the fiber is usually made small (such as less than  $5 \mu\text{m}$ ) to guide a single-transverse mode ( $\text{LP}_{01}$ ). The cladding generally has a much larger cross section (several-hundred-micron diameter) for high-power launching, and the shape of the cladding can be flexible with novel consideration. The shape of the inner cladding of the fiber has a great impact on the absorption efficiency of launched pump light. In the past, the inner cladding is used to be circularly symmetric, which can be drawn with ease and is compatible with the pig-tail fiber of the pump LD. However, the circular symmetry will make large portion of the pump light to be skew light, greatly reducing the absorption efficiency of doping ions. In order to improve the utility efficiency of pump sources, and take the pump light shape into account (compatible with the inner cladding shape), various double cladding fiber structures are invented, as shown in Fig. 1. By using these double cladding fibers, the pump efficiency is significantly enhanced.

### 1.4 $\text{Tm}^{3+}$ -doped fiber laser cavity structure

The fiber laser resonator can be very simple when it is in free-running regime. The commonly adopted three kinds of fiber laser resonators, defined as Fabry-Perot resonator, are shown in Fig. 2. Fig 2 (a) is the simplest cavity, the pump light is launched into the fiber through a dichroic mirror, which is high reflective for laser light. Laser oscillation forms between this dichroic mirror and the distal-end fiber facet ( $\sim 4\%$  Fresnel reflection). In this cavity configuration, addition of output coupler or pump-light reflector will improve the

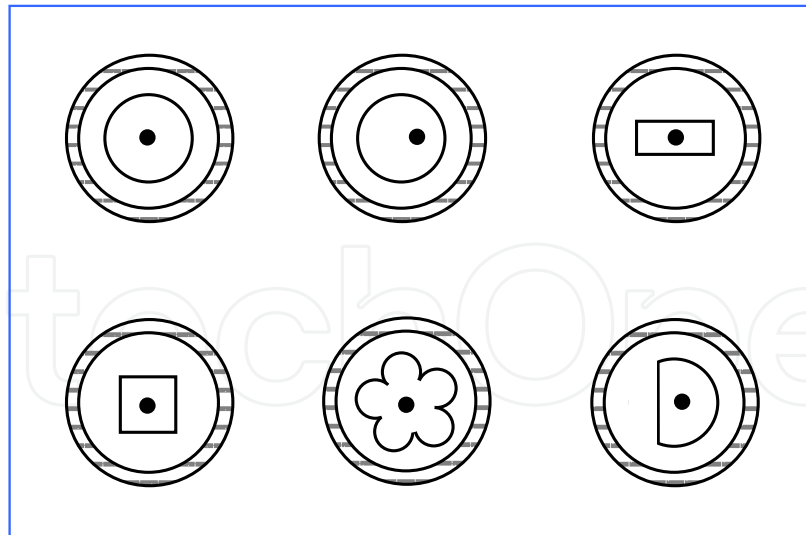


Fig. 1. Various shape of the double cladding fiber cross section

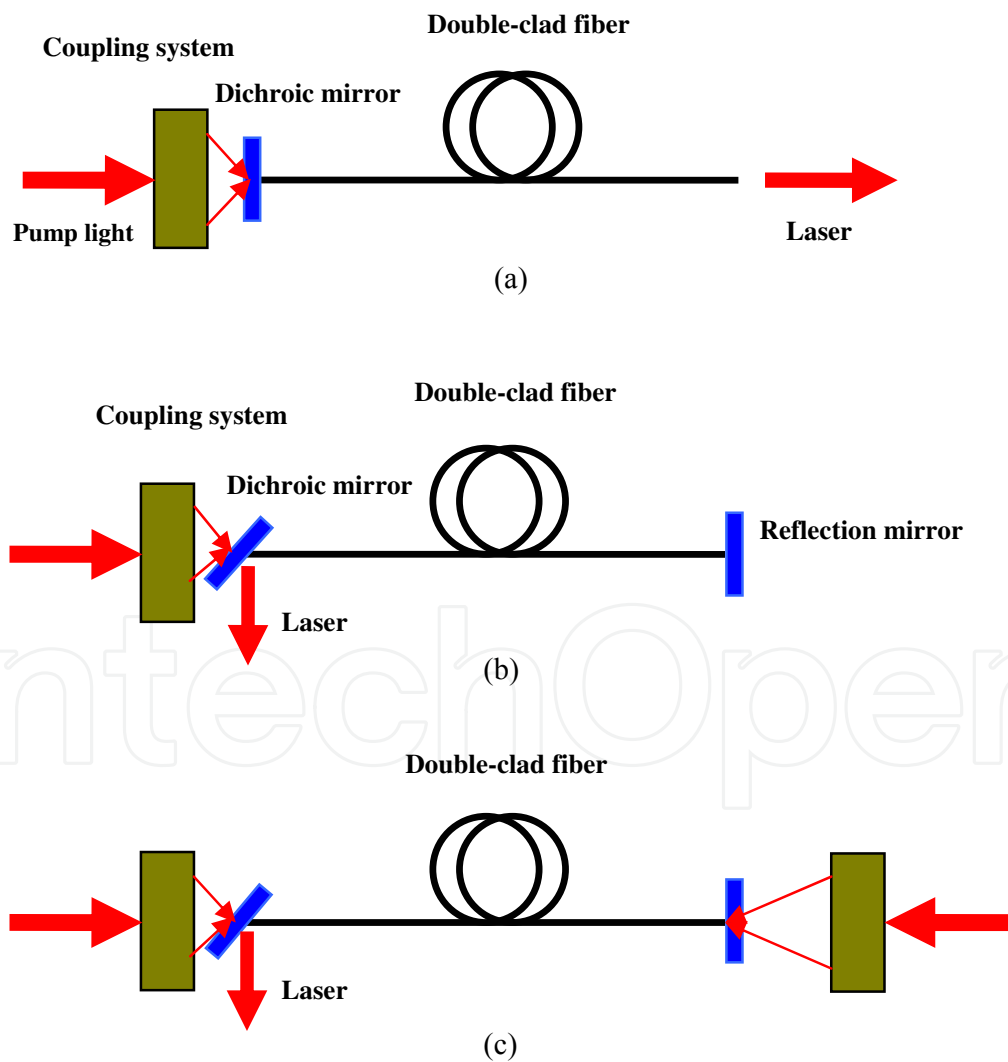


Fig. 2.  $Tm^{3+}$ -doped fiber laser resonators (a) Single-end forward pumping; (b) Single-end backward pumping; (c) Double-end pumping.

optical efficiency of the fiber laser. In Fig 2 (b), the pump light is launched into the fiber from the output end, and the dichroic mirror is set at 45 degree with respect to the fiber axis for extracting laser output. At the distal fiber end, a signal high reflection mirror is added to form the laser resonator. The cavity of Fig 2 (c) is used to further improve the pump power that can be launched into the fiber for the aim of power scaling.

In order to realize wavelength tuning, and at the same time obtain narrow-width laser spectrum, a bulk gratings can be put in the cavity as the output coupler. However, wavelength-tuning with bulk grating is inconvenient, and brings laser instability. The commonly used wavelength-tuning fiber laser resonator is constructed by using fiber Bragg gratings as the feedback device and output coupler, as shown in Fig. 3. This kind of fiber laser resonator can provide not only wavelength tuning, but also narrow spectral width and high stability.

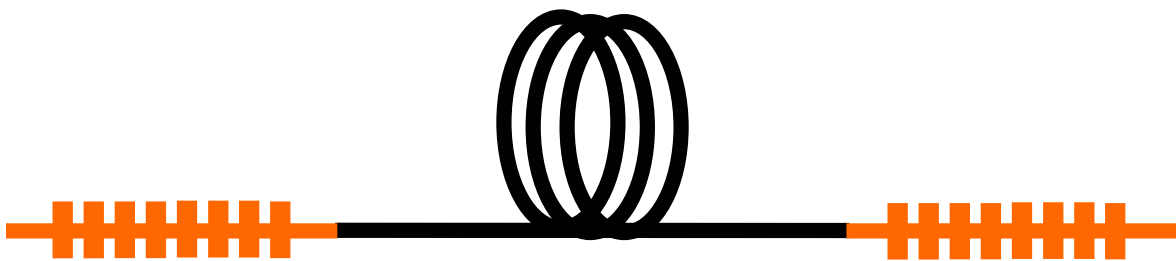


Fig. 3. Complete-fiber resonator with fiber Bragg grating.

### 1.5 Spectral characteristics of $Tm^{3+}$ -doped silica fiber

Our aim is to focus on the development of high-power  $\sim 2\mu m$  fiber laser, so the description about the spectral characteristics is only confined to the  $Tm^{3+}$ -doped silica fiber. The absorption spectrum of  $Tm^{3+}$ -doped silica fiber is shown in Fig. 4 [7]. This spectrum has strong absorption near 790 nm, which has good overlap with the emission band of present fully developed AlGaAs diode lasers. This feature of the  $Tm^{3+}$ -doped fiber laser makes the pump process comparatively easier and less expensive, offering an exciting potential for power scaling in the 2- $\mu m$  wavelength range.

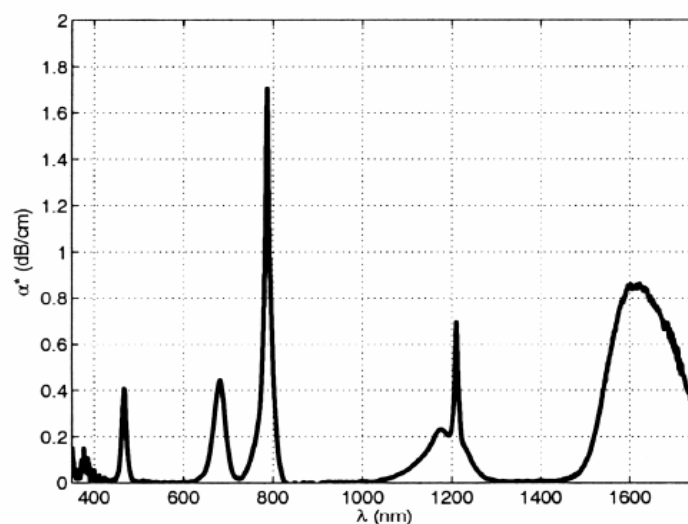


Fig. 4. Absorption spectrum of  $Tm^{3+}$ -doped silica fiber

The simplified energy-level diagram of Tm<sup>3+</sup> ions is shown in Fig. 5. The pump light at ~790 nm excites Tm<sup>3+</sup> ions from <sup>3</sup>H<sub>6</sub> to <sup>3</sup>H<sub>4</sub>, which then nonradiatively decay to the upper laser level of <sup>3</sup>F<sub>4</sub> with a fluorescence lifetime of 0.55 ms [8]. The transition from <sup>3</sup>F<sub>4</sub>→<sup>3</sup>H<sub>6</sub> will radiates photons at wavelength of ~2μm. Due to large Stark splitting of the lower laser level (the ground state level), the Tm<sup>3+</sup>-doped fiber laser is a quasi-four-level system.

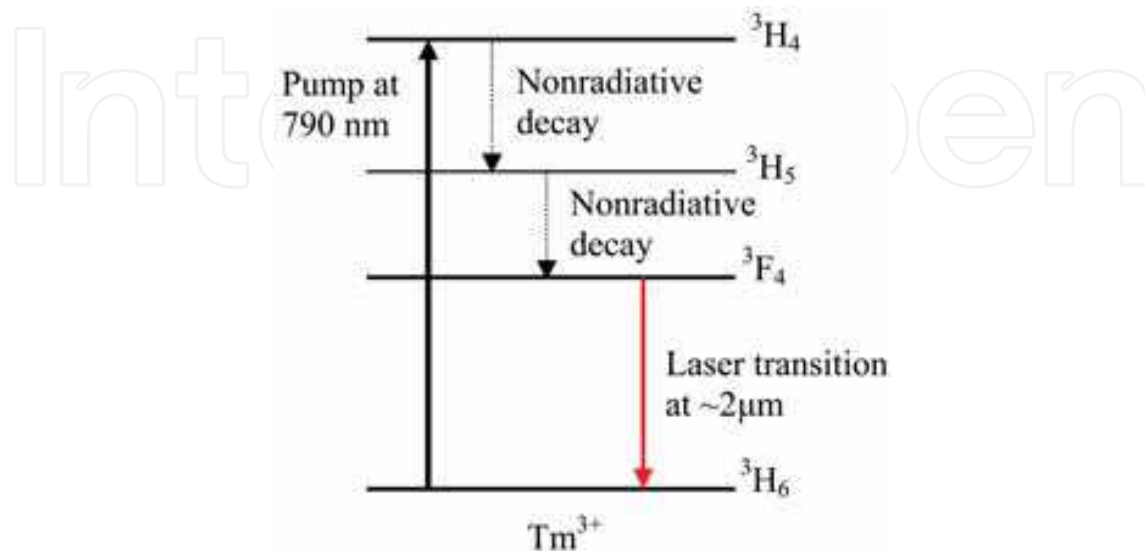


Fig. 5. The simplified energy-level diagram of Tm<sup>3+</sup> ions

The special energy-level structure of Tm<sup>3+</sup> ions provides the Tm<sup>3+</sup>-doped silica fiber laser the advantageous **cross relaxation** process (<sup>3</sup>H<sub>4</sub>+<sup>3</sup>H<sub>6</sub>→<sup>3</sup>F<sub>4</sub>+<sup>3</sup>F<sub>4</sub>). With this process, high quantum efficiencies can be achieved in Tm<sup>3+</sup>-doped fiber lasers by appropriately improving the ion doping concentration. The cross relaxation process, as shown in Fig 6, can produce >100% quantum efficiencies for Tm<sup>3+</sup>-doped fiber lasers [9-10]. In experiment, slope efficiency larger than 60% has been achieved (quantum efficiency>150%) in Tm<sup>3+</sup>-doped fiber lasers [11-12].

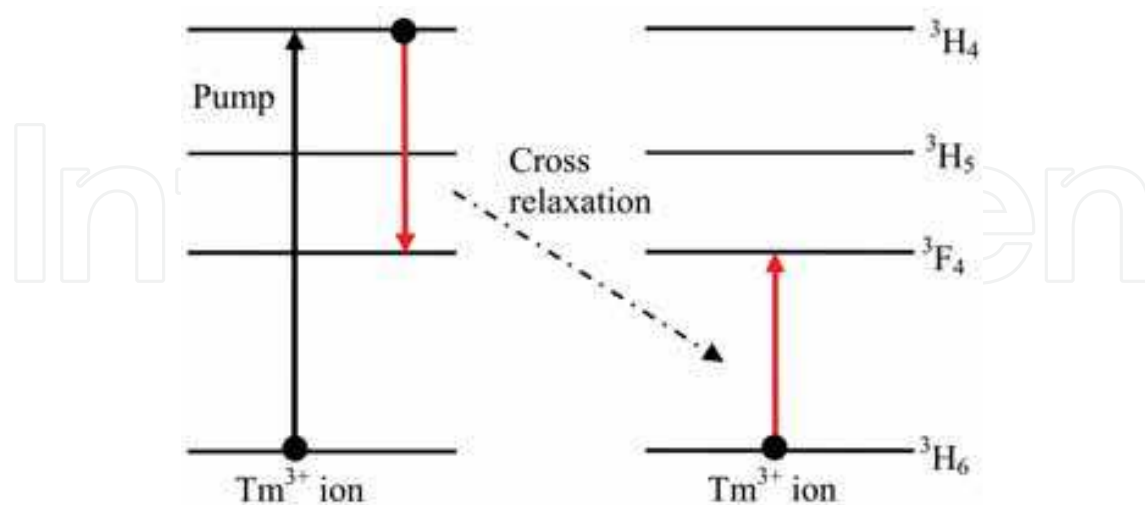


Fig. 6. Cross relaxation between Tm<sup>3+</sup> ions.

In Tm<sup>3+</sup>-doped silica fiber lasers, high-degree Stark splitting of the <sup>3</sup>H<sub>6</sub> level by local electric field produces a broad emission band (>400 nm), as shown in Fig. 7 [13]. This special broad emission band makes Tm<sup>3+</sup>-doped fibers very suitable for wavelength tuning.

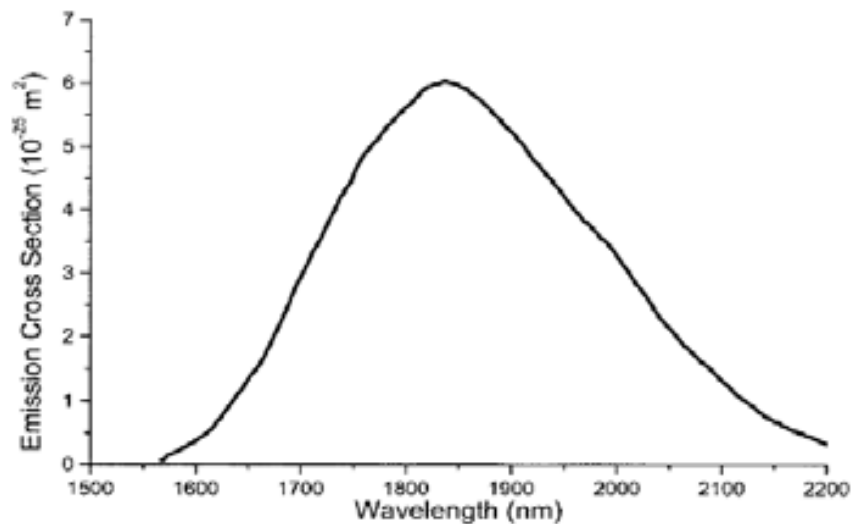


Fig. 7. The emission spectrum of the  ${}^3F_4 \rightarrow {}^3H_6$  transition in  $Tm^{3+}$ -doped silica fiber

### 1.6 Pump sources

With the fully development and decreasing cost of AlGaAs diode lasers, diode lasers are the primary and ultra most preferred pump source in pumping  $\sim 2\mu m$   $Tm^{3+}$ -doped fiber lasers at present. The 790-nm diode lasers pump  $Tm^{3+}$  ions to the  ${}^3H_4$  level, which can lead to the advantageous cross relaxation process, greatly enhancing the quantum efficiency of  $Tm^{3+}$ -doped fiber lasers. From the absorption band of  $Tm^{3+}$  ions, light sources at other wavelength can also be used as the pump. As shown in Fig. 8, apart from 790nm, the pump sources include the 1.064 $\mu m$  and 1.319 $\mu m$  output from Nd:YAG lasers, 1.09  $\mu m$  from Yb-doped fiber lasers, and 1.57 $\mu m$  Er $^{3+}$ -doped fiber lasers.

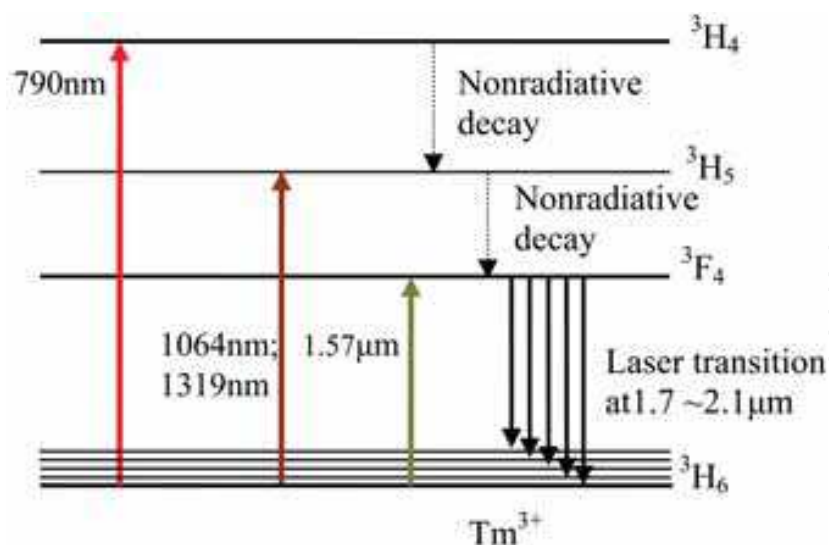


Fig. 8. The schematic of  $Tm^{3+}$  silica fiber with different pump wavelength.

The advantage of the 1.064  $\mu m$  and 1.09  $\mu m$  pumping is that Nd:YAG lasers and Yb-doped fiber lasers have been fully developed, which can be obtained with ease and low cost. This wavelength is used for the  ${}^3H_5$ -band pumping. Due to strong ESA, this band pumping leads to slope efficiencies less than 30% [14-15].

When the 1.319 $\mu$ m Nd:YAG laser is used as the pump source for Tm<sup>3+</sup>-doped fiber lasers, the Tm<sup>3+</sup> ions are pumped to the <sup>3</sup>H<sub>5</sub> level. The small absorption cross section of the pump light limits the slope efficiency of the 1.319 $\mu$ m-pumped Tm<sup>3+</sup>-doped fiber laser. Besides, at this wavelength, excited-state absorption of the pump is strong. Therefore, the slope efficiency of Tm<sup>3+</sup>-doped fiber lasers with this kind of pump source is less than 25% [16].

When the Tm<sup>3+</sup>-doped fiber laser is pumped at 1.57 $\mu$ m wavelength, the system is defined as a resonant pump structure due to the pump level (<sup>3</sup>F<sub>4</sub>) is also the upper laser level. Such a pump scheme has a small Stokes shift, thus can provide high operation efficiencies for Tm<sup>3+</sup>-doped fiber lasers. With this pump technique, M. Meleshkevich reported a slope efficiency of 60% with respect to absorbed pump power [17]. However, this pump scheme cannot make use of the advantageous “cross relaxation” as the 790-nm pumping. Therefore, the highest efficiency is also less than that has been achieved in 790-nm-pumped Tm<sup>3+</sup>-doped fiber lasers.

### 1.7 Recent power scaling of CW Tm<sup>3+</sup>-doped fiber laser

The first ~2 $\mu$ m laser output from the <sup>3</sup>F<sub>4</sub>→<sup>3</sup>H<sub>6</sub> transition in Tm<sup>3+</sup>-doped silica fiber laser was achieved by Hanna et al in 1988 with a 797-nm dye laser as the pump source [18]. With the advent of AlGaAs diode lasers, diode-pumped Tm<sup>3+</sup>-doped silica [19] and fluoride [20] fiber lasers were both realized in 1990.

The first high-power double-clad Tm<sup>3+</sup>-doped silica fiber laser was reported by Jackson in 1998. The maximum output power is 5.4 W, and the slope efficiency is 31% [21]. In 2000, the output power was improved to 14 W with a slope efficiency of 46% [22]. In 2002, the 793-nm laser diode pumped Tm<sup>3+</sup>-doped fiber laser has achieved a power output of 85 W with the slope efficiency of 56%. At the same power level, 75 W 2 $\mu$ m laser output was realized in an Yb-Tm codoped fiber laser, where ytterbium ions are used as sensitizing ions to facilitate pumping with 976 nm diodes. The slope efficiency however is just 32% due to the lack of “cross relaxation” process compared with those directly 790-nm pumped Tm<sup>3+</sup>-doped fiber lasers [24]. In 2007, G. Frith reported a Tm<sup>3+</sup>-doped fiber laser with output power improved to 263 W and the slope efficiency of 59% [25]. In 2009, the 2  $\mu$ m output power from the Tm<sup>3+</sup>-doped fiber laser was significantly enhanced to 885 W with a slope efficiency of 49.2% [26]. In addition, single frequency output has also been over 600 watts [27]. Further improving the 2- $\mu$ m laser output over 1-kilowatt level, comparable with Yb-doped fiber lasers, is just a matter of time.

## 2. Short-length Tm<sup>3+</sup>-doped silica fiber lasers

### 2.1 Introduction

Compared with long fiber lasers, short fiber lasers have many unique advantages. First, short fiber lasers can provide narrow-linewidth laser emission due to large axial mode spacing. From the equation [28]

$$\Delta\nu = \frac{c}{2nL}, \quad (1)$$

the shorter the fiber length, the larger the axial mode spacing. In a same broad gain spectrum, short fiber length leads to fewer axial modes obtaining enough gain to overcome cavity loss achieving oscillation. Therefore, the laser spectrum will be much narrower with

shorter fiber length. Second, in pulsed laser operation, short fiber lasers are preferable to produce short pulse-width emission with high peak power. The laser pulse width can be expressed by [29]

$$\tau_p = \frac{r\eta(r)}{r-1-\ln r} \times \frac{2L}{c\delta_0} \quad (2)$$

where,  $\delta_0$  is the single-pass cavity loss,  $\eta(r)$  is the energy extraction efficiency,  $r$  is the pump strength,  $L$  is the cavity optical length. We can see that the laser pulse width is proportional to the fiber length. Therefore, short fiber laser is preferred to achieved short pulse duration, thus achieve high peak power. In addition, short fiber lasers are free from the undesired nonlinear effects such as stimulated Raman, Brillouin scattering and so on.

Short-length  $\text{Tm}^{3+}$ -doped fiber lasers can be used to achieve single frequency output [7, 30-31], as well as moderate-level laser output [32] in the mid-infrared region. Such kind of compact mid-infrared laser device has great potentials in communication and integrated optical systems. Power scaling of short  $\text{Tm}^{3+}$ -doped fiber lasers will improve the utility of  $2\mu\text{m}$  fiber lasers and speed the development of compact fiber laser systems.

In this section, short thulium-doped fiber lasers with high-power output are introduced. Besides, the performance dependence of such kind of laser on temperature and cavity parameters are discussed.

## 2.2 Experiment and CW output

The double-cladding thulium-doped fiber has a  $30\ \mu\text{m}$  diameter, 0.22 N.A. core doped with  $\sim 2\text{wt.}\%$   $\text{Tm}^{3+}$ . The pure-silica cladding, coated with a low-index polymer, has a  $\sim 410\ \mu\text{m}$  diameter and a N.A. of 0.46. The cladding absorption coefficient at the pump wavelength (790 nm) is  $\sim 7\text{dB/m}$ . These fiber specifications of large fiber cross section, large ratio of core diameter to cladding diameter, high N. A. and high doping concentration make it possible to achieve high output power from short length of fibers. The pump source for the experiment is a single high-power LD bar, operating TM mode centered at 790 nm, shifting to  $\sim 793\ \text{nm}$  at comparatively higher operating temperature. With this pump source, the maximum power launched into the fiber is near 12 W.

The laser cavity configuration is shown in Fig. 9 [33]. The laser pumping beam is reshaped first by a micro-prism stack, and then focused into a circular spot of  $\sim 0.5 \times 0.5\ \text{mm}$  diameter with a cylindrical lens and an aspheric lens. The focused pump beam is launched into the thulium-doped fiber through a dielectric mirror. The pump end of the fiber is butted directly to the dielectric mirror with high reflectivity ( $>99\%$ ) at 1850~2100 nm and high transmission ( $>97\%$ ) at 760~900 nm. The distal end of the fiber is directly butted to the output coupler with  $\sim 90\%$  reflectivity at 1800~2000 nm to build a Fabry-Perot laser resonator. During the course of the experiments, the fiber is clipped between two copper sheets, which are closely fixed onto a water-cooling heat sink. The combination of a dielectric mirror ( $R>99\%$ @1850~2100nm,  $T>99\%$ @790 nm) and a Ge filter is used to extract the laser light and block the unabsorbed pump light.

Figure 10 shows the output power of a 7-cm length fiber laser as a function of launched pump power without water-cooling ( $40^\circ\text{C}$ ) [33]. When the cavity is constructed with an output coupler of 10% transmission, the laser has a threshold pump power of 135 mW and a maximum output power of 1.09 W. When the pump power is over 10 W, rollover of the output power occurred, which probably stemmed from large amount of heat generated in

the fiber due to large quantum defect. The slope efficiency of the fiber laser is about 9.6% with respect to launched pump power, which is much higher than that of silica based DFB fiber lasers [7, 32], but lower than that from a thulium-doped germanate glass fiber laser [31]. The comparatively low slope efficiency can be accounted by poor pump absorption due to relatively low doping concentration and short fiber length. Another alternative explanation can be related to the background loss of the silica-based fiber at wavelengths longer than 1.8  $\mu\text{m}$  [34]. When the output coupler mirror is removed and only the 4% Fresnel reflection of the fiber end is used to complete the laser cavity, the maximum output power and slope efficiency decrease to 0.96 W and 8.7%, respectively. However, below 2.3 W of pump power, the fiber-end output coupler leads to slightly higher output power. Different output coupling seems to have little influence on the threshold pump power, which remains around 135 mW.

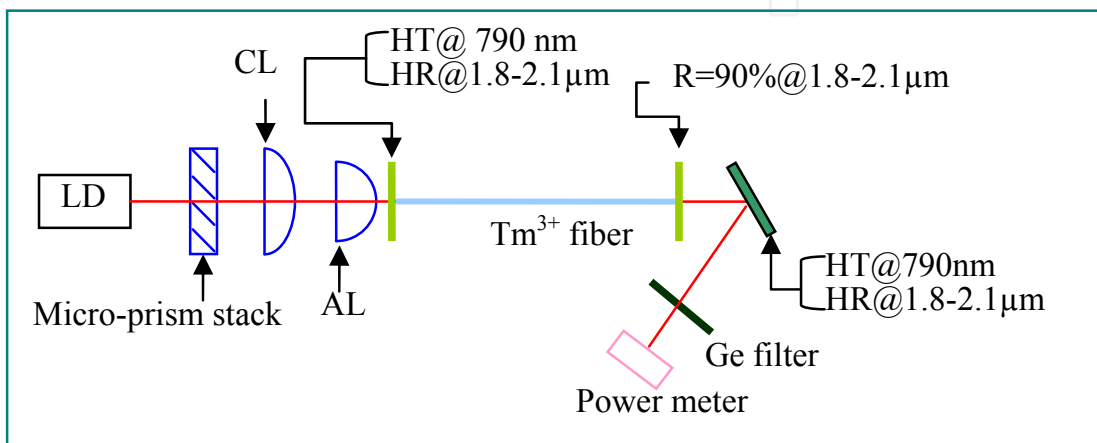


Fig. 9. Schematic diagram of the experimental setup. HT: high transmission; HR: high reflection; CL: cylindrical lens; AL: aspheric lens.

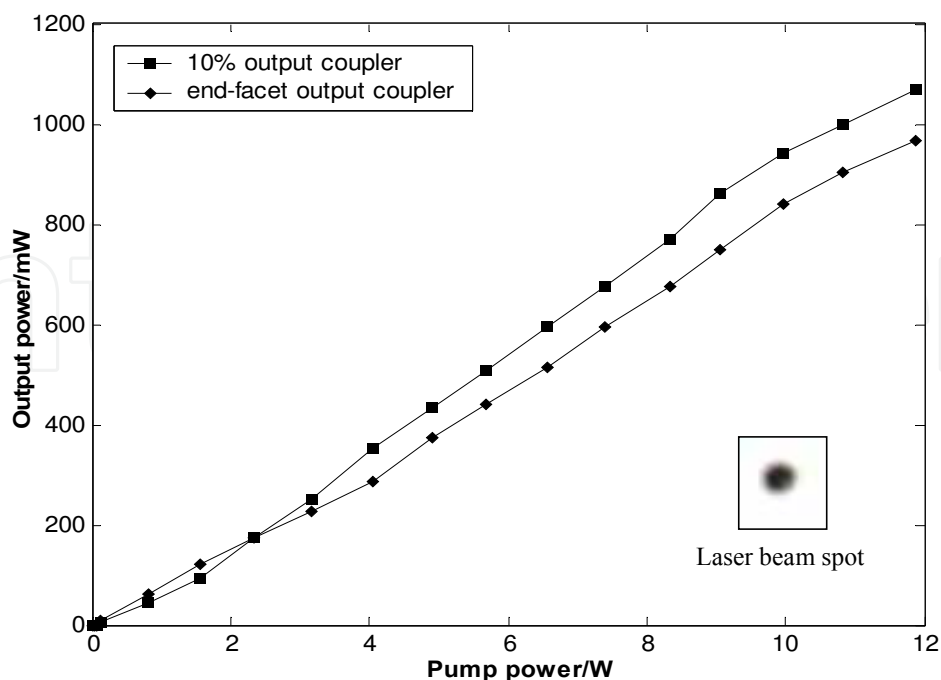


Fig. 10. Output characteristics of a 7 cm-length fiber laser with 10% output coupler and fiber-end-face coupler ( $R \sim 4\%$ ). Inset is the laser beam spot.

In order to find out the influence of the spacing between the rear fiber end and the output coupler, a 6-cm-long fiber is used. The air spacing is denoted by  $L_s$ . This fiber laser is still operated with just air convectional cooling (40°C). The output characteristics are shown in Fig. 11 [33]. When  $L_s = 0$ , a maximum output power of 496 mW and a slope efficiency of 4.6% can be obtained. When  $L_s = 0.5$  and 1 mm, the laser operation efficiency decreases greatly: the maximum output power reduces to 328 mW, and the slope efficiency decreases to 2.95%. This can be accounted by large reduction of the cavity Q factor by strong fiber-end diffraction loss. As far as  $L_s = 0.5$  mm and  $L_s = 1$  mm are compared, no significant different performance can be observed.

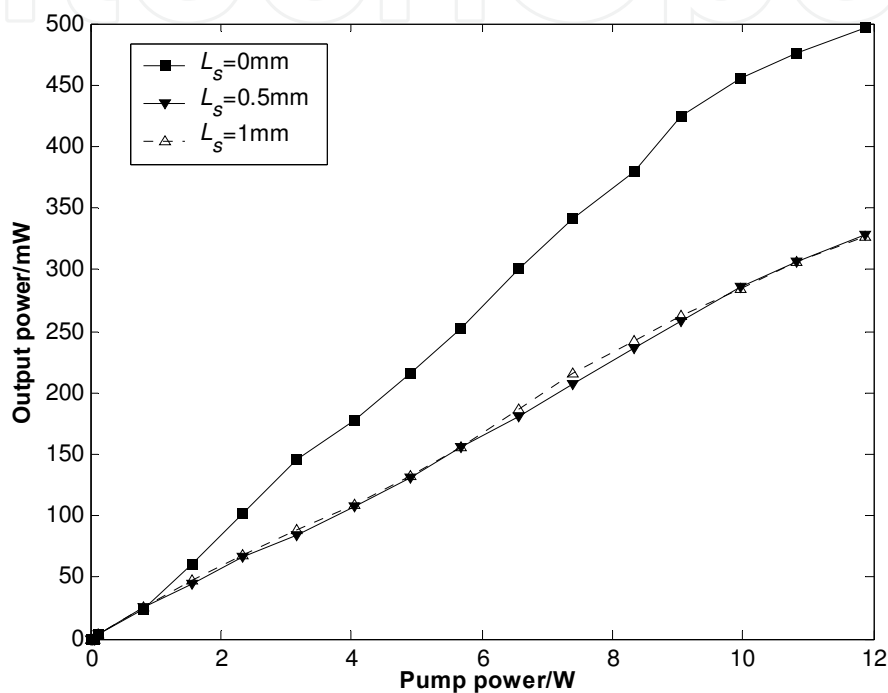


Fig. 11. Output characteristics of a 6 cm-length fiber laser with different air spacing between distal fiber end and output mirror.

### 2.3 Influence of temperature

In  $\text{Tm}^{3+}$ -doped fiber lasers, the ground-state level is Stark splitted into many sub levels. The  $\text{Tm}^{3+}$ -doped fiber laser is a quasi-four-level system, so the operation temperature has an important impact on the laser efficiency. For simplicity, we assume the ground state level of the  $\text{Tm}^{3+}$  ion is spited into just two sub levels  $N_1$  and  $N_2$ .  $N_1$  is the level where pump absorption starts from, and  $N_2$  is the lower laser level. Between these two Stark levels, the population follows the Boltzman distribution [35]

$$\frac{N_2}{N_1} = e^{-\frac{E_2 - E_1}{kT}}, \quad (3)$$

where,  $E_1$  and  $E_2$  are energies of these two levels,  $k$  is the Boltzman constant and  $T$  is temperature. From the above expression, different temperatures will lead to different population distributions between  $N_1$  and  $N_2$ , which in turn has an influence on the

population inversion for the laser transition. Therefore, the laser operation temperature will have an important impact on laser efficiency.

A 5.5-cm long  $\text{Tm}^{3+}$ -doped fiber laser is constructed to observe the impact of the fiber operation temperature on the laser efficiency. The operation temperature of the fiber is controlled by changing the temperature of the circulating water through the copper heat-sink. Without water-cooling, the operation temperature of the fiber is around  $40^\circ\text{C}$ . With water-cooling, the operation temperature can be adjusted from  $\sim 0^\circ\text{C}$  to  $40^\circ\text{C}$ . The output characteristic of the 5.5-cm-length fiber laser with different operation temperatures is plotted in Fig. 12 [33]. Both the maximum output power and slope efficiency exhibit a notable increase as the operation temperature of the fiber laser decreases from  $40^\circ\text{C}$  to  $10^\circ\text{C}$ . The maximum output grows from 345 mW to 531 mW, and the slope efficiency rises from 4% to 5.8%. The threshold pump power drops to 85 mW at operation temperature of  $10^\circ\text{C}$ . At high pump levels, a rollover of the output can be observed for all operation temperatures, which is accounted by saturation of pump absorption and distortion of the fiber end by high light intensity. At the maximum output level, the laser output fluctuation is less than 5% (as shown in the inset of Fig. 12), showing high stability of short-length  $\text{Tm}^{3+}$ -doped fiber lasers.

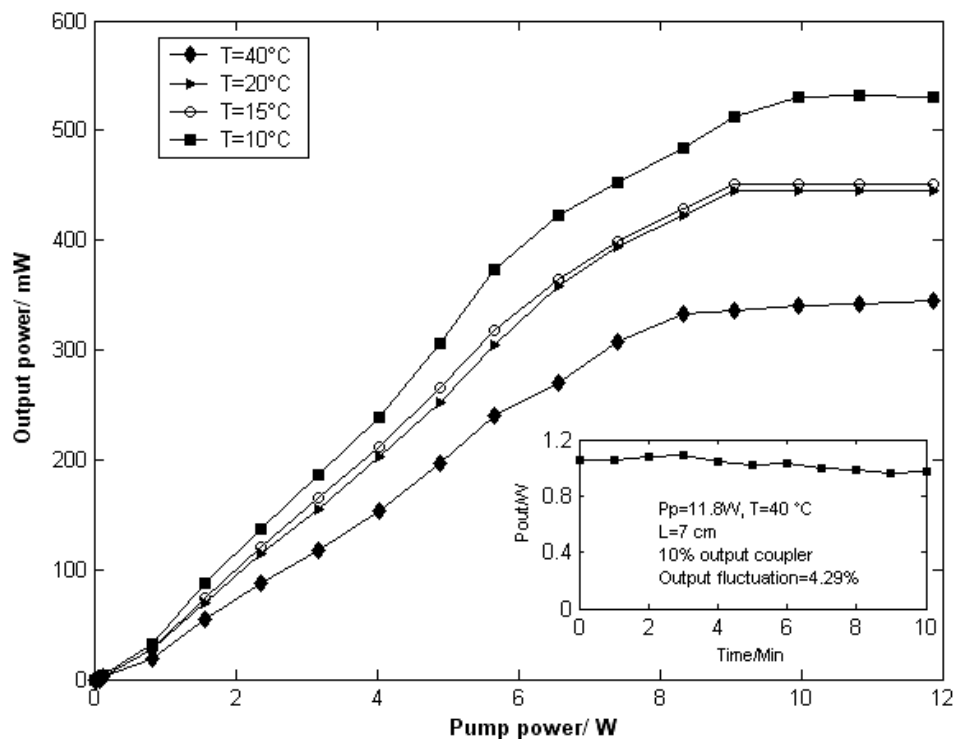


Fig. 12. Output characteristics of a 5.5 cm-length fiber laser with different operation temperatures; inset is the output power versus time (minute) at constant pump (11.8W) and operation temperature ( $40^\circ\text{C}$ ).

#### 2.4 The laser spectra

Fig. 13 is the laser spectrum of the 5cm-length  $\text{Tm}^{3+}$ -doped fiber laser measured at pump power of 10 W (output of  $\sim 500\text{mW}$ ). It is clear that the short fiber laser operates in few

longitudinal modes. This is because that the fiber length is small, leading to a large longitudinal mode spacing, only few modes can obtain enough gain to initiate laser oscillation. The main spectral peak situates at 1970 nm, with a FWHM of  $\sim 3$  nm. This spectral band width is much narrower than that obtained in the longer fiber laser [23], whose laser band width is tens of nm. Therefore, it is much easier to achieve single-frequency laser output with short-length  $\text{Tm}^{3+}$ -doped fibers. The existence of another small spectral peak indicates the mode competition in the short  $\text{Tm}^{3+}$ -doped fiber laser.

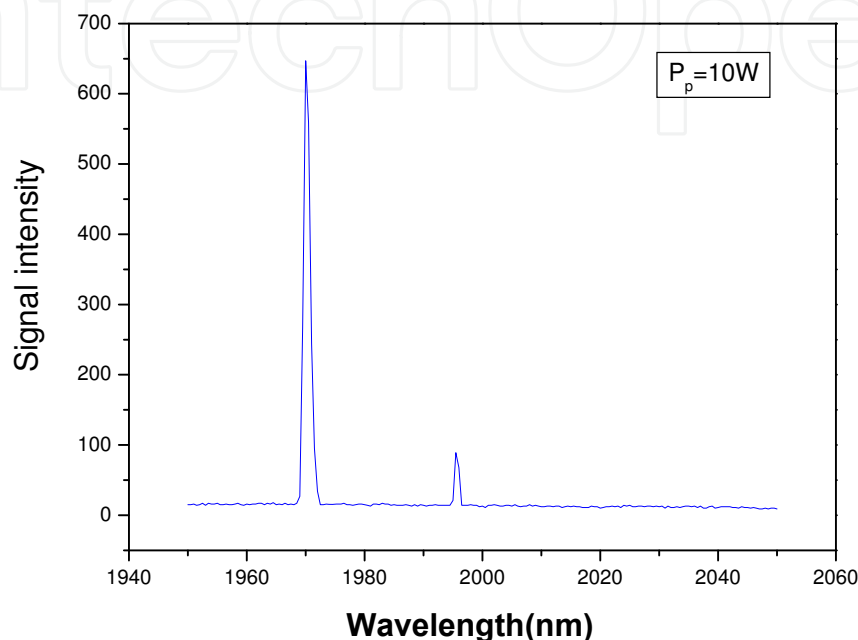


Fig. 13. Laser spectrum of the 5cm-length  $\text{Tm}^{3+}$ -doped fiber laser

The laser spectra of this short fiber laser under different pump power levels are shown in Fig. 14. When the pump power is 0.8 W, the laser only shows one spectral peak. The single-spectral-peak operation preserves with improvement of the pump to 2 W. When the pump is increased to 5W, laser operation changes from single spectral peak to two spectral peaks. At high pump level, mode hopping occurs, e.g. the main spectral peak changes to 1997 nm at the pump power of 8 W. The mode hopping phenomenon is probably due to changes of the cavity configuration parameters induced by the variation of the circumstance (such as fiber temperature or deformation of the cavity mirror).

### 3. High power $\sim 2 \mu\text{m}$ $\text{Tm}^{3+}$ -doped silica fiber laser and its wavelength tunability

The  $\text{Tm}^{3+}$ -doped fiber laser pumped by diode lasers has a great potential to scaling its output comparable to or even over the  $\text{Yb}^{3+}$ -doped fiber laser. This is because that  $\text{Tm}^{3+}$ -doped fiber can be pumped at around 790 nm, where efficient diode lasers are readily available. Another reason is that the  $\text{Tm}^{3+}$ -doped fiber laser can benefit from the cross-relaxation process, obtaining two excited  $\text{Tm}^{3+}$  ions for one pump photon. Therefore, the  $\text{Tm}^{3+}$ -doped fiber laser can provide, in theory, a maximum efficiency of 82% (a maximum

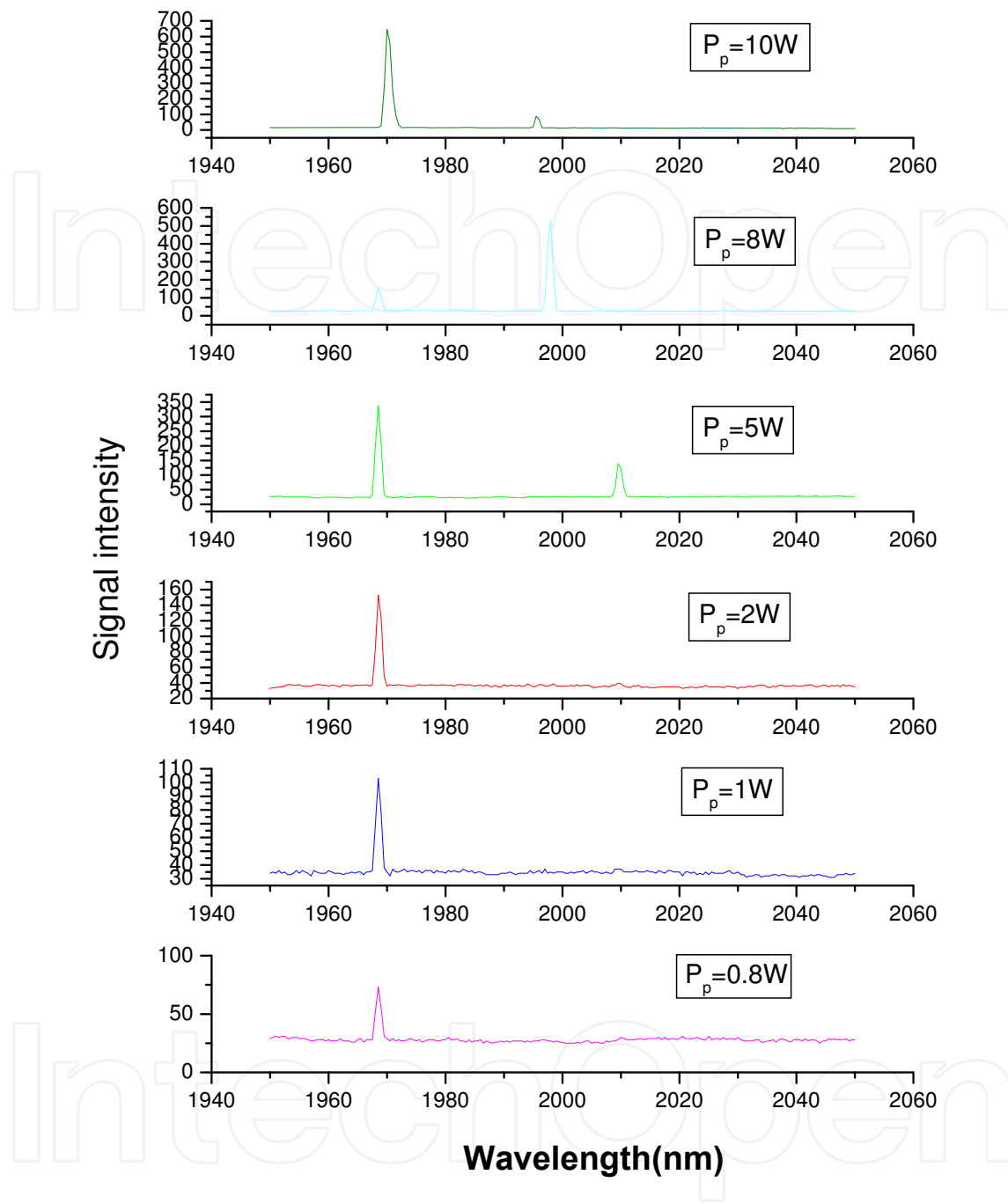


Fig. 14. Laser spectrum of the 5cm-length Tm<sup>3+</sup>-doped fiber laser at different pump levels (quantum efficiency of 200%). Since 1998, the output power of double-clad Tm<sup>3+</sup>-doped fiber laser has scaled steadily, especially when Al was codoped into the fiber to improve the Tm<sup>3+</sup> doping level [36-37]. At present, the maximum CW output from the 2 $\mu$ m Tm<sup>3+</sup>-doped fiber laser has arrived at 885W [26]. With further improvement of the pump diodes and pumping techniques, the 2 $\mu$ m output from the Tm<sup>3+</sup>-doped fiber laser will be over 1 kilowatts and rise to tens of kilowatts.

### 3.1 Power scalability of Tm<sup>3+</sup>-doped fiber laser

In this section, the power scalability and the limitation of Tm<sup>3+</sup>-doped fiber lasers is analyzed and discussed. Detailed analysis shows that Tm<sup>3+</sup>-doped fiber lasers have higher power scaling capabilities than that of Yb fiber lasers, i.e. higher power can be achievable from Tm<sup>3+</sup>-doped fiber lasers than Yb fiber lasers. Thereafter, a 100-W CW Tm<sup>3+</sup>-doped silica fiber laser with 60% slope efficiency is demonstrated experimentally and a design of twisted slab-like Tm<sup>3+</sup>-doped fiber with the modal area of 5000μm<sup>2</sup> is proposed for high-power Tm<sup>3+</sup>-doped fiber lasers.

#### 3.1.1 Introduction

Compared with solid-state lasers, fiber laser has many advantages, such as good heat management (large surface to volume ratio), high beam quality, compactness and high stability [38-39]. Yb-doped fiber lasers have always been the research interest due to its merits such as high output and high slope efficiency. Since the invention of double-clad fiber, the output power of Yb fiber laser follows the Moore's law of fiber laser-Payne's law, i.e. the laser output doubles every two years. The 2μm laser wavelength from the Tm<sup>3+</sup>-doped fiber laser is "eye-safe", which has wide applications in medical treatment, optoelectric Lidar and pump sources for mid-infrared lasers. Although Tm<sup>3+</sup>-doped fiber lasers appear later than the Yb fiber laser [40], and the output power is lower than that of the latter, the output of the Tm<sup>3+</sup>-doped fiber laser also follows Payne's law.

#### 3.1.2 Limitation and advantages for power scalability of Tm<sup>3+</sup>-doped fiber lasers

##### 1. Energy levels of the Tm<sup>3+</sup>-doped fiber laser

In Tm<sup>3+</sup>-doped fiber lasers, the 2μm laser light comes from the transition <sup>3</sup>F<sub>4</sub>→<sup>3</sup>H<sub>6</sub>. the energy level diagram of Tm<sup>3+</sup> ions is shown in Fig. 15 [41]. Due to strong Stark splitting of the <sup>3</sup>F<sub>4</sub> level, the Tm<sup>3+</sup>-doped laser is a quasi-four-level laser system. Besides, ions have a much smaller absorption cross section of 1.14×10<sup>-21</sup>cm<sup>2</sup> [40] than that of Yb<sup>3+</sup> ions (7.7×10<sup>-21</sup>cm<sup>2</sup>). Therefore, the Tm<sup>3+</sup>-doped fiber laser requires more bright pump diode lasers to over its threshold. For the <sup>3</sup>F<sub>4</sub> upper laser level, the emission cross section is σ<sub>emi</sub>=0.6×10<sup>-21</sup>cm<sup>2</sup> [40]. The saturation intensity can be calculated from the expression [42]

$$I_{sat} = \frac{h\nu}{\sigma_{emi}\tau_f}, \quad (1)$$

where τ<sub>f</sub> is the lifetime of the upper laser level.

From the calculation, we obtain the saturation intensity I<sub>sat</sub> = 0.5kW/cm<sup>2</sup>. However, the present output laser intensity of Tm<sup>3+</sup>-doped fiber lasers has arrived at 2GW/cm<sup>2</sup>, far over the saturation intensity. Therefore, high extraction efficiencies near quantum limitation can be achievable. In practice, the accessible laser efficiency is influenced by the physical-chemical features (spectrum, clustering, solubility and re-absorption, et al) of Tm<sup>3+</sup> ions doped in silica fibers. The doping level of Tm<sup>3+</sup> in silica fibers is usually lies in the 5000ppm level, and the fiber length is less than 13 meters. These conditions play a basic limitation in the output and energy-storing capability for the Tm<sup>3+</sup>-doped silica fiber laser.

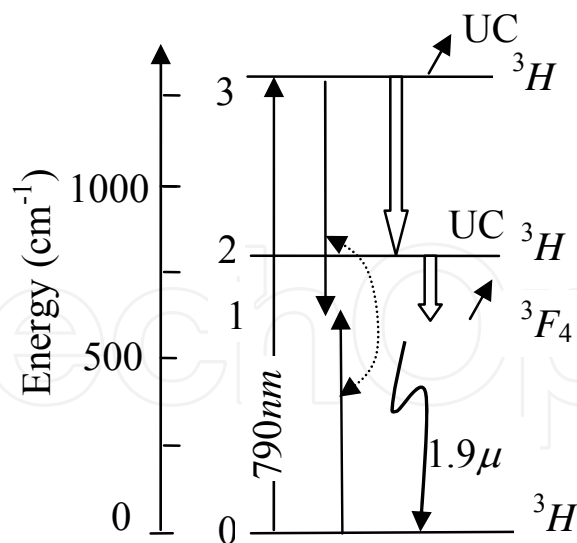


Fig. 15. Diagram of the energy levels of Tm<sup>3+</sup> ions

## 2. Optical damage

Optical damage to fiber is always a factor should be considered when high power output is expected from fiber lasers, because the optical damage of fiber set a upper limit for achieved power. Optical damages to fiber mainly include the material damage by instant light intensity and the photo-darkening effect by long-time illumination. In order to obtain single-transverse-mode operation, the normalized frequency of fiber should be

$$V = \frac{\pi \cdot d \cdot (N.A.)}{\lambda} < 2.4 \quad (2)$$

Where,  $d$  is the fiber diameter, and N.A. is the fiber numerical aperture. Limited by the fiber drawing technique and bend loss, the N.A. of fiber is generally less than 0.06. Therefore, the diameter of single-mode fiber cannot be too large. To obtain the same  $V$ , 2μm-fiber can have a diameter twice that of 1μm-fiber, thus a cross section of 4 times larger. Therefore, the Tm<sup>3+</sup>-doped fiber is more preferred to achieve single-mode high power laser output.

### Damage to bulk fiber

The damage to silica fiber by high-power laser is a complicate process, including many factors such as local heating induced glass fracture, glass evaporation, and non-linear effects, et al. By using 1-μm laser in measurement, damage threshold of silica fiber was obtained from 16GW/cm<sup>2</sup> to 400GW/cm<sup>2</sup>, showing great discrepancy. When Yb<sup>3+</sup> ions are doped, the damage threshold will decrease to be 0.5~0.8 times that of the pure silica fiber [43]. As far as the fiber facet is considered, the damage threshold will drop to 1/4 times that of pure silica fiber due to the impact of surface plasma, being about 40GW/cm<sup>2</sup> [44]. For the passive components in fiber lasers, such as fiber gratings, coated mirrors and fiber couplers, the damage threshold will be further decreased. At present, the maximum light intensity achieved in 1μm fiber laser is 2GW/cm<sup>2</sup>, much lower than the fiber damage threshold.

As shown in Fig. 16, the silica fiber has much stronger absorption at 2μm wavelength than at 1μm wavelength. Therefore, the silica fiber damage threshold will be lower at 2μm wavelength (~40GW/cm<sup>2</sup>) than at 1μm wavelength. On the other hand, the surface plasma

effect will be smaller by 2 $\mu$ m laser, which will improve the damage threshold to some extent. In experiment, the 2 $\mu$ m laser light intensity achieved in the Tm<sup>3+</sup> fiber has arrived at 2GW/cm<sup>2</sup>, being the same order of magnitude with that of 1 $\mu$ m laser.

As far as short-pulse (ps to ns regime) lasers are concerned, when neglecting self-focusing and other factors, the damage threshold of silica fiber follows the integrating law, which can also be applied to silica fiber laser [43].

$$E_{thres} \approx \sqrt{2 / \pi P \Delta t}, \quad (3)$$

where, P is peak power and  $\Delta t$  is the pulse width. The damage threshold peak power P= 475GW/cm<sup>2</sup> is nearly unchanged [43], indicating that heating effect is not the main factor leading to fiber damage. For fs-level laser pulses, self-focusing will be the primary source of fiber laser, and eq. (3) cannot be used.

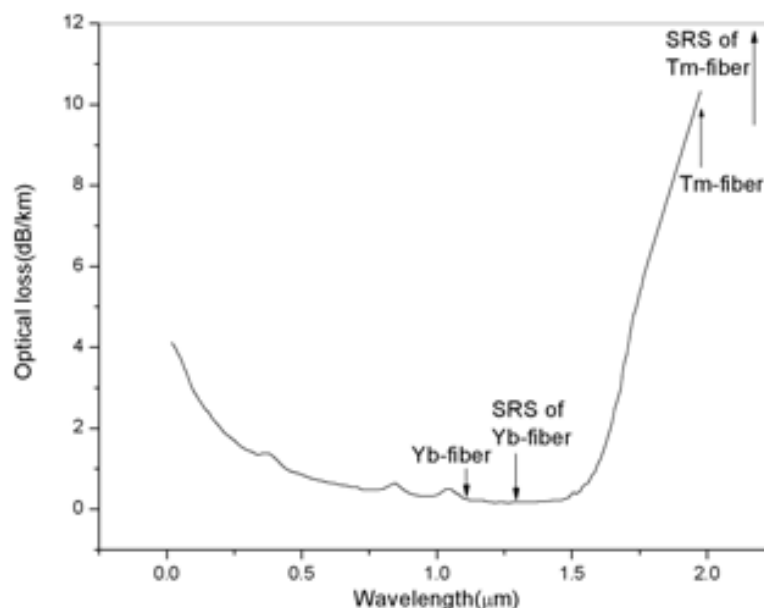


Fig. 16. Optical loss of Yb and Tm lasers, and their respective SRS emissions in silica fiber

#### *Photo-darkening*

Photo-darkening is the phenomenon that, after long time of laser operation, high-energy photons will induce color-center and defects in silica fiber, thus lead to growth of laser absorption and decrease of laser efficiency. Photo-darkening mainly stems from the radiation of UV and visible light. After 4 hours' radiation of 5 mW laser light at 488 nm, photo-darkening can be clearly observed. The photo-darkening-induced absorption primary occurs in the UV and visible spectral range. However, due to the fact that silica fiber itself has very weak absorption at the 1~2 $\mu$ m wavelength range, even slight photo-darkening will reduce the efficiency of fiber lasers [45].

Photo-darkening is extensively observed in Tm<sup>3+</sup>-doped fiber lasers. Therefore, photo-darkening was considered a hamper limiting long-time operation of Tm<sup>3+</sup>-doped fiber lasers pumped by 790 nm diode lasers. However, present experiment has shown that Tm<sup>3+</sup>-doped fiber laser can operate stably over 2000 hours [46], close to that of Yb fiber lasers. Employing pre-radiation with UV light will decrease photo-darkening effect, thus enhance the lifetime of Tm<sup>3+</sup>-doped fiber lasers.

### 3. Thermal issues

Larger ratio of surface to volume of fiber provides fiber lasers a good heat management system [47]. The heat generated in fiber core through multiphonon relaxation can be effectively dissipated by radiation and convection from the outer surface of the fiber. Most important is that, due to the guiding effect of fiber, even large temperature gradient exists will not deteriorate the light beam quality severely. However, with enhancement of output power, thermal issues of the Tm<sup>3+</sup>-doped fiber laser become serious and should be considered carefully.

#### *Heat effects*

Just as the Yb fiber laser, the key factor deciding how high power the Tm<sup>3+</sup>-doped fiber laser can endure is the melting temperature of the fiber core. By adopting positive cooling, the heat resistance ability of the Tm<sup>3+</sup>-doped fiber laser is about 100 W/m.

The 790nm-pump Tm<sup>3+</sup>-doped fiber laser has the “one-for-two” energy-transfer process-cross relaxation [23], there exist three transitions leading to occurrence upper laser level ions from absorbing a pump photon. They are (1)  $n_3 \rightarrow 2n_1$  (cross relaxation); (2)  $n_3 \rightarrow n_2 \rightarrow n_1$ ; and (3)  $n_3 \rightarrow n_1$ . Taking into account the up-conversion and re-absorption, the quantum efficiency of achieving upper laser level ions is

$$\eta = [2\eta_{3101} + \eta'_{3101} + \eta_{3201}] \eta_{las} - \eta_{up} - \eta_{reabs} \quad (3)$$

Neglecting some weak effects, the expression can be simplified to

$$\eta = 2\eta_{31} + (1 - \eta_{31})(\beta_{31} + \beta_{32}) \quad (4)$$

From the parameters of Tm<sup>3+</sup>-doped silica fiber, we can obtain  $\eta = 0.74$ , which is comparable with that of Nd:YAG laser. The quantum efficiency of Tm<sup>3+</sup>-doped fiber laser is also related to the doping concentration, operation temperature and other cavity parameters. Based on the heat management capability, it is concluded that the Tm<sup>3+</sup>-doped fiber laser can provide a output potential of about 300W/m.

#### *Efficiency decrease by operation temperature*

The ground state energy level of Tm<sup>3+</sup> ions is consisted of a series of sublevels, forming a continuous energy band with a broad bandwidth of 5770 cm<sup>-1</sup> [48]. This feature provides the Tm<sup>3+</sup>-doped fiber laser a quasi-four level laser system, possessing high temperature stability. At kilowatt level, the reduction of population inversion of Tm<sup>3+</sup>-doped fiber laser due to temperature growth is less than 1%.

Based on a 5.5cm-length Tm<sup>3+</sup>-doped fiber laser, the influence of temperature on the laser's efficiency has been observed, as shown in Fig. 12. When the temperature is increased from 10°C to 40°C, the output and slope efficiency decrease about 30% [33]. The primary reason leading to the reduction of output power is the 0.3nm/°C wavelength shift of the pump diode laser, which making the pump light cannot overlap well with the Tm<sup>3+</sup> absorption band, decreasing the pump absorption efficiency. If only the absorbed pump power is taken into account, the power reduction is just 5%. Another alternative explanation is that the fluorescence spectrum of Tm<sup>3+</sup>-doped fiber is broadened with temperature, decreasing the gain per unit-length of fiber. As far as long fiber lasers are concerned, the influence of these

two factors is weak. Our 100-W Tm<sup>3+</sup>-doped fiber laser experiment shows that, when the fiber length is 10 meters, the reduction of output power and slope efficiency induced by the temperature growth from 10°C to 40°C is less than 5%.

#### 4. Non-linear optical effects

The silica glass itself is non-symmetric, so no intrinsic second-order non-linear effect exists [49]. However, the existence of third-order non-linear effect such as stimulated Raman scattering (SRS) and stimulated Brillouin scattering (SBS) has significant impact on high-power CW lasers, especially single-frequency output is expected. Self-phase-modulation (SPM) and cross-phase-modulation (XPM) has negligible effects on CW-mode lasers, but has obvious impact on ultra-short pulsed lasers. Self-focusing can greatly decrease the damage threshold of fiber. The parameter of fiber material that is closely related with third-order non-linear effects is the second-order refractive index  $n_2$ , which differs greatly when different doping and fiber drawing techniques are used. For silica fiber operating at 2 $\mu$ m, the second-order refractive index  $n_2$  is about  $2.5 \times 10^{-20} \text{ m}^2/\text{W}$  [49].

##### *SRS and SBS*

Both SRS and SBS are elastic scattering processes. SRS originates from the elastic scattering of optical phonons, and has a frequency shift of  $\sim 13\text{THz}$ , and is hardly influenced by the band width of input laser; SBS stems from the elastic scattering of acoustic phonons, and has a frequency shift of  $\sim 17\text{GHz}$ , and can be significantly influenced by the band width of input laser. When the band width of the input laser is larger than 0.5GHz, the SBS threshold will be significantly improved, and the SRS will be the dominant limitation for power scaling of fiber lasers.

In fiber, the power threshold of SRS and SBS can be expressed as [49]

$$P_0 \approx C_1 A_{\text{eff}} / g_R L_{\text{eff}} \quad (5)$$

Where,  $C_1$  is the threshold parameter ( $C_{\text{SRS}}=16$  and  $C_{\text{SBS}}=21$ ),  $A_{\text{eff}}$  and  $L_{\text{eff}}$  is effective mode area and interaction length, respectively. At the wavelength of 2 $\mu$ m, the effective SRS coefficient  $g_R=5 \times 10^{-14} \text{ m/W}$  [40], is just a half of the one at the wavelength of 1 $\mu$ m; while the SBS coefficient  $g_R=5 \times 10^{-11} \text{ m/W}$  [40], is the same as the one at the wavelength of 1 $\mu$ m. In fiber, the Stocks loss is also important to SRS. From Fig. 16, we can see that the Stocks loss will higher than the pump when laser wavelength is longer than 1.55 $\mu$ m. The optical loss at 2 $\mu$ m ( $\sim 10\text{dB/km}$ ) is 10 times that at 1 $\mu$ m, so the SRS threshold in 2 $\mu$ m fiber lasers will be 20 times that in 1 $\mu$ m fiber lasers. In Tm<sup>3+</sup>-doped silica fiber lasers, the SRS threshold is 30~100MW/ $\mu\text{m}^2$ .

##### *Self-focusing*

Self-focusing is the light beam focusing phenomenon induced by the intensity-related change of refractive index of the material. Due to long interaction length in fiber lasers, even a weak self-focusing effect will induce laser beam focusing, thus damage the fiber. The threshold for self-focusing in fiber is expressed by [50]

$$P_{\text{self}} = \frac{0.15\lambda^2}{n_0 n_2} \quad (6)$$

The threshold  $P_{self}$  is proportional to the square of laser wavelength. At 2 $\mu$ m, Both  $n_0$  and  $n_2$  are slightly smaller than that at 1 $\mu$ m. Therefore, the self-focusing threshold at 2 $\mu$ m is more than 4 times that at 1 $\mu$ m. For 2 $\mu$ m fiber lasers, the self-focusing threshold is about 16MW, with no relation to fiber diameter.

#### SPM and XPM

In fiber lasers, SPM and XPM change the phase of ultra-short laser pulses, playing a severe role in the reshaping of pulses. The phase change can be calculated by

$$B = \frac{2\pi}{\lambda} \int n_{2l}(z) I(z) dz, \quad (7)$$

where,  $n_{2l}$  is non-linear refractive index,  $I$  is light intensity and  $\lambda$  is laser wavelength.

Generally, in order to keep a small phase distortion in the propagation of ultra-short pulses, the B integral should less than  $\pi$ . With the same  $n_2$ , 2 $\mu$ m laser pulses have a smaller B integral than that of 1 $\mu$ m. Solving the propagation equations of laser pulse in fiber, the frequency change induced by SPM and XPM can be expressed by a non-linear character parameter

$$\gamma = \frac{2\pi n_2}{\lambda A_{eff}}. \quad (8)$$

The 2 $\mu$ m fiber laser has a comparatively smaller  $n_2$  and a comparatively larger  $A_{eff}$  than that of 1 $\mu$ m lasers. Therefore, the 2 $\mu$ m fiber laser has a non-linear character parameter about 1/10 times that of 1 $\mu$ m fiber laser, providing a much higher peak-power enduring capability of ultra-short pulses.

### 3.1.3 Power scaling techniques for the Tm<sup>3+</sup>-doped fiber laser

#### Experimental results

For achieving high power laser output, the double-clad Tm<sup>3+</sup>-doped silica fiber has a large doped core diameter of 27.5  $\mu$ m with the N.A. of 0.20 and. High Tm<sup>3+</sup> ions doping concentration of 2.5 wt.% is chosen to facilitate the cross relaxation process. A small portion of Al<sup>3+</sup> ions were also doped into the fiber to suppress the energy transfer upconversion (ETU) processes. The pure silica inner cladding, coated with a low-index polymer, has a 400- $\mu$ m diameter and the N.A. of 0.46. The hexagonal cross section of the inner clad helps to improve pump absorption.

Fig. 17 is the experimental setup for realizing the high-power Tm<sup>3+</sup>-doped fiber laser. Two high-power fiber-coupled LD arrays operating at  $\sim$ 793 nm was used as the pump source. The pump beam was launched into the fiber by aspheric-lens coupling system through dichroic mirrors. The right-hand side dichroic mirror is used to guide the 2  $\mu$ m laser light out. The launched efficiency was as high as  $\sim$ 90%, and the largest pump power of 180 W can be launched into the fiber. The pump end of the fiber was butted directly to the dichroic mirror with high reflectivity ( $>$ 99.7%) at 2.0  $\mu$ m and high transmission ( $>$ 97%) at 790 nm. Both fiber ends were cleaved perpendicularly to the axis and polished carefully. The ends of the fiber were clamped tightly in water-cooled copper heat-sinks, and the remaining fiber was immersed into water to achieve maximum efficiency.

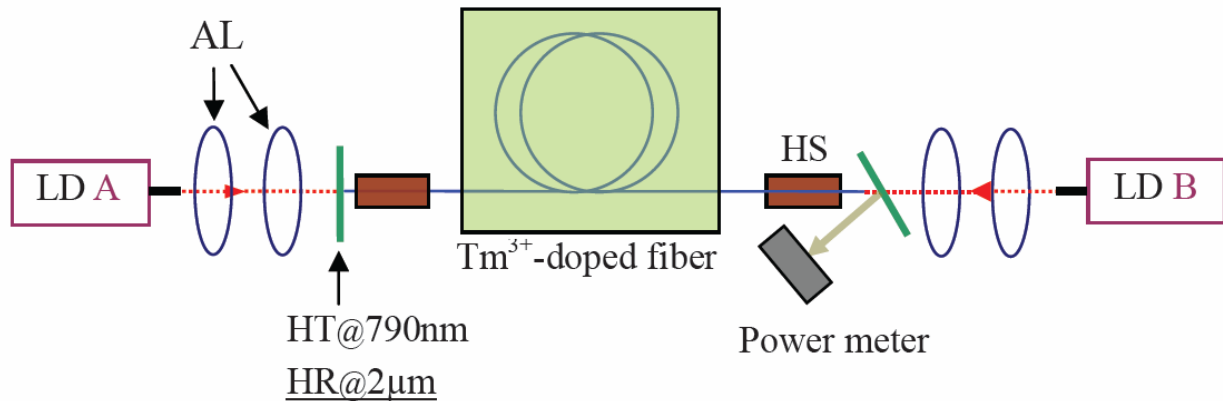


Fig. 17. Experimental setup of the  $\text{Tm}^{3+}$ -doped fiber laser. LD: laser diode; AL: aspheric lens; HT: high transmission; HR: high reflection; HS: heat sink.

Fig.18 shows the 100-W level  $\text{Tm}^{3+}$ -doped silica fiber laser achieved in our laboratory. When pumped by 790 nm diode laser, the laser output is 102 W with a slope efficiency of 58.6%. In this  $\text{Tm}^{3+}$ -doped fiber laser, the power density is just  $30\text{kW}/\text{cm}^2$ , far lower than the previously mentioned power density limit. Therefore, power scaling this  $\text{Tm}^{3+}$ -doped fiber laser to over 1 kW power level is only limited by obtaining high brightness pump diode lasers [51].

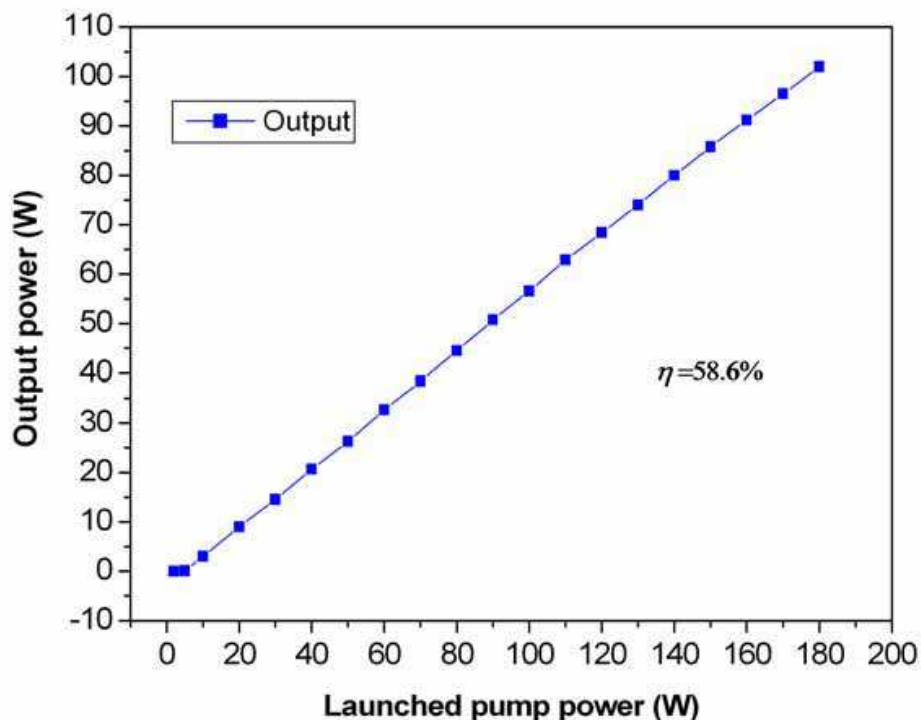


Fig. 18. Output characteristics of the  $\text{Tm}^{3+}$ -doped fiber laser.

Fig. 19 is the laser output spectrum. The laser spectrum is centered at 2070 nm, and has a full band width of about 25 nm. Due to a broad gain bandwidth, the fiber laser operates in the multi-mode regime. Therefore, there are many spectral peaks in the measured spectrum.

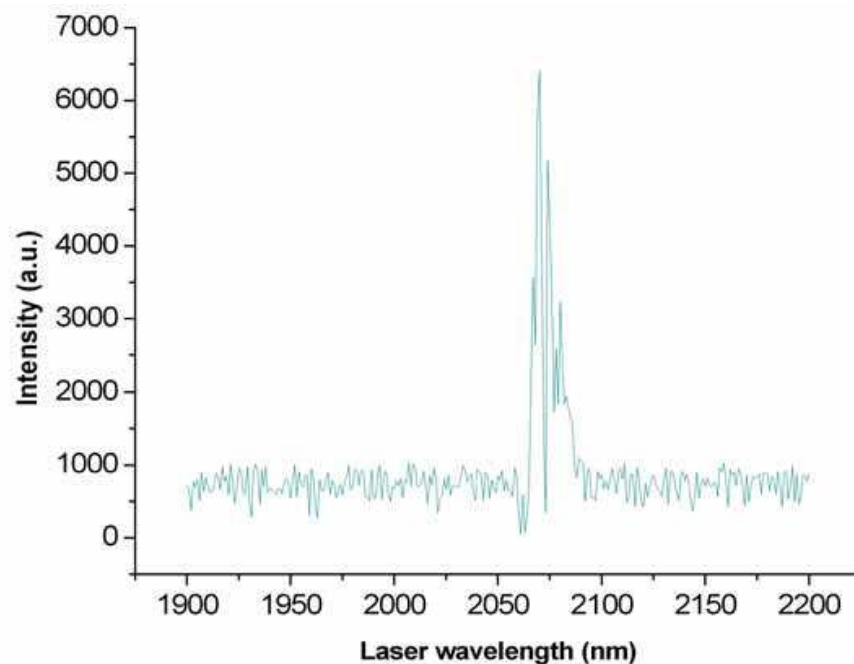


Fig. 19. Laser spectrum of the Tm<sup>3+</sup>-doped fiber laser.

*A novel power-scaling method*

There are two technical ways to improve the output power of the 2 $\mu$ m Tm<sup>3+</sup>-doped fiber laser over 1kW: one is by using large mode area (LMA) fibers or multi-mode fibers through special fiber-structure design; another way is adopting different laser cavity configurations such as multi-stage cavity (different cladding-size fibers are used in different stages), master oscillator power amplifier (MOPA) structure or laser beam combination.

From the analysis in the previous section, we found that the limitation of power scaling of fiber lasers is the finite fiber diameter. In order to obtain LMA fiber together with high beam quality, photonic crystal fiber (PCF) can be used. Another alternative is designing the fiber with a W-shape refractive index. By using this method, we design a slab-core fiber, achieving a core mode area larger than 5000 $\mu$ m<sup>2</sup> [52]. In such kind of fiber, laser in the width direction is multi-mode, so the key thing is to control the beam quality in this direction. Using the V-groove method can improve the beam quality in the width direction, but will decrease the mechanical feature of the fiber. Therefore, we proposed the rotating slab-core fiber configuration, as shown in Fig. 20. The slab-core rotates at an angular rate of  $\theta$ , the trace of the slab-core edge can be described as

$$\begin{aligned} x &= d \cos(\theta z) \\ y &= d \sin(\theta z) \end{aligned} \quad (9)$$

Where,  $d$  is the slab-core width and  $z$  is the coordinate in the length direction.

With different  $\theta$ , the rotating strength of the slab core will be changed. The winding of the fiber core induce much higher loss for higher-order modes (suppressing the higher-order modes), thus laser oscillation occurs for lower-order modes. Fig. 20 shows the loss of different orders of modes as a function of the rotating rate of the slab core. It can be seen that higher-order modes can be effectively suppressed when the rotating rate of the fiber core is less than  $2\pi/5\text{cm}^{-1}$ .

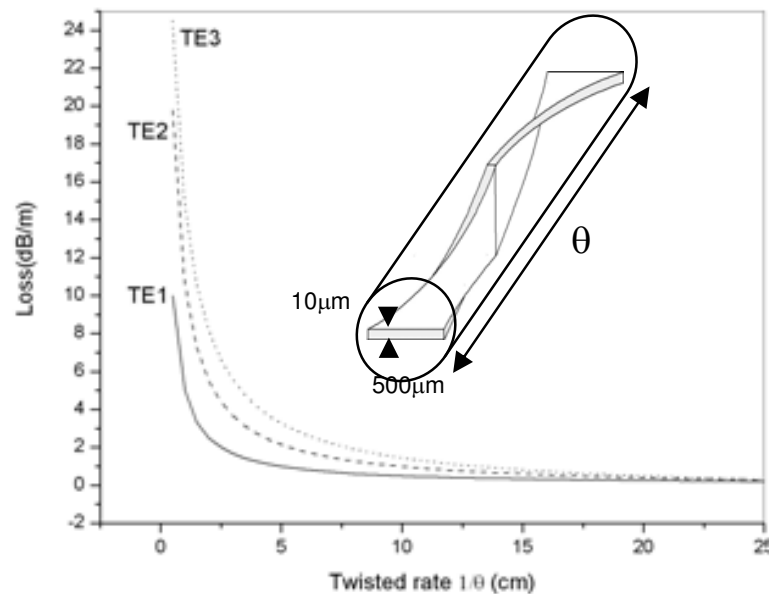


Fig. 20. Mode loss of the rotating rectangular-core fiber versus the angular rotating rate.

#### Conclusion and prospect

The  $\text{Tm}^{3+}$ -doped silica fiber laser as a kind of high efficient  $2\mu\text{m}$  laser source, its further power scalability is not limited by the intrinsic physical mechanism of fiber. At present, the limitation for power scaling lies in obtaining high bright laser diodes and ultra-low-loss  $\text{Tm}^{3+}$ -doped silica fibers. Compared with the  $1\mu\text{m}$  Yb fiber lasers,  $\text{Tm}^{3+}$ -doped fiber laser has a higher power scalability. Besides, the  $\text{Tm}^{3+}$ -doped fiber laser has a longer lifetime of the upper laser level and a much broader emission band, providing itself a much better advantage in achieving pulsed laser output. The  $\text{Tm}^{3+}$ -doped fiber laser has great potentials in high-power "eye-safe" laser output and high-peak-power pulsed laser.

### 3.2 Wavelength tuning of high-power $\text{Tm}^{3+}$ -doped fiber laser

#### 3.2.1 Introduction

The large degree of Stark splitting of the  $^3\text{H}_6$  ground state, as shown in Fig. 8, provides the  $^3\text{H}_4 \rightarrow ^3\text{H}_6$  transition in the  $\text{Tm}^{3+}$ -doped silica fiber with a very broad emission spanning  $>400$  nm. This feature provides the  $\text{Tm}^{3+}$ -doped fiber laser the great potential of being wavelength tuning in a large spectral range. The emission spectrum of the  $^3\text{F}_4 \rightarrow ^3\text{H}_6$  transition in  $\text{Tm}^{3+}$ -doped silica fiber is shown in Fig. 7 [18].

Apart from being doped into silica fiber, the  $\text{Tm}^{3+}$  ions can also achieve very broad emission band when doped into other host materials. For instance, an emission band of  $\sim 300$  nm can be obtained when  $\text{Tm}^{3+}$  is doped into ZBLAN fiber, as shown in Fig. 21 [53]. Therefore,  $\text{Tm}^{3+}$ -doped fiber lasers have a particular advantage in wavelength tuning regime.

According to the character of fiber laser, many methods can be used to achieve the wavelength tuning function. As far as the  $\text{Tm}^{3+}$ -doped fiber laser is concerned, the wavelength tuning techniques include temperature-tuning, length-tuning, birefringence-tuning and grating-tuning et al. Among these tuning techniques, the most widely used and most skillful is the grating wavelength tuning technique. Along with the mature of the fiber Bragg grating, the grating tuning technique is becoming more and more important.

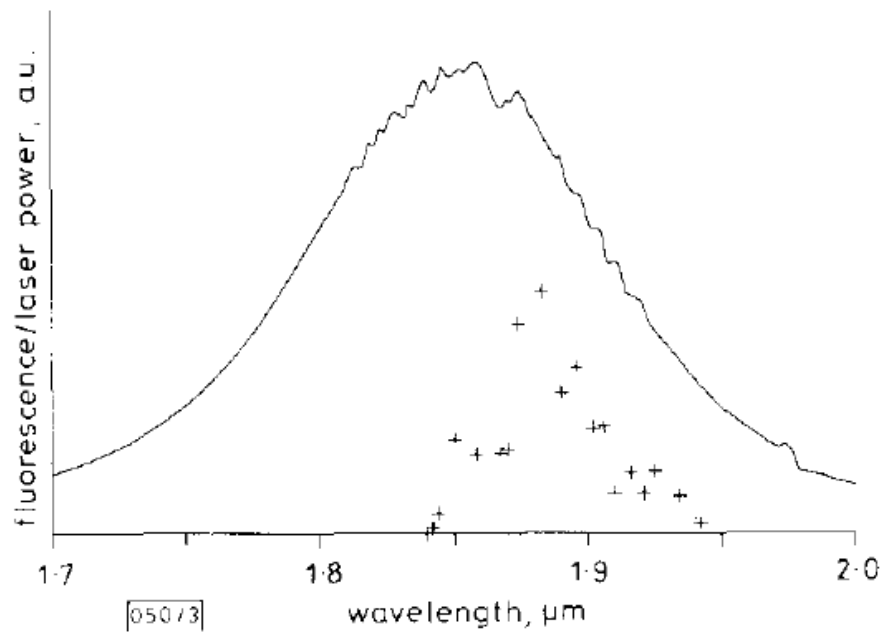


Fig. 21. The fluorescence spectrum of  ${}^3F_4 \rightarrow {}^3H_6$  transition in Tm<sup>3+</sup>-doped ZBLAN fiber

Several kinds of wavelength tuning techniques in Tm<sup>3+</sup>-doped fiber lasers:

1. Fiber-length tuning.

Due to the quasi-four-level system feature, the Tm<sup>3+</sup>-doped fiber laser can be wavelength tuned by changing the fiber length. When the fiber length is elongated, re-absorption of the signal light will increase, leading to red-shift of laser wavelength. This tuning method is simple and convenient for manipulating, but the tuning range is limited. The broadest tuning wavelength spanning is less than 100 nm [54-55]. The most dominated shortcoming of this wavelength tuning technique is that laser wavelength cannot be tuned continuously. In the tuning process, the replacement of fiber requires re-adjusting the laser cavity, complicating the tuning work. This tuning method has little potential in practical applications.

2. Birefringence-tuning.

This wavelength tuning method is based on changing the birefringence characteristic of the signal light in the cavity. By using a birefringence filter, the Tm<sup>3+</sup>-doped fiber laser has been tuned over a 200 nm spectral range [56]. Although this method can provide a wide tuning range, the tuning laser configuration is rather complicated, and very inconvenient for tuning. Besides, this technique is confined by the free-spectral range of the birefringence filter. Therefore, this method is far from practical application.

3. Temperature-tuning.

Due to the circumstance-field impact, the ground-state level of Tm<sup>3+</sup> ions is Stark splitted into many sub levels. As one of the Stark sub levels, the lower laser level has a population distribution significantly influenced by the circumstance temperature (according to the Boltzman distribution). This leads to the wavelength shift with temperature. Electrical oven has been used to heat the Tm<sup>3+</sup>-doped fiber laser for wavelength tuning [57], and a tuning

range of 18 nm was achieved when the fiber temperature was changed during a 109°C range. With a Peltier plate, a wavelength tuning range of 40 nm was realized with the tuning rate of  $\sim 2\text{nm}/^\circ\text{C}$  in a 6-meter-length  $\text{Tm}^{3+}$ -doped fiber [58]. This tuning technique is simple and convenient, but the tuning range is also narrow. The melting point of the fiber polymer cladding set a upper limit for the temperature, and low temperature operation cannot be practically used, which limits the wide application of this tuning method.

#### 4. Grating-tuning.

At present, the grating tuning method is the most fully developed and widely used. This is primarily due to the fast development of the grating fabrication technique. By using the grating-tuning technique,  $\text{Tm}^{3+}$ -doped fiber laser has achieved tuning range over 200 nm [59-61]. Compared with the above mentioned three methods, the grating tuning technique can provide a broader tuning range with a much narrower linewidth. This method is, up to date, the most mature wavelength tuning technique.

### 3.2.2. High-power $\text{Tm}^{3+}$ -doped fiber laser tuned by a variable reflective mirror

Due to the quasi-four-level system feature, the  $\text{Tm}^{3+}$ -doped fiber laser can be wavelength tuned by changing the transmittance of the output coupler. With a variable reflective mirror (VRM) as the output coupler, high-power  $\text{Tm}^{3+}$ -doped fiber laser can be wavelength tuned over a range of  $>200\text{ nm}$  [47]. The combination of high power and wavelength tuning of the  $\text{Tm}^{3+}$ -doped fiber laser provides an excellent kind of laser source in the  $\sim 2\ \mu\text{m}$  spectral range.

In the experiment, the double-clad  $\text{Tm}^{3+}$ -doped silica fiber has a doped core with the N.A. of 0.20 and diameter of  $27.5\ \mu\text{m}$ . High  $\text{Tm}^{3+}$  ions doping concentration of 2.5 wt.% is essential to facilitate the CR energy transfer process. A small portion of  $\text{Al}^{3+}$  ions were also doped into the fiber to suppress the energy transfer upconversion (ETU) processes, which may cause the quenching of the  $^3\text{F}_4$  multiplet lifetime. The pure silica inner cladding, coated with a low-index polymer, has a  $400\text{-}\mu\text{m}$  diameter and the N.A. of 0.46. The hexagonal cross section of the inner clad helps to improve pump absorption. The absorption coefficient at the pump wavelength (790 nm) is  $\sim 2.8\ \text{dB/m}$ .

Fig. 22 shows the experimental setup [47]. High-power LD arrays operating at 790 nm and TM mode was used as the pump source. The outputs from two LD arrays were polarizedly combined to form a single pump beam. This pump beam was reshaped by a micro-prism stack at first, and then focused into a circular spot using a cylindrical lens and an aspheric lens. Through a dichroic mirror, the pump light was launched into the fiber. The launched efficiency was measured through a 4-cm-long  $\text{Tm}^{3+}$ -doped fiber. The largest pump power of 51 W can be launched into the fiber. The pump end of the fiber was butted directly to the dichroic mirror with high reflectivity ( $>99.7\%$ ) at  $2.0\ \mu\text{m}$  and high transmission ( $>97\%$ ) at 790 nm. Both fiber ends were cleaved perpendicularly to the axis and polished carefully. The output coupler was formed by a VRM or the bare fiber-end facet. The transmission of the VRM can be changed continuously from 5% to 80% (the reflection  $R$  is changed from  $\sim 94.8\%$  to  $18.4\%$ ) at  $2\ \mu\text{m}$  by simply horizontally displacing the VRM with a one-dimensional stage. The ends of the fiber were clamped tightly in water-cooled copper heat-sinks, and the remaining fiber was immersed into water to achieve maximum efficiency. During the experiment, both cavity mirrors were carefully adjusted with five-dimensional holders.

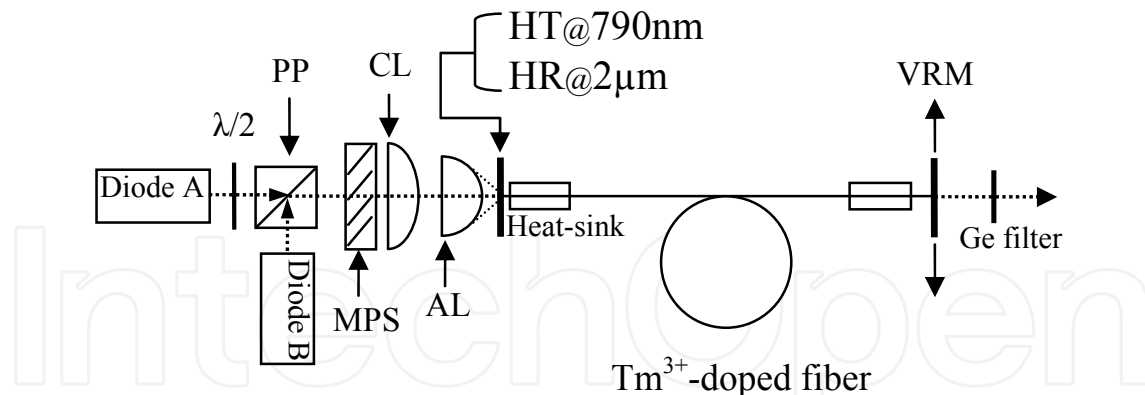


Fig. 22. Schematic of the experimental setup. PP: polarizing plate; MPS: micro-prism stack; CL: cylindrical lens; AL: aspheric lens; HT: high transmission; HR: high reflection; VRM: variable reflective mirror.

The lasing characteristics obtained with relative higher output couplings in a 4-m long fiber laser are shown in Fig. 23 [47]. When the VRM was moved away from the fiber end and the bare fiber-end facet was used as the output coupler ( $T \approx 96\%$ ), the laser reached threshold at a launched pump power of 5.9 W, and produced a maximum output power of 32 W at 1949 nm for 51-W launched pump power, corresponding to a slope efficiency of 69% and a quantum efficiency of 170%. The high efficiency was attributed to high  $\text{Tm}^{3+}$ -doping concentration, suppression of ETU with  $\text{Al}^{3+}$  ions [38], and efficient fiber-cooling. With  $T=80\%$  output coupling, a slightly lower output power of 29.8 W was generated at 1970 nm, and the slope efficiency with respect to launched pump power was  $\sim 65\%$ . When the output coupling decreased to 60%, the output power dropped to 27.4 W at 1994 nm with a slope efficiency of  $\sim 58\%$ . In all these cases, the output power increased linearly with the launched pump power, suggesting that the laser can be power scaled further by increasing the pump power. The power stability of the laser output, monitored by an InAs PIN photodiode and a 100 MHz digital oscilloscope, was less than 1% (RMS) at  $\sim 30$  W power levels.

After carefully optimization the position of the coupler, the fiber laser was wavelength tuned by simply horizontally moving the VRM coupler. The peak wavelength of the laser spectrum is taken as the laser wavelength. Fig. 24 shows the dependence of the laser wavelength on the output coupling [47]. When the output coupling decreased from  $\sim 96\%$  to 5% in the 4-m long fiber laser, the laser wavelength was tuned from 1949 to 2055 nm with a tuning range of 106 nm. The nearly linear dependence provides a basic knowledge to choose the wavelength from  $\text{Tm}^{3+}$ -doped silica fiber lasers. The phenomenon can be explained by the enhanced re-absorption of laser in the high-Q cavity. Since the photon lifetime in the cavity is increased with higher reflective mirrors, the photon travels more round-trips, and undergoes more re-absorption before escapes from the cavity.

Employing different fiber lengths from 0.5 m to 10 m, as shown in Fig. 24, the laser can be tuned from 1866 to 2107 nm. The total tuning range is over 240 nm at above-ten-watt levels. A typical laser spectrum obtained with the 4-m fiber at coupling of  $T=15\%$  and 16-W output power is shown as inset in Fig. 24. The laser spectra under different couplings and fiber lengths hold nearly identical features. The spectrum has a bandwidth (FWHM) of  $\sim 15$  nm and several lasing peaks. The multi-peak spectrum indicates the laser operated in multiple longitudinal modes.

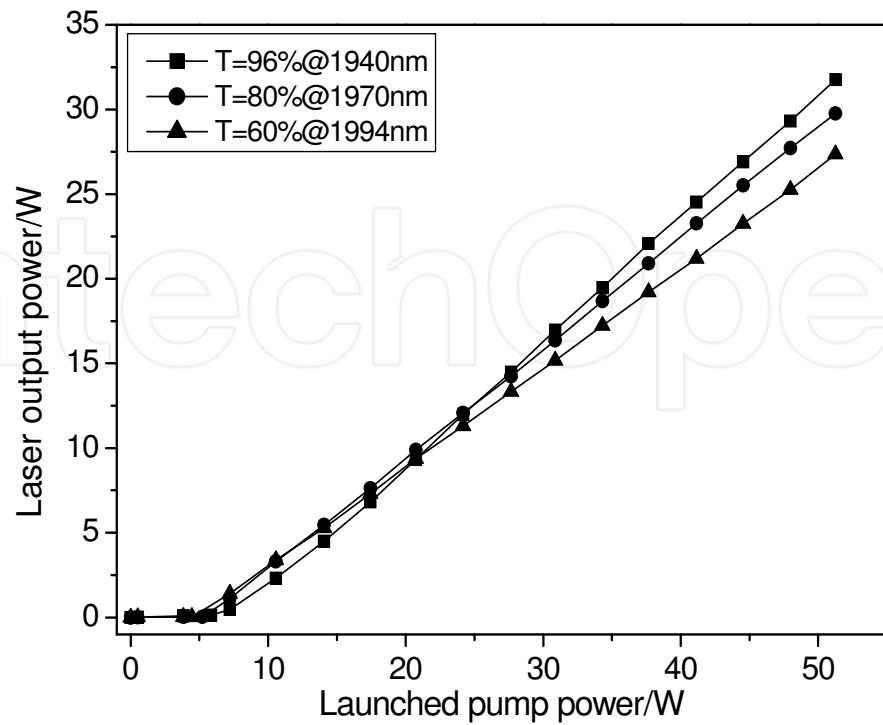


Fig. 23. Laser output power versus launched pump power with three high output couplings.

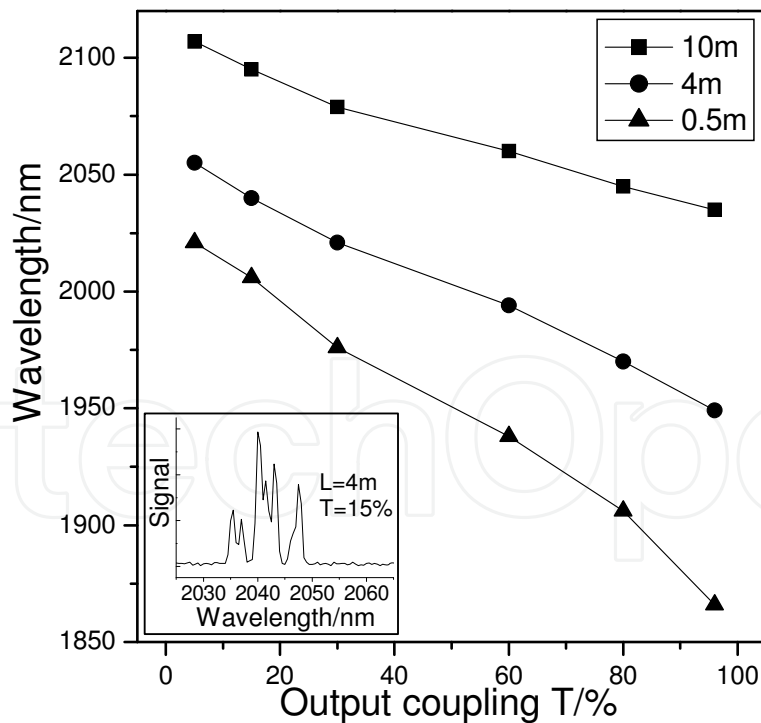


Fig. 24. Laser peak wavelength as a function of output coupling; inset is the laser spectrum obtained with the 4-m fiber at coupling of  $T=15\%$ .

The maximum output power and launched threshold pump power as functions of the output coupling are shown in Fig. 25 [47]. When the output coupling decreases from  $\sim 96\%$

to 5%, the threshold pump power reduces almost linearly from 5.9 to 1.0 W, and the maximum output power drops from 32 W to 9.0 W. The sharp decreasing of the output power with <15% output coupling is mainly due to low output transmission and increased re-absorption of laser light. Between the output coupling of 20% and 96%, the laser output power exceeds 20 W over a tuning range of 90 nm from 1949 to 2040 nm (see Fig. 24). This presents the potential of Tm<sup>3+</sup>-doped silica fiber lasers to generate multi-ten-watt output over a hundred-nanometer tuning range.

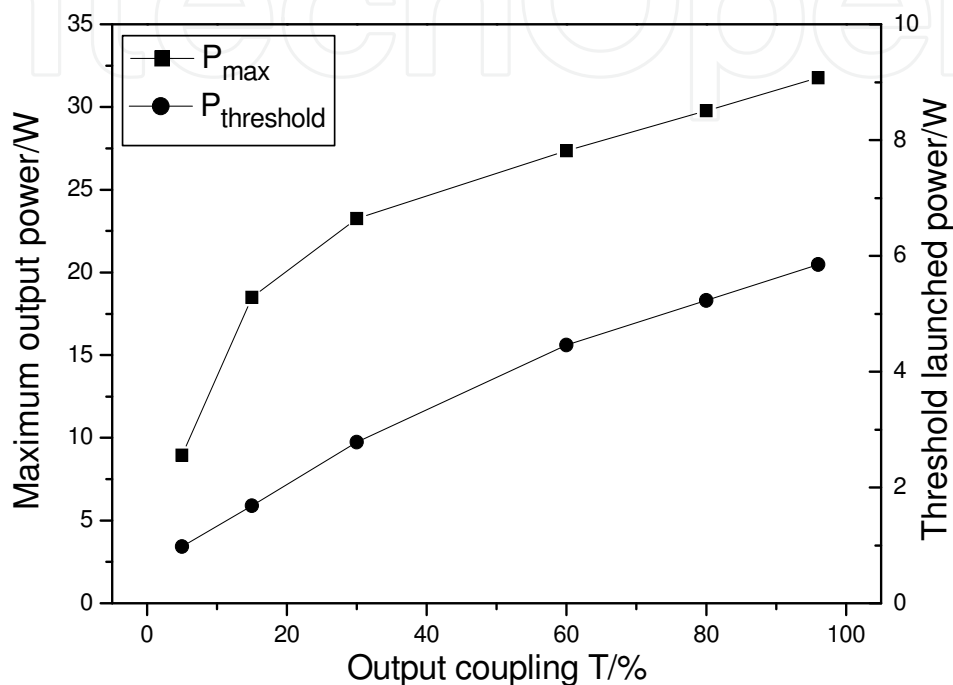


Fig. 25. Maximum laser output power and threshold launched power as functions of the output coupling.

### 3.2.3 Conclusion

At present, high-power widely tunable Tm<sup>3+</sup>-doped silica fibers must make use of high-power diode lasers as the pump source. Due to the comparatively low damage threshold of grating and difficulty in fabricating 2 $\mu$ m grating, wavelength tuning high-power Tm<sup>3+</sup>-doped fiber laser with fiber Bragg grating is still unpractical. Using the variable reflective output coupler to tune high-power 2 $\mu$ m fiber lasers is a feasible alternative. The combination of high power, high efficiency, and wide tunability of Tm<sup>3+</sup>-doped fiber lasers will provide a great opportunity for applications of eye-safe lasers.

## 4. Self-pulsing and passively Q-switched Tm<sup>3+</sup>-doped fiber laser

Due to its special energy-level structure and the wave-guiding effect of fiber, Tm<sup>3+</sup>-doped fiber lasers can produce fluent dynamical behaviors, including self-pulsing, self-mode-locking and et al [62-63]. On the other hand, the particular broad emission band of Tm<sup>3+</sup> ions provides the potential to achieve ultra-short pulses from the Tm<sup>3+</sup>-doped fiber laser.

## 4.1 Self-induced pulsing in $\text{Tm}^{3+}$ -doped fiber lasers with different output couplings

### 1. Introduction

It's well known that self-pulsing can be achieved in any lasers with an adequate saturable absorber [64]. Erbium-doped fiber lasers have demonstrated a large variety of dynamical behaviors, including self-pulsing operations [65], static and dynamic polarization effects [66], antiphase and chaotic dynamics [67]. The dynamic behaviors have been attributed to the presence of ion-pairs or clusters acting as a saturable absorber [68-69], bidirectional propagation in "high-loss cavity" and Brillouin scattering effects in the fiber [70]. Ion pair concentration can play an important role in self-pulsing dynamic behaviors [71].

It has been shown that the  $\text{Tm}^{3+}$ -doped fiber laser can operate successively in continuous-wave (CW) mode, self-pulsing mode and quasi-CW mode with increase of pump power [62]. Self-mode-locking phenomenon has also been observed in the  $\text{Tm}^{3+}$ -doped fiber laser, which was supposed to stem from saturable absorption or strong interactions between the large number of longitudinal modes oscillating in the cavity [63].

### 2. Experimental observation

In order to understand the mechanism and features of self-pulsing in  $\text{Tm}^{3+}$ -doped fiber lasers, different output couplers are used to construct the fiber laser cavity. Self-pulsing behavior was observed under various pumping rates.

The experimental arrangement for observing self-pulsing operation is shown in Fig. 26 [72]. The  $2\ \mu\text{m}$   $\text{Tm}^{3+}$ -doped fiber laser is pumped by a single CW-diode laser, operating TM mode centered at 790 nm, shifting to  $\sim 793\ \text{nm}$  at comparatively higher operating temperature. With this pump source, the maximum power launched into the fiber was near 12 W.

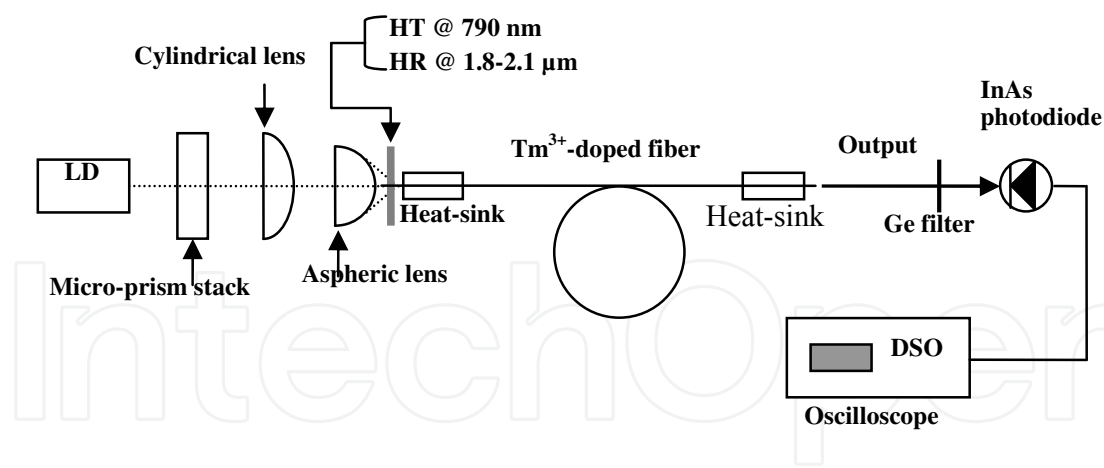


Fig. 26. Experimental arrangement of LD-pumped  $\text{Tm}^{3+}$ -doped fiber laser

The double-clad MM-TDF with  $\sim 10\ \text{m}$  length (Nufern Co.) had a  $30\ \mu\text{m}$  diameter, 0.22 N.A. core doped with  $\text{Tm}^{3+}$  of  $\sim 2\ \text{wt.}\%$  concentration (the  $V$  value is about 9.42 when laser wavelength is of  $\sim 2\ \mu\text{m}$ ). The pure-silica cladding, coated with a low-index polymer, had a  $410\ \mu\text{m}$  diameter and a NA of 0.46. The fiber has an octagon-shape clad, which helps to improve the pump absorption. The fiber ends were perpendicularly cleaved and carefully polished carefully to ensure flatness, so that the loss was minimized.

The laser pumping beam was reshaped first by a micro-prism stack, and then focused into a circular spot of  $\sim 0.5 \times 0.5\ \text{mm}$  diameter with a cylindrical lens and an aspheric lens. The

focused pump beam was launched into the thulium-doped fiber through a dielectric mirror. The pump end of the fiber is butted directly to the dielectric mirror with high reflectivity (>99%) at 1850~2100 nm and high transmission (>97%) at 760~900 nm. The Fabry-Perot laser cavity was formed between the dielectric mirror and the output-end fiber facet (with Fresnel reflection of ~3.55% providing feedback for laser oscillation). Both ends of the fiber were held in metallic heat-sinks, and the remaining fiber was wrapped on a water-cooling metallic drum to prevent possible thermal damage to the fiber.

The threshold pump power of the long fiber laser with the output coupler of the fiber-end facet is about 5.8 W. Various self-pulsing regimes obtained with increasing pump level are shown in Fig. 27 [72]. When the pump power is near the threshold ( $P=6$  W), the laser delivers a regular train of pulses, as shown in Fig. 28(a). The pulse duration is 7.2  $\mu$ s, and the frequency is 42 kHz. When the pump power is increased to  $P=7$  W, the pulse width narrows to 6.5  $\mu$ s and the pulse frequency grows to 63 kHz, as seen in Fig. 28(b). At high pump levels, a second set of pulses began to appear as shown (the arrow point to) in Fig 28(b) and (c). This is due to that the high peak power confined in the fiber core may favor the excitation of a Brillouin backscattered wave, especially in the "high-loss cavity" configuration (high output coupling) [70].

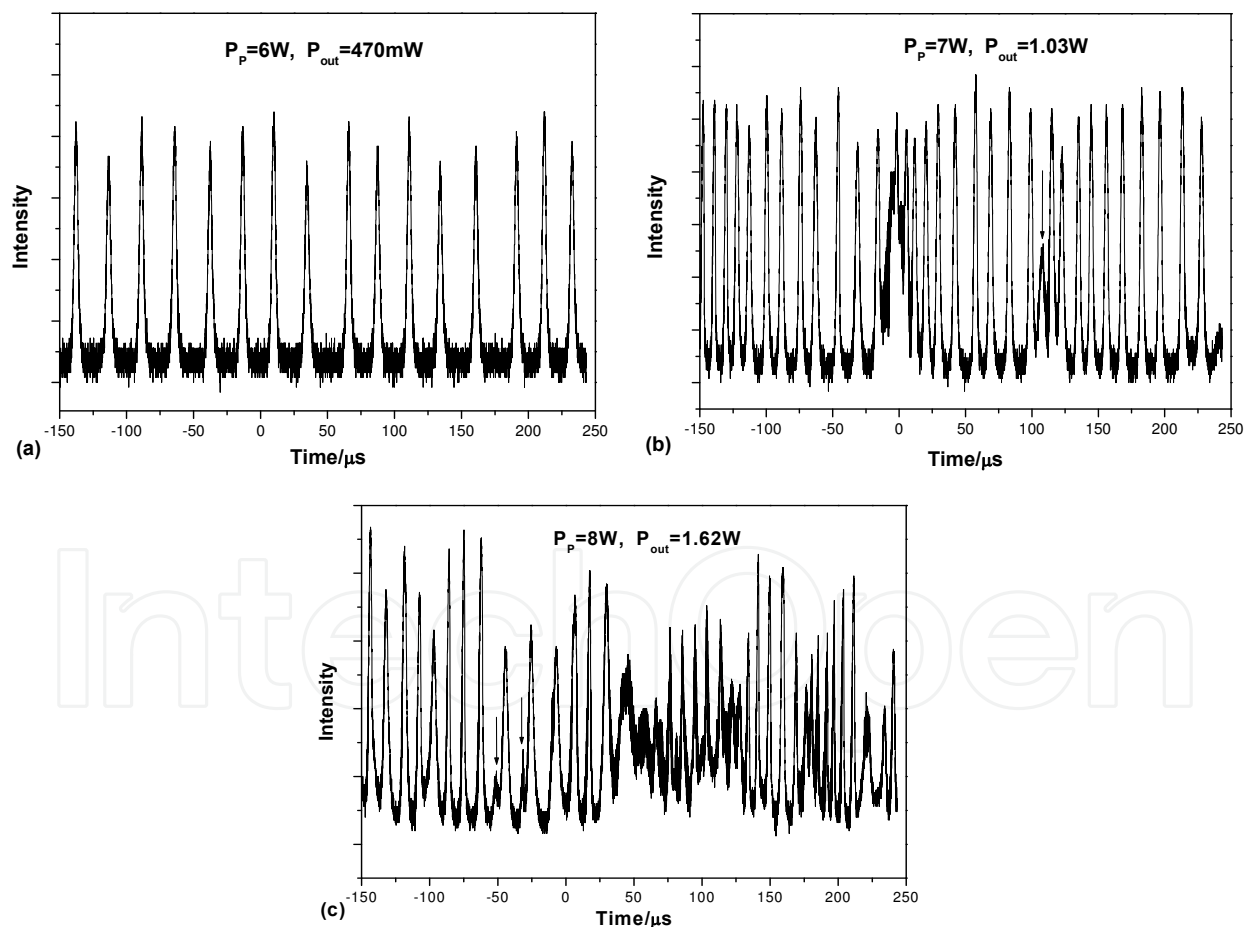


Fig. 27. Output intensity time trace of 10 m fiber laser with end-facet output coupler for (a)  $P_p=6$  W, (b)  $P_p=7$  W, (c)  $P_p=8$  W.

When the pumping level is high enough, the laser output becomes quasi-CW, as shown in Fig. 28 [72]. This result is in agreement with that obtained in previously studies [62, 69]. In the case

of 10 W of pump power, the pulse repetition rate increases to 132 kHz, but the pulse width randomizes. At this time, the laser operates in a similar self mode-locking state [63, 71].

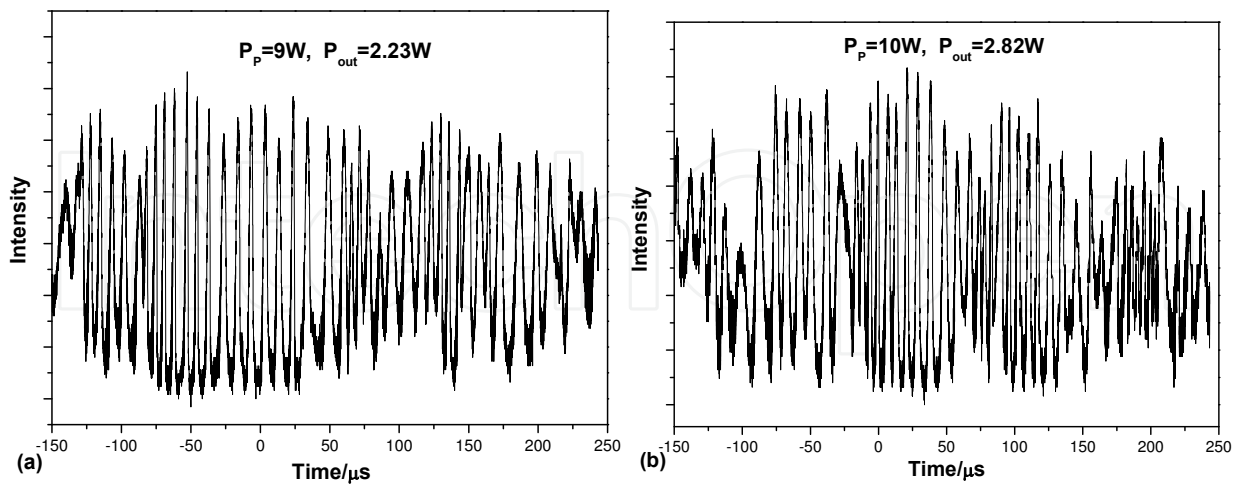


Fig. 28. Quasi-CW operation for pumping power (a)  $P_p=9$  W, (b)  $P_p=10$  W.

With the fiber-end coupler, the pulse width and frequency as functions of pump power are indicated in Fig. 29 [72]. The pulse width decreases, but the pulse repetition rate increases, near linearly with enhanced pump power. At high pump levels, e.g. over 9 W, the pulse width begins saturating. Therefore, it seems hard to derive short pulse duration through self-pulsing in  $Tm^{3+}$ -doped fiber lasers.

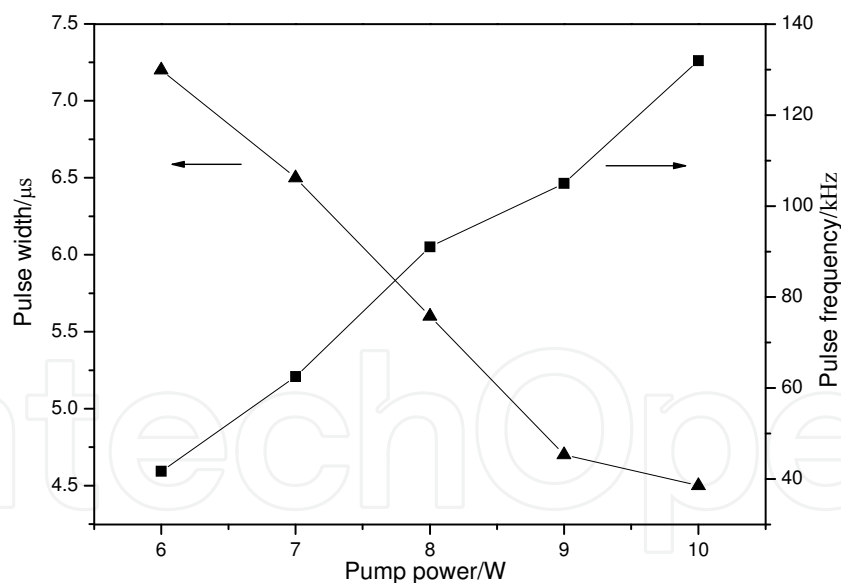


Fig. 29. Pulse width and pulse frequency versus pump power.

When a dielectric mirror with  $T=10\%$  at  $2 \mu m$  is used as the output coupler, the dynamics behavior is somewhat different from that obtained with the fiber-end coupler, as indicated in Fig. 30 [72]. For this cavity configuration, the threshold pump power is about 3 W. Near the threshold, a regular train of pulses is observed, as shown in Fig. 30(a). The pulse duration is around  $18 \mu s$ , and the pulse frequency is about 21 kHz. Increasing the pump power to 4 W, the pulse duration decreases to  $16 \mu s$  and the frequency increases to 37 kHz, respectively. However, when the pump power is further increased to 5 W and 6 W, only the

pulse frequency shows a definite changing trend, becoming higher and higher. The pulse width indicates an indefinite advancing trend: some become broader and some become narrower. The irregularity of the pulse increases significantly with pump power enhanced.

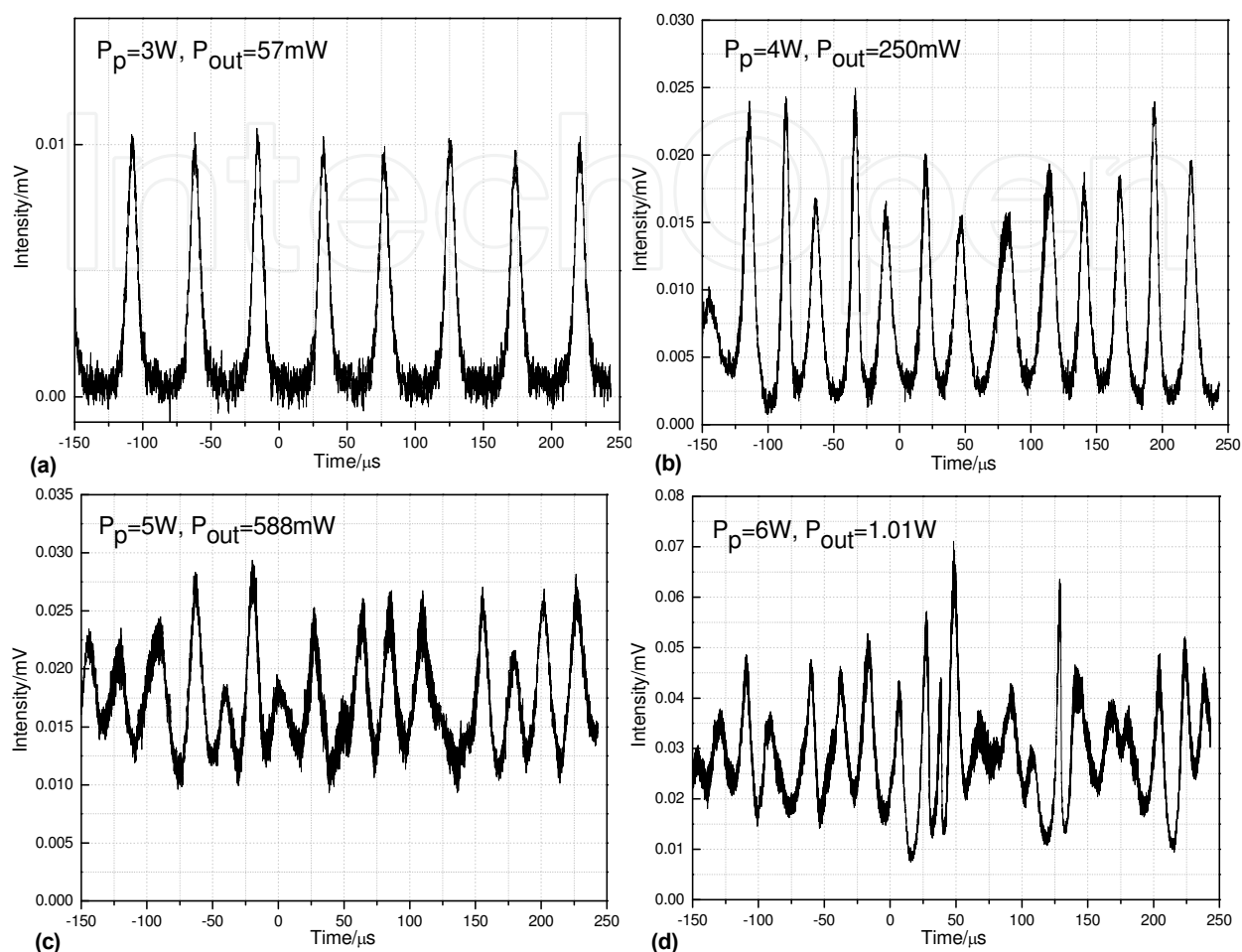


Fig. 30. Output intensity time trace of 10 m fiber laser with 10% output coupler for (a)  $P_p = 3$  W, (b)  $P_p = 4$  W, (c)  $P_p = 5$  W, (d)  $P_p = 6$  W.

When a dielectric mirror with  $T=5\%$  at  $2 \mu\text{m}$  is used as the output coupler, the dynamics behavior is completely different from the previous results, as indicated in Fig. 31 [72]. For this cavity configuration, the threshold pump power is also about 3 W. However, even near the threshold, the pulse train is very irregular, as shown in Fig. 31(a). The pulse duration is around  $23 \mu\text{s}$ , and the pulse frequency is about 28 kHz. Increasing the pump power to 4 W, the laser output becomes near-CW. With 5 W of pump power, the output is completely CW. This clearly demonstrates that the self-pulsing behavior of heavily doped fiber lasers can be suppressed by using low-transmission output couplers.

The dependence of the pulse width and frequency on the output coupler transmission ( $T$ ) is shown in Fig. 32 [72]. The pulse width and pulse frequency were obtained near respective pump threshold. It is clear that the pulse width decreases near linearly with  $T$ . This is because that the pulse width scales similar to the photon cavity lifetime [73]. A laser cavity with a lower  $T$  has a longer photon cavity lifetime due to less output loss, thus has broader pulse duration. The pulse frequency first decreases and then increases with increasing  $T$ . Considering that the threshold pump power is different for different cavities, we

normalized pulse frequency to pump power. As shown in Fig. 32(b), the normalized pulse frequency increases with decreasing  $T$ . When  $T < 10\%$ , the pulse frequency grows sharply, transforming to CW operation.

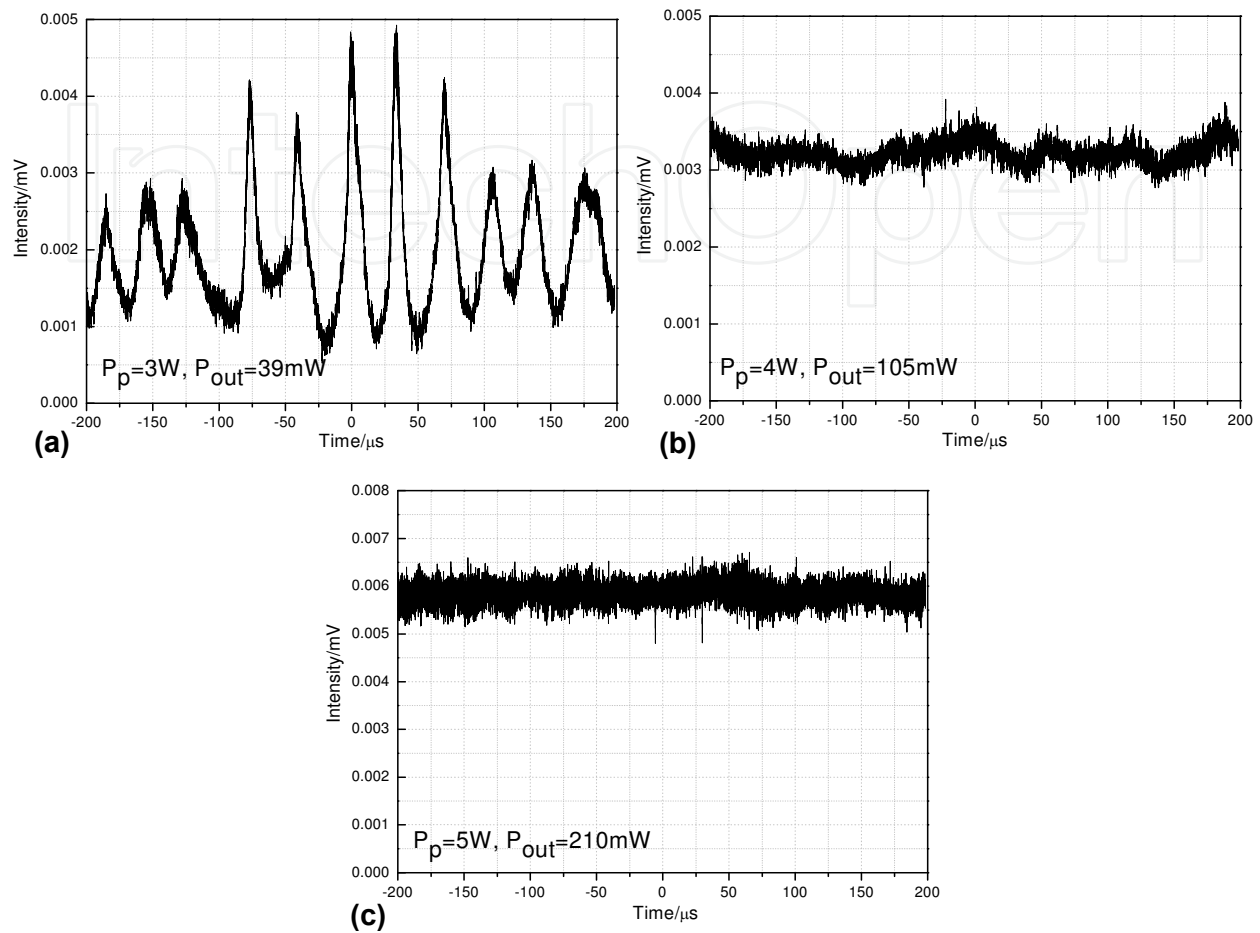


Fig. 31. Output intensity time trace of 10 m fiber laser with 5% output coupler for (a)  $P_p = 3$  W, (b)  $P_p = 4$  W, (c)  $P_p = 5$  W.

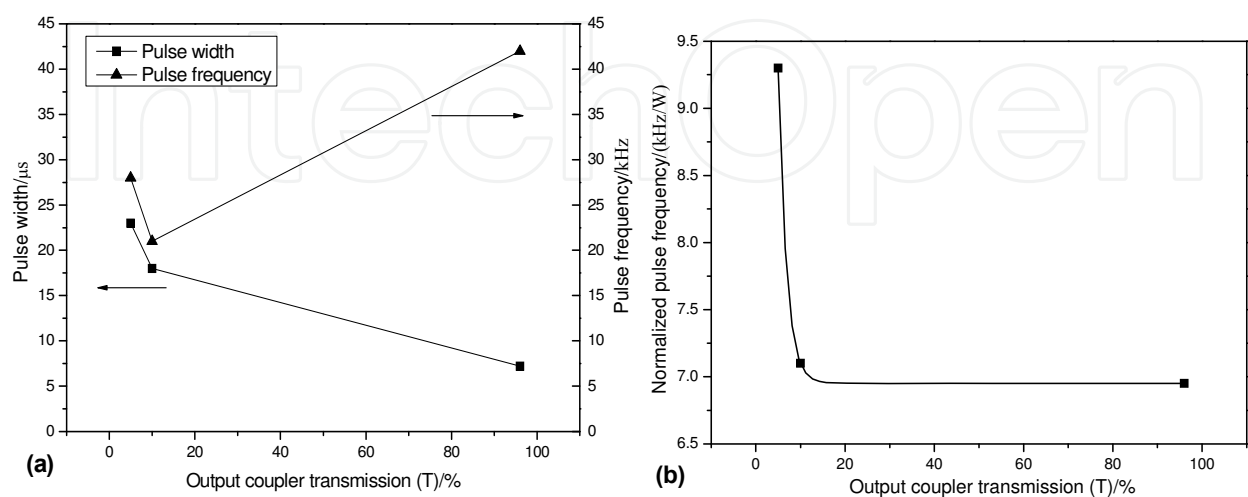


Fig. 32. Output coupler transmission dependence of (a) pulse width and frequency, and (b) normalized pulse frequency near pump threshold.

### 3. Several possible loss mechanisms for self-pulsing formation

In heavily Tm<sup>3+</sup>-doped fibers, the distance between Tm<sup>3+</sup> ions decreases, leading to the formation of ion pairs or clusters, this in turn strengthens the interaction between ions. Such interactions occur among the ions doped in fibers, leading to several energy-transfer processes, one of which is dubbed as the up-conversion process [74].

For Tm<sup>3+</sup>-doped fiber lasers, as shown in Fig. 35, the pump light at 790 nm excites the ions from <sup>3</sup>H<sub>6</sub> state to <sup>3</sup>H<sub>4</sub> state, which quickly relaxes to the upper laser level <sup>3</sup>F<sub>4</sub>. In Tm<sup>3+</sup>-doped fibers, the up-conversion processes include <sup>3</sup>F<sub>4</sub>, <sup>3</sup>F<sub>4</sub>→<sup>3</sup>H<sub>4</sub>, <sup>3</sup>H<sub>6</sub> and <sup>3</sup>F<sub>4</sub>, <sup>3</sup>H<sub>5</sub>→<sup>3</sup>H<sub>6</sub>, <sup>3</sup>F<sub>3</sub>, as shown in Fig 32 (1) and (2). This effect results in one ground ion and one up-converted ion, which quickly relaxes to the <sup>3</sup>F<sub>4</sub> level. Consequently, this energy transferring process losses one potential stimulated photon. High Tm<sup>3+</sup> ion doping concentration leads to high ion-pair and ion-cluster concentration, thus induces large quenching effect.

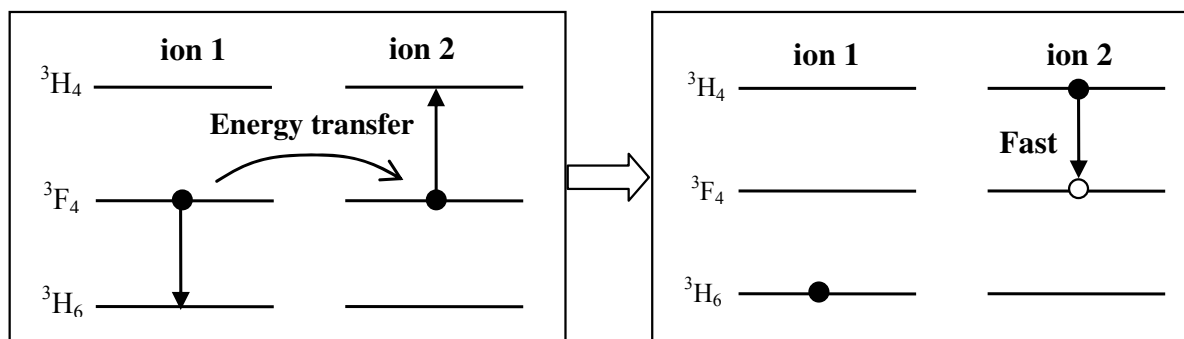


Fig. 33 (1). Up-conversion energy transfer process between the same energy levels in Tm<sup>3+</sup>-doped fiber lasers

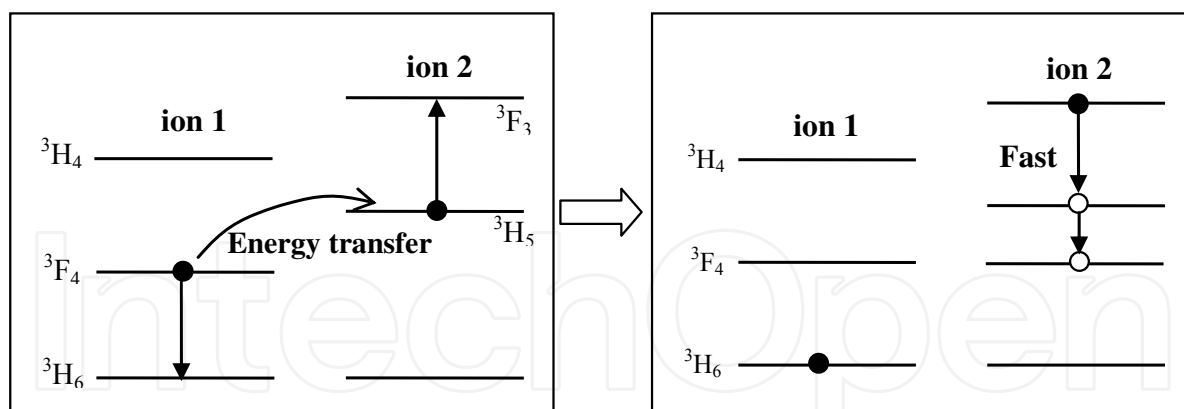


Fig. 33 (2). Up-conversion energy transfer process between different energy levels in Tm<sup>3+</sup>-doped fiber lasers

Another photon loss mechanism may be due to laser self-absorption (ground-state absorption) through the <sup>3</sup>F<sub>4</sub>, <sup>3</sup>H<sub>6</sub>→<sup>3</sup>H<sub>6</sub>, <sup>3</sup>F<sub>4</sub> energy transfer process, as shown in Fig. 34. When one excited ion and a ground-state ion stay near enough, the excited ion will transfer its energy to the latter and relaxes to ground state, while the latter ion will absorb the energy and transits to higher levels. When such process occurs repeatedly between a large number of ions, the energy migration process happens, acting as a loss mechanism. These above mentioned energy-transfer processes all have the possibility to act as saturable absorbers.

In the  $\text{Tm}^{3+}$ -doped fiber laser, self-pulsing is a commonly observed phenomenon, which is considered as an output instability. The true mechanism leading to the formation of this interesting phenomenon is still unclear. In the following section, the origin of self-pulsing in the  $\text{Tm}^{3+}$ -doped fiber laser will be discussed.

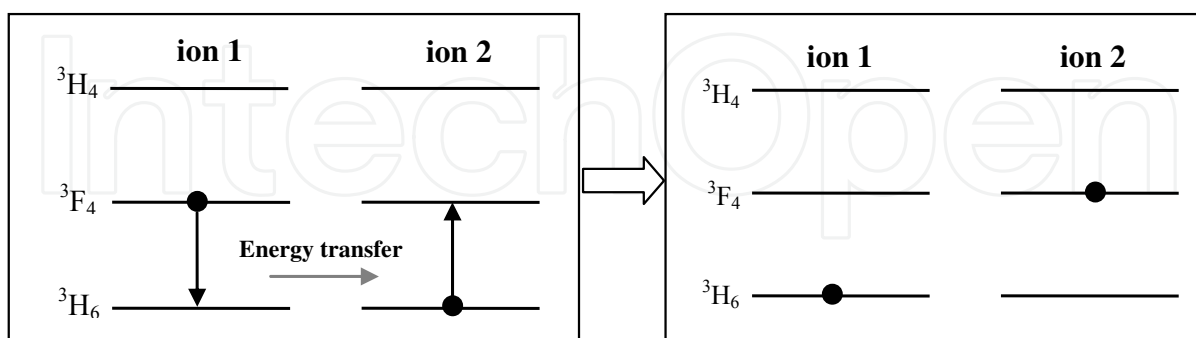


Fig. 34. schematic diagram of self-absorption process in heavily  $\text{Tm}^{3+}$ -doped fiber lasers

## 4.2 Theoretical modeling and simulation of Self-pulsing in $\text{Tm}^{3+}$ -doped fiber laser

### 4.2.1 Effects of Excited-state Absorption on Self-pulsing in $\text{Tm}^{3+}$ -doped Fiber Lasers

#### Introduction

Followed various experimental observations, many mechanisms have been proposed to explain the origin of self-pulsing in  $\text{Tm}^{3+}$ -doped fiber lasers. Some of them are controversial, and consistent agreement has not been satisfied. The in-depth understanding for self-pulsing formation in  $\text{Tm}^{3+}$ -doped fiber lasers is required.

In this section, mechanisms of self-pulsing in  $\text{Tm}^{3+}$ -doped fiber lasers are theoretically investigated by taking into account several important energy-transfer processes. A simplified model is constructed to explain the self-pulsing characteristics in  $\text{Tm}^{3+}$ -doped fiber lasers.

#### Numerical model

The four lowest energy manifolds of trivalent thulium ions are sketched in Fig. 35. The pump transition, laser transition, and different energy transfer mechanisms including cross relaxation, energy transfer up-conversion and spontaneous decay are indicated. The energy manifolds were numbered 1-4 and these denominations will be used throughout this paper. The rate equations for the local population densities of these levels are as follows [75-77]:

$$\begin{aligned} \frac{dN_4}{dt} = & R(z,t)(N_1 - N_4) - k_{4212}N_1N_4 \\ & + k_{2124}N_2^2 - \frac{N_4}{\tau_4} + \sigma_{sa}c\phi(z,t)(N_3 - N_4) \end{aligned} \quad (1)$$

$$\begin{aligned} \frac{dN_3}{dt} = & k_{2123}N_2^2 + \beta_{43} \frac{N_4}{\tau_4} - \frac{N_3}{\tau_3} \\ & - \sigma_{sa}c\phi(z,t)(N_3 - N_4) \end{aligned} \quad (2)$$

$$\begin{aligned} \frac{dN_2}{dt} = & 2k_{4212}N_1N_4 - 2(k_{2124} + k_{2123})N_2^2 + \beta_{42} \frac{N_4}{\tau_4} \\ & + \beta_{32} \frac{N_3}{\tau_3} - \frac{N_2}{\tau_2} - c\phi(z,t)\sigma_e \left( N_2 - \frac{g_2}{g_1} N_1 \right) , \\ & + c\phi(z,t)\sigma_{ga}(N_1 - N_2) \end{aligned} \quad (3)$$

$$\begin{aligned} \frac{d\phi}{dt} = & c\phi(z,t)\sigma_e \left( N_2 - \frac{g_2}{g_1} N_1 \right) + m \frac{N_2}{\tau_2} , \\ & - \sigma_{ga}c\phi(z,t)(N_1 - N_2) - r_c\phi(z,t) \end{aligned} \quad (4)$$

$$N_1 = N_{tot} - N_2 - N_3 - N_4 , \quad (5)$$

$$R(z,t) = R(0,t) \cdot e^{-\alpha_p \cdot z} , \quad (6)$$

where  $N_i$  are the populations of four energy manifolds  ${}^3H_6$ ,  ${}^3F_4$ ,  ${}^3H_5$ ,  ${}^3H_4$ , and  $N_{tot}$  is the total density of Tm<sup>3+</sup> ions.  $R$  is the pump rate, and  $\phi$  is the average photon density of the laser field.  $\sigma_e$  is the stimulated emission cross section of signal light,  $\sigma_{ga}$  and  $\sigma_{sa}$  are the absorption cross sections of ground state and excited state, respectively. Where  $g_1$  and  $g_2$  are the degeneracies of the upper and lower laser levels,  $\tau_i$  is the level lifetimes of four manifolds, and  $r_c$  is the signal photon decay rate.  $\beta_{ij}$  are branch ratios from the  $i$  to  $j$  level,  $m$  is the ratio of laser modes to total spontaneous emission modes. The coefficients  $k_{ijkl}$  describe the energy transfer processes:  $k_{4212}$  and  $k_{3212}$  are the cross relaxation constants, and  $k_{2124}$  and  $k_{2123}$  are the up-conversion constants. The coefficient  $\alpha_p$  is the pump absorption of the fiber, which is calculated by  $\alpha_p = \sigma_{ap} \cdot N_{tot}$ , where  $\sigma_{ap}$  is the pump absorption cross section. In the simulation, the phonon-assisted ESA process of  ${}^3F_4$ ,  ${}^3H_5 \rightarrow {}^3H_6$ ,  ${}^3H_4$  and ground-state absorption (GSA) through the  ${}^3F_4$ ,  ${}^3H_5 \rightarrow {}^3H_6$ ,  ${}^3F_3$  energy transfer process are considered. The corresponding parameters for Tm<sup>3+</sup> ions doped in silica host are listed in Table 1 [12, 77-79].

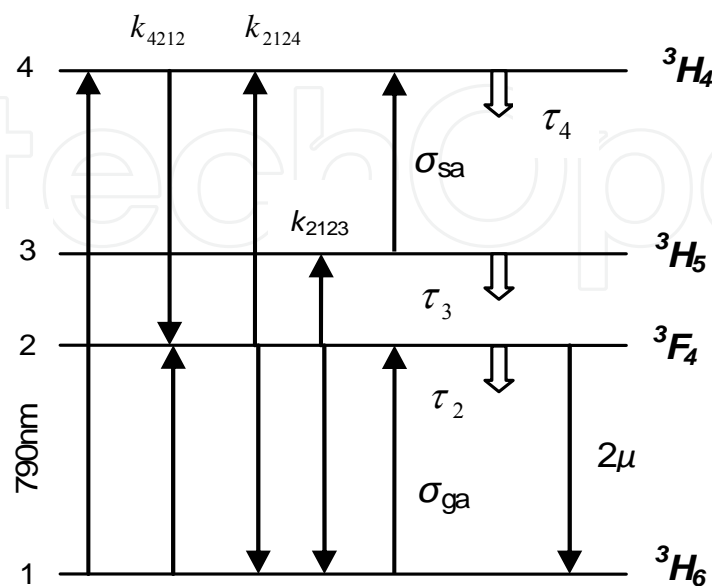


Fig. 35. Schematic of the four lowest energy manifolds in Tm<sup>3+</sup> ions.

| Parameter     | numerical value   |
|---------------|---|
| $k_{4212}$    | $1.8 \times 10^{-16} \text{ cm}^3\text{s}^{-1}$   |
| $k_{2123}$    | $1.5 \times 10^{-18} \text{ cm}^3\text{s}^{-1}$   |
| $k_{2124}$    | $1.5 \times 10^{-17} \text{ cm}^3\text{s}^{-1}$   |
| $\tau_i$      | $\tau_4 = 14.2 \mu\text{s}$<br>$\tau_3 = 0.007 \mu\text{s}$<br>$\tau_2 = 340 \mu\text{s}$ |
| $\beta_{ij}$  | $\beta_{43} = 0.57$<br>$\beta_{42} = 0.051$<br>$\beta_{32} \approx 1$                     |
| $\sigma_e$    | $2.5 \times 10^{-21} \text{ cm}^2$  |
| $\sigma_{sa}$ | Variable ( $4 \times 10^{-21} \text{ cm}^2$ )   |
| $\sigma_{ga}$ | variable  |
| $m$           | $8 \times 10^{-7}$  |
| $r_c$         | $9.7 \times 10^6 \text{ s}^{-1}$  |
| $\sigma_{ap}$ | $1 \times 10^{-20} \text{ cm}^2$  |
| $N_{tot}$     | $1.37 \times 10^{20} \text{ cm}^{-3}$   |

Table 1. The parameters in the rate equations

*Theoretical calculation*

As can be seen from table 1, the lifetime of level  $N_3$  (0.007  $\mu\text{s}$ ) is much shorter than that of level  $N_2$  (340  $\mu\text{s}$ ), we can simplify the energy manifolds to three levels. In the above rate equations, we assume the relaxation from  $N_3$  to  $N_2$  is very fast so that  $N_3 \sim 0$ . Let  $N_{23} = N_2 + N_3$  and add Eq. (2) and (3), we get

$$\frac{dN_{23}}{dt} = 2k_{4212}N_1N_4 - (2k_{2124} + k_{2123})N_{23}^2 + (\beta_{43} + \beta_{42})\frac{N_4}{\tau_4} - \frac{N_{23}}{\tau_2} - c\phi\left[\sigma_e\left(N_{23} - \frac{g_2}{g_1}N_1\right) + \sigma_{sa}(N_{23} - N_4) - \sigma_{ga}(N_1 - N_{23})\right] \quad (7)$$

By replaced Eq. (2) and (3) with Eq. (7), the rate equations Eq. (1–6) are simplified to a three-level system. All important energy transfer processes, ESA, and GSA are kept in the simplified rate equations. The simplified model is sufficiently to investigate the dynamic characteristics involved these processes.

Suppose the laser operating in the steady-state (or CW, continuous-wave) regime, the rate of change of the photon density and population must be equal to zero,

$$\frac{d\phi}{dt} = 0, \quad (8)$$

$$\frac{dN_i}{dt} = 0. \quad (9)$$

Neglecting GSA, the rate equations (1), (4) and (7) lead to

$$R(N_1 - N_4) - k_{4212}N_1N_4 + k_{2124}N_{23}^2 - \frac{N_4}{\tau_4} + \phi c \sigma_{sa}(N_{23} - N_4) = 0 \quad (10)$$

$$c \phi \sigma_e(N_{23} - \frac{g_2}{g_1}N_1) + m \frac{N_{23}}{\tau_2} - r_c \phi = 0, \quad (11)$$

$$2k_{4212}N_1N_4 - (2k_{2124} + k_{2123})N_{23}^2 + (\beta_{42} + \beta_{43})\frac{N_4}{\tau_4} - \frac{N_{23}}{\tau_2} - \phi[c \sigma_e(N_{23} - \frac{g_2}{g_1}N_1) + c \sigma_{sa}(N_{23} - N_4)] = 0 \quad (12)$$

From Eq. (10-12) and Eq. (5), we can solve  $\phi$ ,  $N_1$  and  $N_{23}$  with the prerequisite that  $\phi > 0$ ,  $N_{\text{tot}} > N_1$  and  $N_{23} > 0$ .

Solving the equations, we find that there is a certain range of pump rate  $R$  (defined as  $\Delta R$ ), where the steady-state solution for the rate equations can not be found, as shown in Fig. 36 [80]. In this range, the laser will not be operated in the continuous-wave state. With increase or decrease of pump power out of the range  $\Delta R$ , the operation of Tm<sup>3+</sup>-doped fiber lasers undergoes phase transition (changes to CW operation). Such a case is in good agreement with the experimental observation in the self-pulsing operation in Tm<sup>3+</sup>-doped fiber lasers.

The non-CW range  $\Delta R$  is calculated as varying the ESA cross section and the cross relaxation parameter  $k_{4212}$ . The variation of  $\Delta R$  as a function of the ESA cross section is shown in Fig. 37 [80]. It is clear that the ESA cross section has an important impact on the self-pulsing operation of Tm<sup>3+</sup>-doped fiber lasers. The non-CW range  $\Delta R$  increases with the larger ESA cross section, especially, increases exponentially when the ESA cross section is larger than  $3 \times 10^{-21}$  cm<sup>2</sup>. When the ESA cross section is less than  $1 \times 10^{-21}$  cm<sup>2</sup>, the range  $\Delta R$  shrinks sharply, and goes to zero with a small value of ESA cross section. The CW operation of Tm<sup>3+</sup>-doped fiber lasers can sustain for any pump rate when the ESA cross section is sufficiently small. On the other hand, with a larger ESA cross section, the CW operation will always be broken in certain pump range.

The influence of the cross relaxation on the self-pulsing of Tm<sup>3+</sup>-doped fiber lasers is evaluated. The non-CW range  $\Delta R$  is calculated as a function of cross relaxation strength  $k_{4212}$  as shown in Fig. 38 [80]. Large values of  $k_{4212}$  will obviously enlarge the range  $\Delta R$ . However, even when the cross relaxation  $k_{4212}$  is decreased to zero, the breaking of CW operation still preserves, implying that the cross relaxation energy-transfer process is not the key process in the formation of self-pulsing in Tm<sup>3+</sup>-doped fiber lasers.

In order to investigate exactly the revolution of the photon density in Tm<sup>3+</sup>-doped fiber lasers, numerical simulation based on complete rate equations Eq. (1-6) is carried out in the following section.

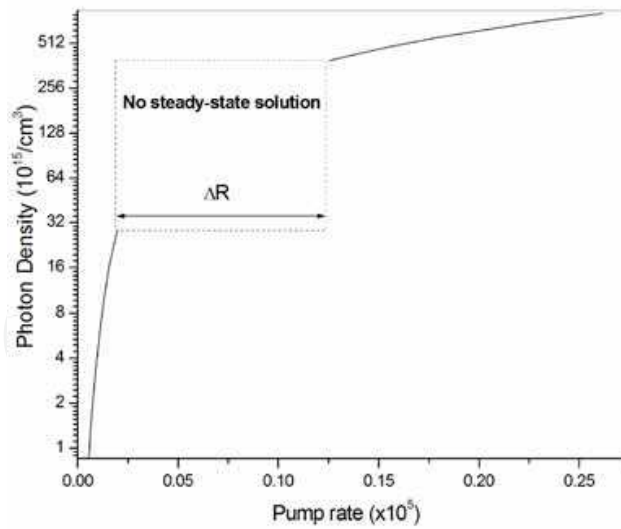


Fig. 36. Photon density as a function of pump rate  $R$ .

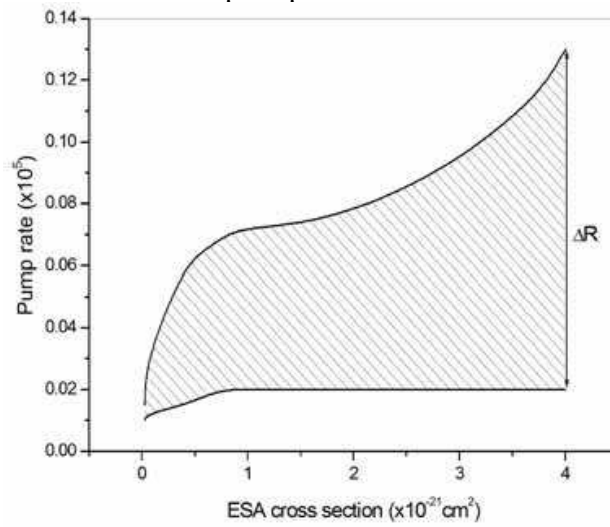


Fig. 37. The non-CW pump range  $\Delta R$  as a function of the ESA cross section.

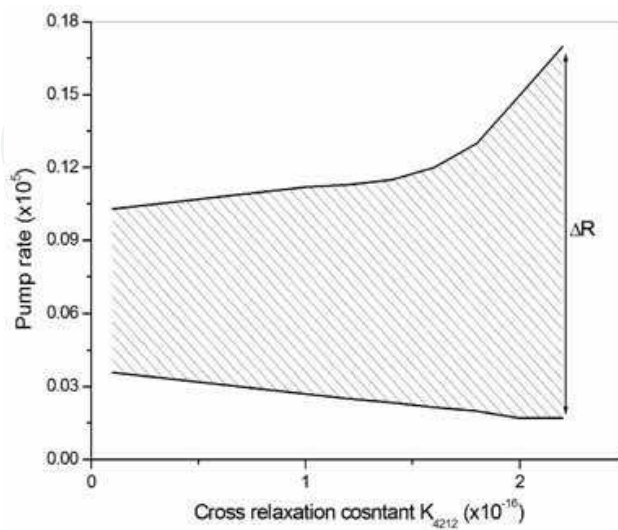


Fig. 38. The non-CW pump range  $\Delta R$  as a function of the cross relaxation strength.

### Simulation results

In order to compare with our experiments, the fiber laser is made up of a 10-m long Tm<sup>3+</sup>-doped silica fiber with the doping concentration of ~2 wt.%. One fiber end is attached with a dichroic mirror, which is high reflective ( $R=100\%$ ) at laser wavelength and anti-reflective at pump wavelength. Another fiber-end facet is used as the output coupler with signal light transmission of  $T\sim 96\%$ . The pump light is coupled into fiber through the dichroic mirror and the pump rate is set to be  $8\times 10^3\text{ cm}^{-3}\text{s}^{-1}$ .

In the simulation, the fiber is divided into 100 gain segments. The coupled rate equations are solved in every segment sequentially. The output of previous segment is used as the input of the next segment. The photon intensity in the last segment transmitted through the fiber end is assumed to be the laser output intensity. The returned light is used as the input for the next calculation cycle.

Four energy-transfer processes: cross relaxation, energy transfer up-conversion, GSA and ESA are calculated separately to analyze their influence on the formation of self-pulsing.

#### A. Cross relaxation

In this sub-section, only the cross relaxation process is taken into account and the processes of energy-transfer up-conversion, GSA and ESA are all neglected. The impact of cross relaxation is evaluated by varying the value of the parameter  $k_{4212}$ . The simulation results are shown in Fig. 39 [80]. Stable CW laser operation preserves over a very large region of  $k_{4212}$  from  $1.8\times 10^{-20}$  to  $1.8\times 10^{-12}\text{ cm}^3\text{s}^{-1}$ . Further decreasing or increasing the cross relaxation strength does not change the nature of the stable CW laser operation. Clearly, the cross relaxation process is not the determinate process leading to self-pulsing formation. With the increase of  $k_{4212}$ , the decay of the laser relaxation oscillation will be lengthened, and the laser intensity be increased. A strong cross relaxation parameter may be helpful for improving the slope efficiency of heavily-doped Tm<sup>3+</sup>-doped fiber lasers.

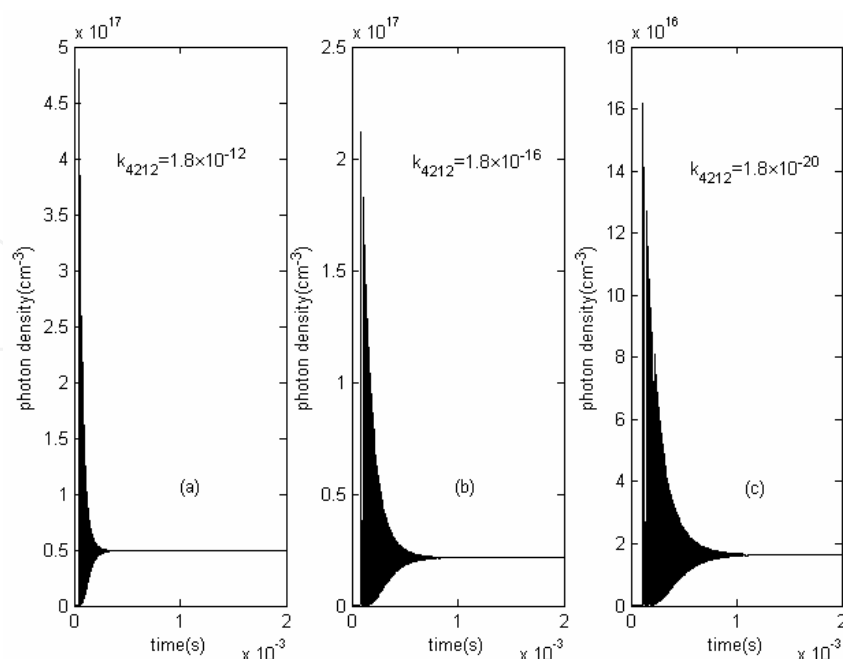


Fig. 39. Laser photon density dynamics characteristics with different cross-relaxation strength  $k_{4212}$ .

### B. Energy-transfer up-conversion process – $k_{2123}$ and $k_{2124}$

In this sub-section, the energy-transfer up-conversion process  ${}^3F_4, {}^3F_4 \rightarrow {}^3H_6, {}^3H_5$  ( $k_{2123}$ ) and  ${}^3F_4, {}^3F_4 \rightarrow {}^3H_6, {}^3H_4$  ( $k_{2124}$ ) are taken into account. The simulation results are shown in Fig. 40 and 41 [80].

The behaviors of the parameters  $k_{2123}$  and  $k_{2124}$  are very similar. The up-conversion processes  ${}^3F_4, {}^3F_4 \rightarrow {}^3H_6, {}^3H_5$  or  ${}^3F_4, {}^3F_4 \rightarrow {}^3H_6, {}^3H_4$  consume the population inversion. When the energy-transfer up-conversion is too strong, *i.e.*,  $k_{2123} > 1.5 \times 10^{-17}$  or  $k_{2124} > 1.5 \times 10^{-16} \text{ cm}^3\text{s}^{-1}$ , the laser

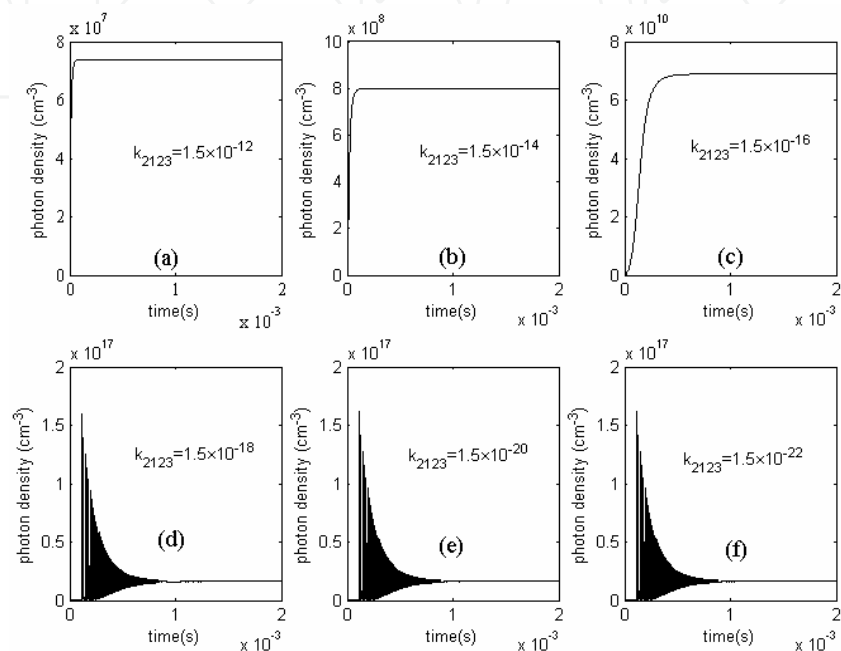


Fig. 40. Laser photon density dynamics characteristics with different energy-transfer up-conversion strength  $k_{2123}$ .

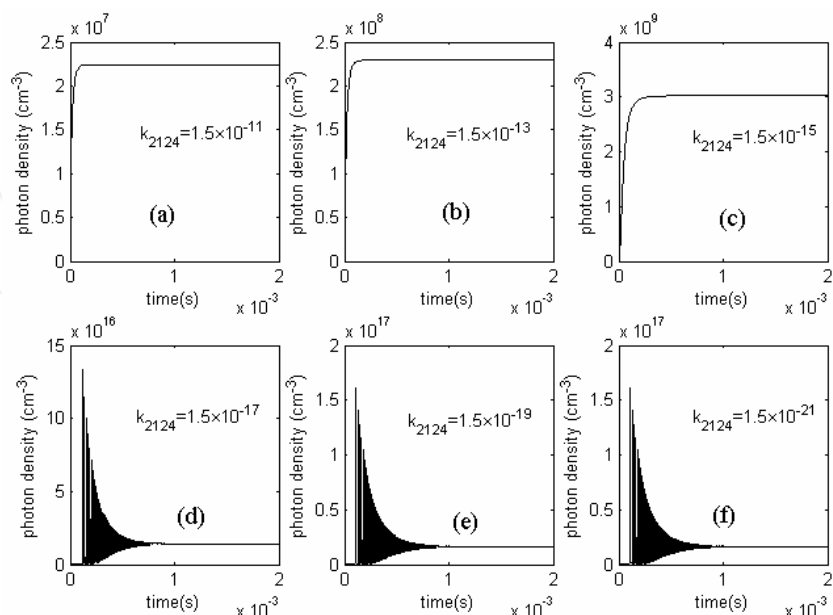


Fig. 41. Laser photon density dynamics characteristics with different energy-transfer up-conversion strength  $k_{2124}$ .

relaxation oscillation is suppressed when the pump rate is  $8 \times 10^3 \text{ cm}^{-3}\text{s}^{-1}$ , as shown in Fig. 40(a)-(c) and 41(a)-(c). The photon density is clamped in a very low level. The laser threshold is run up by the stronger up-conversion.

When the parameters  $k_{2123} < 1.5 \times 10^{-18}$  or  $k_{2124} < 1.5 \times 10^{-17} \text{ cm}^3\text{s}^{-1}$ , the laser relaxation oscillation occurs again. The smaller the parameters are, the longer the relaxation oscillation suspends. No matter which values of the parameters (from  $1.5 \times 10^{-6} \text{ cm}^3\text{s}^{-1}$  to zero) are chosen, no self-pulsing phenomenon is observed. The up-conversion process does not directly connect to the self-pulsing operation in Tm<sup>3+</sup>-doped fiber lasers.

In the practical Tm<sup>3+</sup>-doped system, the values of  $k_{2123}$  and  $k_{2124}$  are around  $10^{-17}$  -  $10^{-18} \text{ cm}^3\text{s}^{-1}$ . The main influence of up-conversion is increasing the laser threshold.

### C. Ground-state absorption (GSA)

The GSA is also called as the re-absorption in the Tm<sup>3+</sup>-doped fiber lasers because the laser will be re-absorbed by the ions in the ground state when it propagates along the fiber. The GSA looks like the saturable absorption at the first sight, and had been thought as a possible mechanism for the self-pulsing formation. However, because the photon absorbed by the GSA will be re-emitted back, the laser can not be switched off by the GSA. In such a situation, it is impossible to form the self-pulsing by the GSA.

The GSA process  ${}^3H_6 \rightarrow {}^3F_4$  can be thought as a reverse process of the laser transition  ${}^3H_6 \rightarrow {}^3F_4$ . The photon resonates between the levels  ${}^3H_6$  and  ${}^3F_4$  back and forth, which effectively extends the lifetime of  $N_2$  ( ${}^3F_4$ ). Consequently, the laser threshold is lowered with a relative large GSA cross section.

In Fig. 42 [80], the revolution of photon density is plotted for various GSA cross section  $\sigma_{ga}$ . Obviously, the laser can generate only when the GSA cross section  $\sigma_{ga}$  is less than the emission cross section  $\sigma_e$ . As the GSA cross section  $\sigma_{ga}$  is taken the value from  $1 \times 10^{-21}$  to  $1 \times 10^{-23} \text{ cm}^2$ , stable CW operation always occurs after the relaxation oscillation. The final photon density decreases with the smaller GSA cross section  $\sigma_{ga}$ .

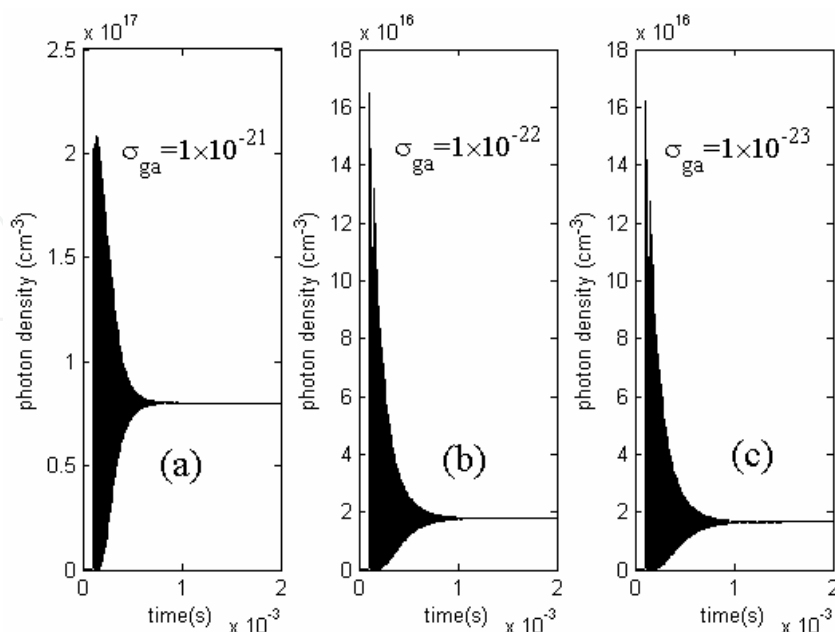


Fig. 42. Laser photon density dynamics characteristics with different ground-state absorption strength  $\sigma_{ga}$  ( $\text{cm}^2$ ).

#### D. Excited-state absorption (ESA)

As the theoretical analysis in the previous section, the ESA is the key process in the self-pulsing operation of  $\text{Tm}^{3+}$ -doped fiber lasers. In this sub-section, the cross relaxation  $k_{4212}$ , up-conversion  $k_{2123}$  and  $k_{2124}$ , and GSA cross section  $\sigma_{ga}$  are set to be zero, and only the ESA process  ${}^3H_5 \rightarrow {}^3H_4$  is taken into account. The evolution of photon densities for various ESA cross sections  $\sigma_{sa}$  are shown in Fig. 43 [80]. When the ESA cross section  $\sigma_{sa}$  is chosen in the range from  $4 \times 10^{-21}$  to  $4 \times 10^{-19}$   $\text{cm}^2$ , it is clear to observe stable, regular self-pulsed trains. This verifies the theoretical predication that the ESA process is the key reason leading to the self-pulsing dynamics in the  $\text{Tm}^{3+}$ -doped fiber lasers. The pulse width is about several microseconds and the pulse frequency is tens of kilohertz, showing excellent agreement with the previous experimental results.

When the ESA cross section  $\sigma_{sa}$  is much lower, the ESA is too weak to hinder accumulation of the population in the level  ${}^3H_5$  ( $N_3$ ), and CW operation occurs after relative long relaxation oscillation as shown in Fig. 43 (c) and (d). With the increase of the ESA cross section  $\sigma_{sa}$ , the decay time of the relaxation oscillation becomes longer and longer, and finally, the relaxation oscillation evolves to a stable self-pulsed train. On the other hand, when the ESA cross section is very large, a great number of population in the level  ${}^3H_5$  ( $N_3$ ) is depleted by the ESA. Consequently, the population inversion in the level  ${}^3F_4$  ( $N_2$ ) is not enough to sustain the laser oscillation.

As shown in Fig. 43 (a) and (b), the self-pulse repetition rate and pulse width are reduced as increase of the ESA cross section. Although the self-pulsing is induced by the ESA, the pulse properties are influenced by the cross relaxation, up-conversion, and GSA.

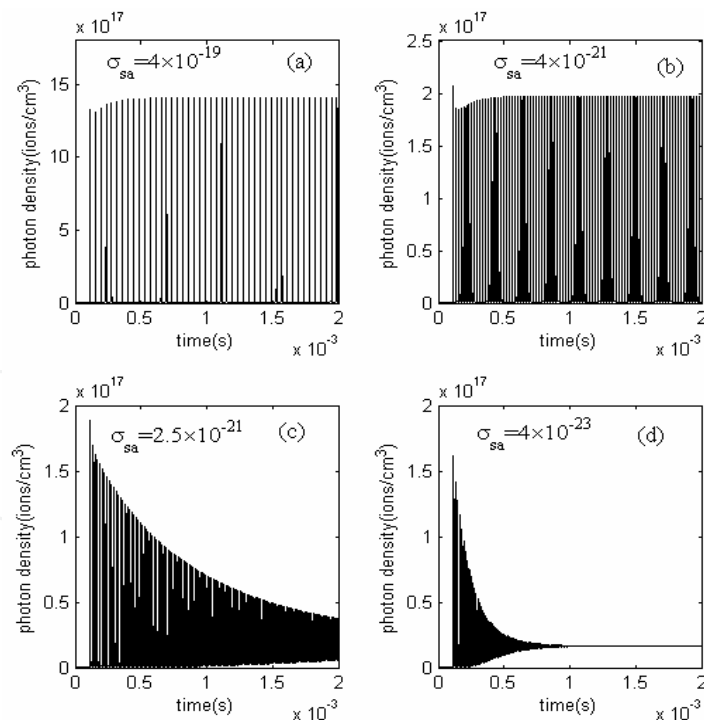


Fig. 43. Laser photon density dynamics characteristics with different ESA strength  $\sigma_{sa}$  ( $\text{cm}^2$ ).

#### Conclusion

Based on theoretical analysis and numerical simulation, the ESA (excited-state absorption) process is clarified as the key reason leading to the formation of self-pulsing in  $\text{Tm}^{3+}$ -doped

fiber lasers. Increasing the ESA cross section can reduce both the self-pulse frequency and pulse width. With increase of the pump rate, the operation of Tm<sup>3+</sup>-doped fiber lasers will undergo phase transition (CW to self-pulsing, and then back to CW). The laser threshold and efficiency are influenced by the cross relaxation, up-conversion and the GSA.

#### 4.2.2. Theoretical study on self-pulsing in Tm<sup>3+</sup>-doped fiber lasers

##### 1. Introduction

In the previous section, explicit theoretical analysis has proved that the ESA process is responsible for self-pulsing formation in fiber lasers [80]. In this section, the self-pulsing characteristics in Tm<sup>3+</sup>-doped fiber lasers are theoretically investigated by changing several key parameters—the output coupling, pump rate and active ion doping concentration. Besides, how to optimize these corresponding parameters for obtaining expected laser pulse frequency and pulse width, and potential applications of self-pulsing are discussed.

##### 2. Simulation results

The simulation process and the adopted rate equations and corresponding parameters are described in the previous section.

##### 2.1. Influence of output coupling T on the self-pulsing characteristics

In this section, the ESA cross section is kept at  $4 \times 10^{-21}$  cm<sup>2</sup>, and the impact of the output coupling strength on the self-pulsing characteristics is simulated. It is found that too low pump rate will not lead to self-pulsing with any output coupling T. The minimum pump rate required to initiate self-pulsing operation is defined as self-pulsing pump threshold  $R_{\text{threP}}$ . The self-pulsing threshold  $R_{\text{threP}}$  as a function of output coupling is shown in Fig. 44 (a) [81]. The self-pulsing threshold increases first moderately and then quickly with the output coupling. This is due to that high output coupling causes high cavity loss. After

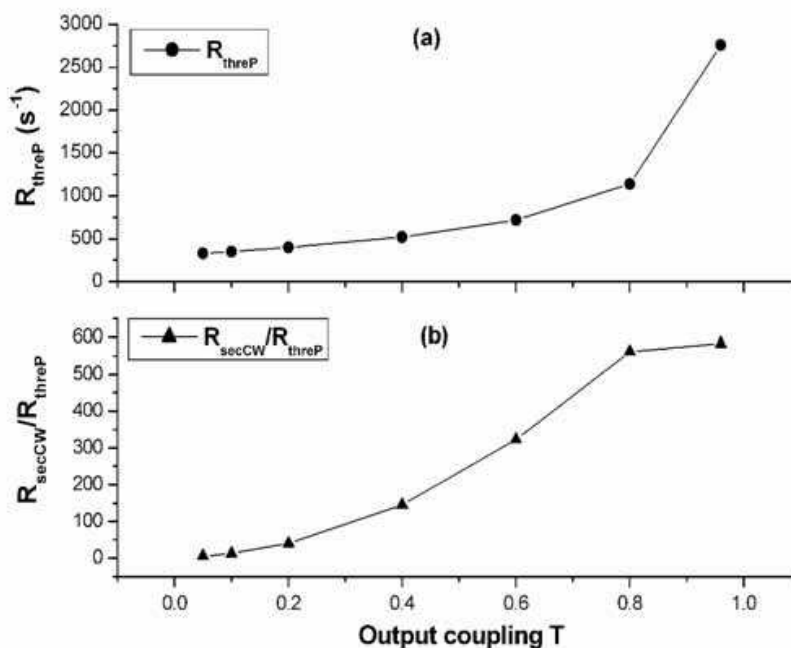


Fig. 44. Self-pulsing threshold (a) and the ratio of second CW threshold to self-pulsing threshold (b) as a function of output coupling.

being initiated, the self-pulsing state will preserve stably for a certain pump range. Further improving the pump rate, self-pulsing operation will be transferred to continuous-wave (CW) state. Because the laser operates in CW mode both before and after the occurrence of self-pulsing, the pump rate that renders the laser to CW mode after the self-pulsing regime is defined as the second CW threshold  $R_{\text{secCW}}$ . The ratio of the second CW threshold ( $R_{\text{secCW}}$ ) to the self-pulsing threshold ( $R_{\text{threP}}$ ) will indicate the capability of a fixed output coupling to support self-pulsing operation in the fiber laser. This threshold ratio  $R_{\text{secCW}}/R_{\text{threP}}$  as a function of output coupling is shown in Fig. 44 (b) [81]. It is clear that the ratio ( $R_{\text{secCW}}/R_{\text{threP}}$ ) increases near linearly with output coupling. Therefore, in order to achieve self-pulsing operation over a large power range, high output-coupling cavity configurations should be adopted. Stable operation of self-pulsing over a large power range will offer a new alternative to obtain pulsed laser output. Therefore, self-pulsing modulation has the potential to become a novel Q-switching technique.

Fig. 45 shows the numerically calculated self-pulsing train of the  $\text{Tm}^{3+}$ -doped fiber laser with output coupling of  $T=96\%$  at the threshold pump rate [81]. This regular self-pulsing train has a pulse width and repetition rate of  $7.68 \mu\text{s}$  and  $16.89 \text{ kHz}$ , respectively. Self-pulsing begins after the pump power being switched on for  $0.4 \text{ ms}$ .

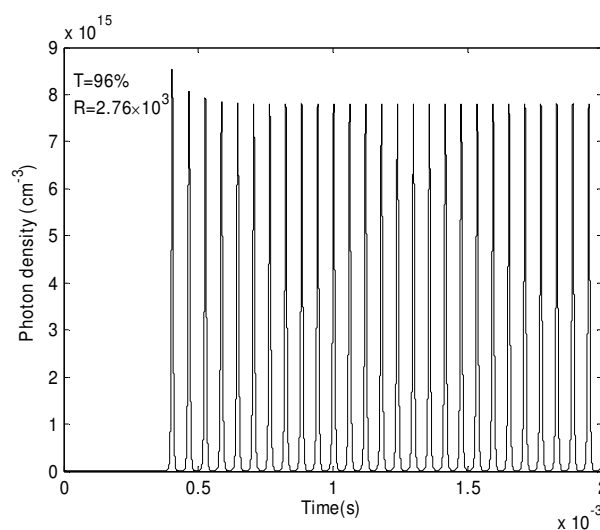


Fig. 45. Self-pulsing train at corresponding threshold pump rate with output coupling  $T=96\%$ .

At respective self-pulsing threshold pump rates, the laser pulse width and pulse frequency as a function of the output coupling are shown in Fig. 46 [81]. Increasing the output coupling, the laser pulse frequency and pulse width respectively increases and decreases near linearly. As shown in Fig. 46, higher output couplings need higher pump rates to initiate self-pulsing. Higher pump rate induces higher population inversion and higher gain, leading to higher self-pulsing repetition rate. Narrower pulse width at higher coupling is due to the reduction of cavity lifetime resulted from higher coupling loss. This offers a clue that, in order to achieve shorter pulse width and higher repetition rate simultaneously in self-pulsing fiber lasers, higher output couplings should be adopted.

In order to further the understanding about the influence of output coupling on the self-pulsing features, we carry out simulation with different output coupling strengths at a identical pump rate of  $R=4 \times 10^3$ . With this pump rate, self-pulsing operation can be achieved

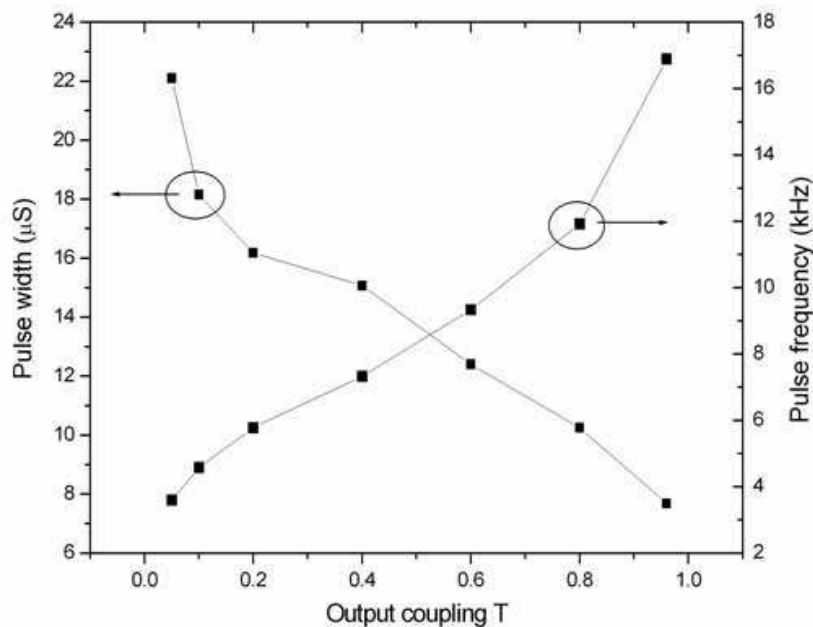


Fig. 46. Pulse width and frequency for different couplings at respective threshold pump rate.

between  $T=96\%$  and  $T=10\%$ . When  $T<10\%$ , self-pulsing cannot be sustained. Detailed values about the pulse width and pulse repetition rate are shown in Fig. 47 [81]. The output coupling of  $T=10\%$  provides the maximum pulse frequency of  $\sim 75$  kHz. As the output coupling increases from  $T=10\%$  to  $T=96\%$ , the pulse frequency drops down sharply first and then more slowly, reaching a minimum value of 30 kHz. Higher pulse frequency at lower output coupling is due to that lower output coupling provides less cavity loss thus a faster

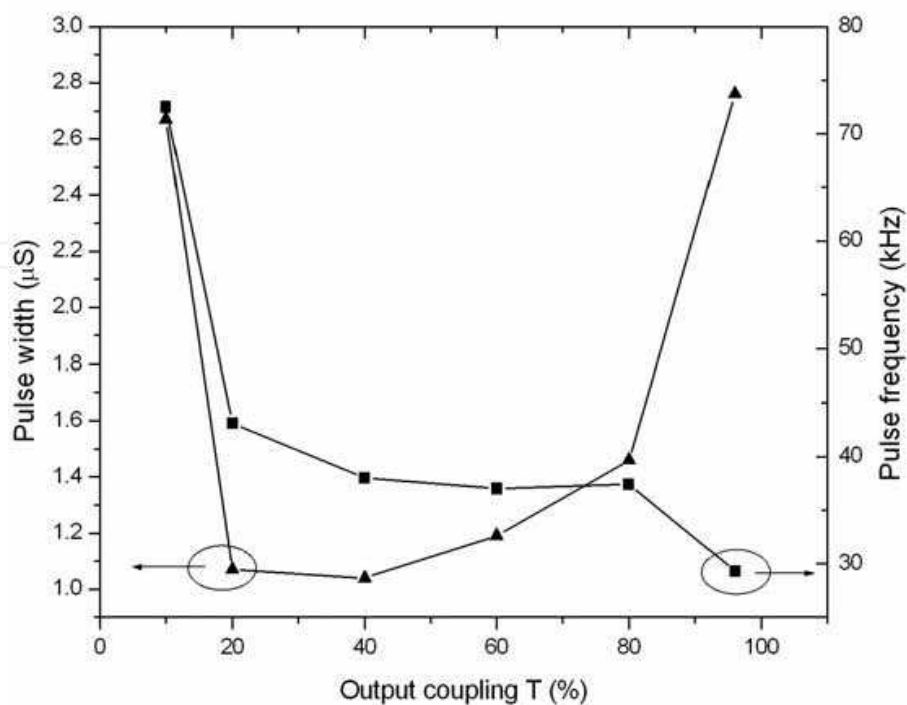


Fig. 47. Pulse width and frequency for different output couplings at pump rate  $R=4\times 10^3$ .

gain recovery. Therefore, in making use of self-pulsing to obtain high-frequency pulses, lower output couplings are preferred. As the output coupling increases from  $T=10\%$  to  $T=96\%$ , the pulse width decreases sharply first, then arrives at a minimum value, thereafter increases steadily and then significantly. Increasing the output coupling reduces the population inversion, but also the photon lifetime in the cavity, which play opposite roles on the pulse width. Therefore, an optimum output coupling ( $\sim 40\%$ ) exists that produces the shortest pulse duration of  $\sim 1 \mu\text{s}$ .

## 2.2. Influence of pump rate $R$ on the self-pulsing characteristics

In this section, fiber-end facet is considered as the output coupler ( $T=96\%$ ), the ESA cross section is kept at  $4 \times 10^{-21} \text{ cm}^2$ , and the pump rate is changed to investigate its impact on the self-pulsing characteristics. Increasing the pump rate, the laser operation undergoes several stages. First, the CW operation occurs at a comparatively low pump rate. Thereafter, self-pulsing begins when the pump rate arrives at the self-pulsing threshold  $R_{\text{threP}}=2.76 \times 10^3$ . The self-pulsing operation maintains for some pump power range, and then transfers to CW mode as the pump rate further reaches the second CW threshold  $R_{\text{secCW}}$ . In the self-pulsing regime, the pulse width and pulse frequency as a function of pump rate are depicted in Fig. 48 [81]. As the pump rate increases, the pulse frequency increases first slowly, and then rapidly. On the contrary, the pulse width decreases sharply first, and then saturates to about 200 ns, finally shows a little rise again. At the self-pulsing threshold, the pulse width and pulse frequency are  $7.68 \mu\text{s}$  and  $16.89 \text{ kHz}$ , respectively. As the pump rate increases to  $5.72 \times 10^3$ , the pulse width and pulse frequency decreases and increases to  $1.83 \mu\text{s}$  and  $38.3 \text{ kHz}$ , respectively. The maximum pulse frequency approaches  $900 \text{ kHz}$ , and the minimum pulse width is about  $200 \text{ ns}$ . An interesting phenomenon is that the pulse width keeps nearly constant at the minimum value over a very large pump range (as the double arrow line denotes). From this phenomenon, several conclusions can be arrived at. First, the self-pulsing must originate from some intra-ionic processes. This excludes such mechanisms as

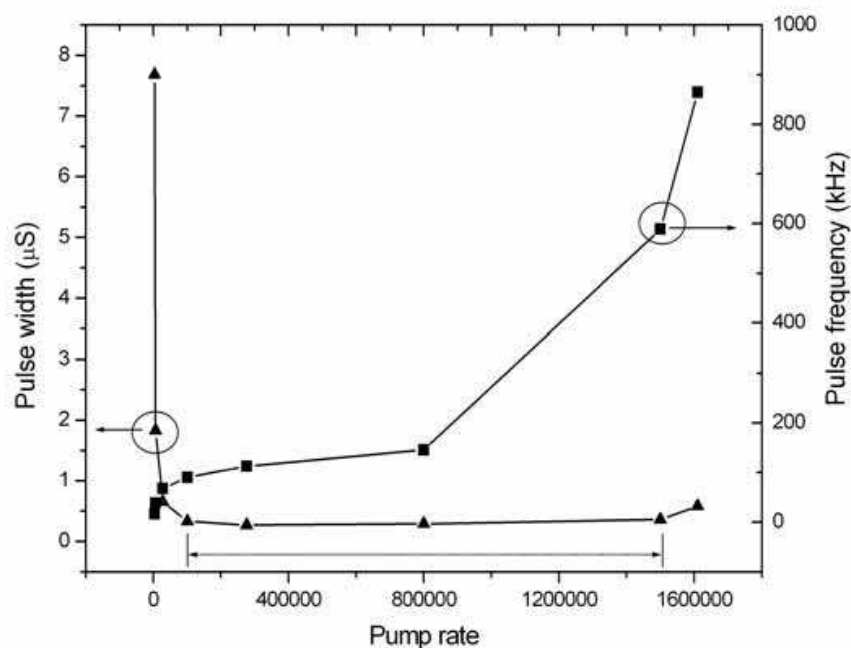


Fig. 48. The pulse width and pulse frequency versus the pump rate for  $T=96\%$  output coupling.

Brillouin scattering and interaction between longitudinal modes from accounting for self-pulsing formation. Secondly, stable self-pulsing operation can be realized with high output power, showing a great power scalability of this pulsing technique. Thirdly, there is a limitation in the achievable minimum pulse width. Further narrowing the pulse width may require combining with other modulation techniques, such as nonlinear polarization control et al.

### 2.3. Influence of active-ion doping concentration $N_{\text{tot}}$ on the self-pulsing characteristics

In Tm<sup>3+</sup>-doped fiber lasers, appropriately high Tm<sup>3+</sup> doping concentration can strengthen the cross relaxation process, which significantly enhances the quantum efficiency of the laser. However, too high Tm<sup>3+</sup> doping concentration will form Tm<sup>3+</sup> ion clusters thus present concentration quenching. Besides, high doping level can induce strong energy up-conversion processes, leading to reduction of population inversion. So in fact, there is an appropriate Tm<sup>3+</sup> doping concentration, which provides the fiber laser the maximum laser efficiency.

In this section, simulation is carried out with constant output coupling  $T=96\%$  and constant pump rate  $R=4\times 10^3$ . Self-pulsing operation is observed by changing the particle density  $N_{\text{tot}}$  (Tm<sup>3+</sup> ion density). As the particle density increases from  $1.37\times 10^{20}$  to  $1.37\times 10^{21}$  cm<sup>-3</sup>, the self-pulsing threshold  $R_{\text{threP}}$  decreases more than ten times. The pulse width and repetition rate as a function of  $N_{\text{tot}}$  are shown in Fig. 49 [81]. As the particle density increases from  $1.37\times 10^{20}$  to  $1.5\times 10^{21}$  cm<sup>-3</sup>, the pulse frequency grows from 30 kHz to ~145 kHz near linearly. Higher doping concentration leads to higher cross relaxation, energy up-conversion and signal light re-absorption. The combination of these processes can speed the recovery of population inversion after a pulse output, thus improve the pulse repetition rate. Increasing the particle density, the laser pulse width decreases sharply first, and then slowly. Therefore, comparatively higher doping concentration is preferred to simultaneously

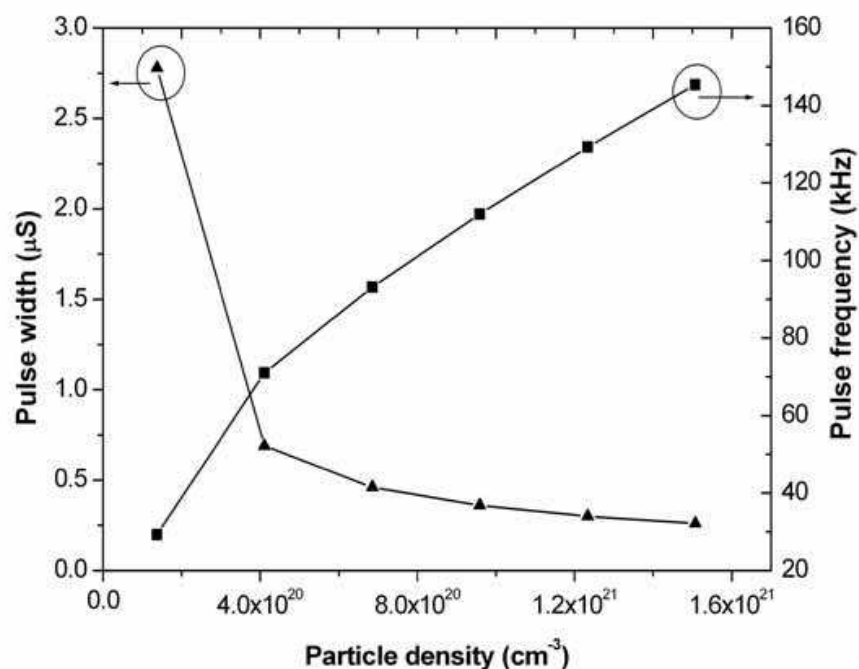


Fig. 49. Pulse width and frequency as a function of doping concentration at pump rate  $R=4\times 10^3$ .

achieve high pulse frequency and narrow pulse width in self-pulsing fiber lasers. However, especially high active-ion doping in fibers is impracticable. In addition, too high doping concentration will cause ion clustering, thus decrease laser efficiency. Therefore, there is a tradeoff between obtaining narrow pulse width and achieving high laser efficiency. Further narrowing the pulse duration requires combining self-pulsing with other modulation techniques.

### 3. Conclusion

Through numerical simulation, self-pulsing behavior of  $\text{Tm}^{3+}$ -doped fiber lasers is theoretically analyzed, and the influence of pump rate, output coupling and ion doping concentration is explicitly studied. In order to achieve self-pulsing over a large pump range, high output couplings are preferred. At a fixed pump level, higher output coupling decreases pulse frequency, but narrowest pulse width can only be achieved with an optimum output coupling. For a given output coupling, higher pump strength increases the pulse frequency, but decreases and saturates the pulse width. Reduction of total cavity loss helps narrowing the pulse width. Increasing doping concentration significantly decreases the self-pulsing threshold. In self-pulsing  $\text{Tm}^{3+}$ -doped fiber lasers, high pulse frequency and narrow pulse width can be simultaneously achieved with appropriately higher active-ion doping concentration.

Understanding the self-pulsing characteristics and methods as how to make use of it will help improving the performance and utility of 2- $\mu\text{m}$   $\text{Tm}^{3+}$ -doped fiber lasers. The excellent features of self-pulsing provide it the potential to become a new competitive Q-switching technique. Self-pulsing has great prospects in applications such as constructing self-switching pulsed lasers, improving pulsed lasers' output power, and simplifying the cavity configuration of ultra-short-pulse-width laser systems.

## 4.3 Passively Q-switching $\text{Tm}^{3+}$ -doped fiber laser with $\text{Cr}^{2+}:\text{ZnSe}$

### 1. Introduction

Thulium-doped fiber lasers have an especially broad emission band, providing great potential for achieving ultra-short mid-infrared pulses. For obtaining pulsed laser output, various modulation techniques, can be used, e.g., gain-switching, Q-switching, cavity dumping and mode-locking. Gain-switched  $\text{Tm}^{3+}$ -doped silica fiber lasers have generated high pulse energy over 10 mJ in several hundred nanosecond pulse duration [82-83], while Q-switched  $\text{Tm}^{3+}$ -doped silica double-clad fiber lasers have produced several-kW peak power with the pulse durations around 100 ns [84-85]. Ultra-short 2- $\mu\text{m}$  pulses have been achieved from mode-locked thulium-doped fiber lasers with the pulse durations as less as several hundred femto-seconds [86].

Compared with the positive Q-switching techniques, Passive Q-switching is an attractive approach to construct simple, robust, and cost-efficient pulsed lasers.

Many saturable materials have been utilized as the modulation elements in the 2- $\mu\text{m}$  spectral range, including  $\text{Ho}^{3+}:\text{CaF}_2$ ,  $\text{Co}^{2+}:\text{ZnSe}$ , and  $\text{Cr}^{2+}:\text{ZnSe}$  crystals [87].  $\text{Tm}^{3+}$ -doped silica fiber lasers near 2  $\mu\text{m}$  passively Q-switched by a  $\text{Cr}^{2+}:\text{ZnSe}$  crystal have been demonstrated with the pulse duration of 330 ns and peak power of 15 W [87]. Passive Q-switching  $\text{Tm}^{3+}$ -doped silica fiber lasers by a  $\text{Ho}^{3+}$ -doped silica fiber has also been investigated with the pulse width of  $\sim 1 \mu\text{s}$  [88].

In this section, short-length passively Q-switched  $\text{Tm}^{3+}$ -doped silica fibers (5-50 cm) are described with polycrystalline  $\text{Cr}^{2+}:\text{ZnSe}$  microchips as the saturable materials.

## 2. Experimental setup

The polycrystalline  $\text{Cr}^{2+}:\text{ZnSe}$ , prepared by CVD technique and doped by thermal diffusion method, has a relaxation time of 5  $\mu\text{s}$  [89], which is significantly shorter than the lifetime of the upper laser level of  $\text{Tm}^{3+}$  ions ( $3\text{F}_4 \rightarrow 3\text{H}_6$ ) of  $\sim 335 \mu\text{s}$  in silica [12]. The  $\text{Cr}^{2+}$  doping concentration of the polycrystalline is  $\sim 7 \times 10^{18} \text{ cm}^{-3}$ . Double-clad large-mode-area fibers are used to increase the extractable energy from short-length fibers. The core, doped with approximate 2.5 wt.%  $\text{Tm}^{3+}$  ions, is 27.5  $\mu\text{m}$  in the diameter and 0.20 of numerical aperture (NA). The pure silica inner cladding, coated with a low-index polymer, has a 400- $\mu\text{m}$  diameter and NA of 0.46.

Fig. 50 shows the experimental setup [90]. A high-power laser-diode array operating at 790 nm is used as the pump source. The pump beam is reshaped to a square beam pattern by a micro-prism stack, and then focused into the fiber using a cylindrical lens and an aspheric lens. The pump beam is launched into the fiber through a dichroic mirror with high reflectivity ( $>99.7\%$ ) at 2.0  $\mu\text{m}$  and high transmission ( $>97\%$ ) at 790 nm. The output end of the fiber is butted directly to the polycrystalline  $\text{Cr}^{2+}:\text{ZnSe}$ . Whole fiber is clamped in an air-cooled copper heat-sink. At the same time, the polycrystalline  $\text{Cr}^{2+}:\text{ZnSe}$  microchip is fixed separately on a water-cooled heat-sink to prevent it from thermal-induced fracture.

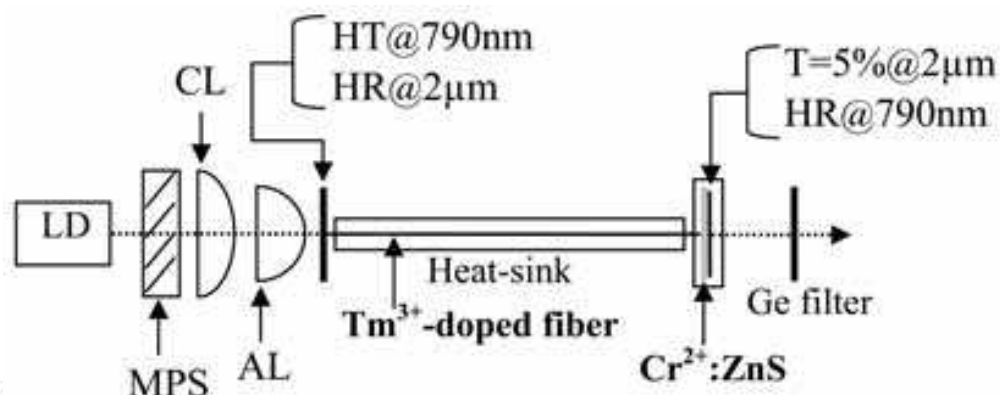


Fig. 50. Schematic of the experimental setup; LD: laser diode, MPS: micro prism stack, CL: cylindrical lens, AL: aspheric lens, HT: high transmission, HR: high reflection.

Laser output power is measured with a pyroelectric power meter after the leaky pump light being blocked by a Ge filter ( $T=0.1\%$  at 790 nm). Laser spectra are examined by a mid-infrared spectrograph with a resolution of 0.2 nm and a TEC-cooled InAs detector (J12 series). An InAs PIN photodiode and a 500 MHz digital oscilloscope are used to measure the laser temporal characteristics.

## 3. Results and discussion

The bleaching experiment is carried out with an uncoated polycrystalline  $\text{Cr}^{2+}:\text{ZnSe}$  microchip with thickness of 1 mm. A 2- $\mu\text{m}$   $\text{Tm}^{3+}$ -doped silica fiber laser with output power

up to 3 W is used as the test source. The 2- $\mu\text{m}$  laser was focused onto the crystal with an objective lens of 11-mm focal length and NA of 0.25. The beam diameter at the focus is measured to be 30  $\mu\text{m}$  by using the knife edge method. Figure 51 shows the power transmission for various laser intensities onto the crystal [90]. The transmission nearly remains a constant  $\sim 0.6$  as the incident intensity is above 164  $\text{kW}/\text{cm}^2$ . The saturation intensity  $I_s \sim 164 \text{ kW}/\text{cm}^2$  is higher than that from  $\text{Cr}^{2+}:\text{ZnSe}$  crystal [87]. The higher saturation intensity is probably attributed to uncoated surfaces and additional scattering loss in the polycrystal. From the saturation intensity  $I_s$  and fiber diameter, the laser power to saturate the polycrystal is calculated to be  $\sim 1.3 \text{ W}$ .

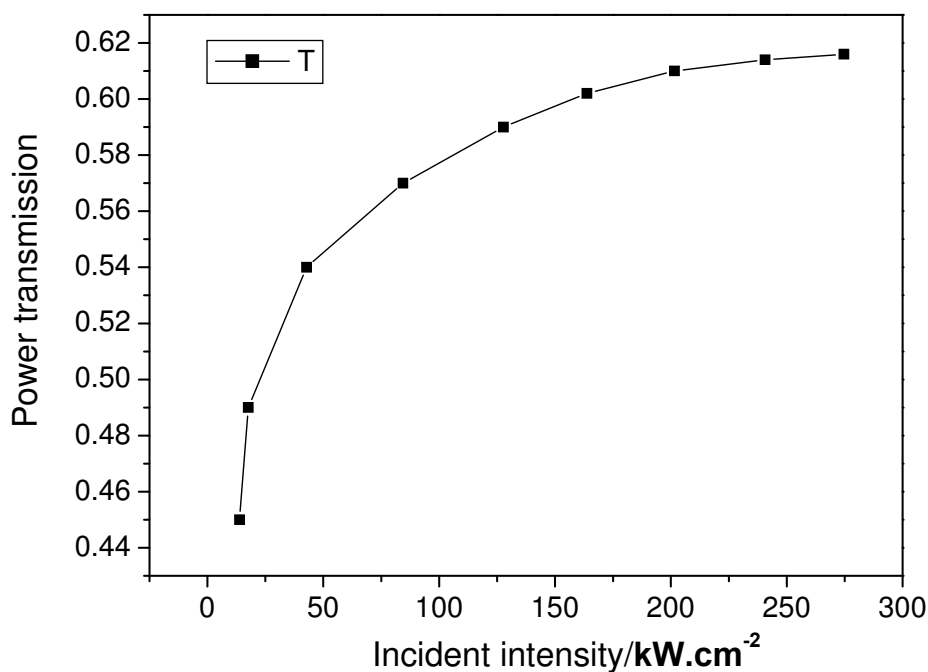


Fig. 51. Power transmission characteristics by 1 mm thick  $\text{Cr}^{2+}:\text{ZnSe}$  polycrystalline showing saturation intensity  $I_s=164 \text{ kW}/\text{cm}^2$ .

One surface of the polycrystalline microchip is precisely polished and the other one is coated with partial reflectivity ( $R=95\%$ ) at  $\sim 2 \mu\text{m}$  wavelength and high reflectivity ( $R>99.8\%$ ) at 790 nm. To Q-switch the fiber laser, different thicknesses of polycrystalline  $\text{Cr}^{2+}:\text{ZnSe}$  microchips are chosen for various fiber lengths. The selected thickness of polycrystalline  $\text{Cr}^{2+}:\text{ZnSe}$  microchip for various fiber lengths is shown in Table 2 [90].

|  |     |     |     |    |
|--|-----|-----|-----|----|
| Fiber length (cm)                              | 5   | 10  | 20  | 50 |
| Thickness of $\text{Cr}^{2+}:\text{ZnSe}$ (mm) | 0.3 | 0.4 | 0.5 | 1  |

Table 2. Parameters of the fiber length and thickness of  $\text{Cr}^{2+}:\text{ZnSe}$

The characteristics of a 5-cm long Q-switched fiber laser are shown in Fig. 52 and 53 [90]. The fiber laser has a threshold pump power of  $\sim 3 \text{ W}$ . Maximum average output power is

around 50 mW, corresponding to a slope efficiency of ~0.5% with respect to ~10 W launched pump power. The output power increases nearly linearly with increasing launched pump power. When the pump power higher than 10.5 W, the dielectric film on the Cr<sup>2+</sup>:ZnSe is damaged. The low output power and slope efficiency arise primarily from insufficient pump absorption in short fibers and reflection loss at the uncoated surface of the polycrystalline Cr<sup>2+</sup>:ZnSe microchips.

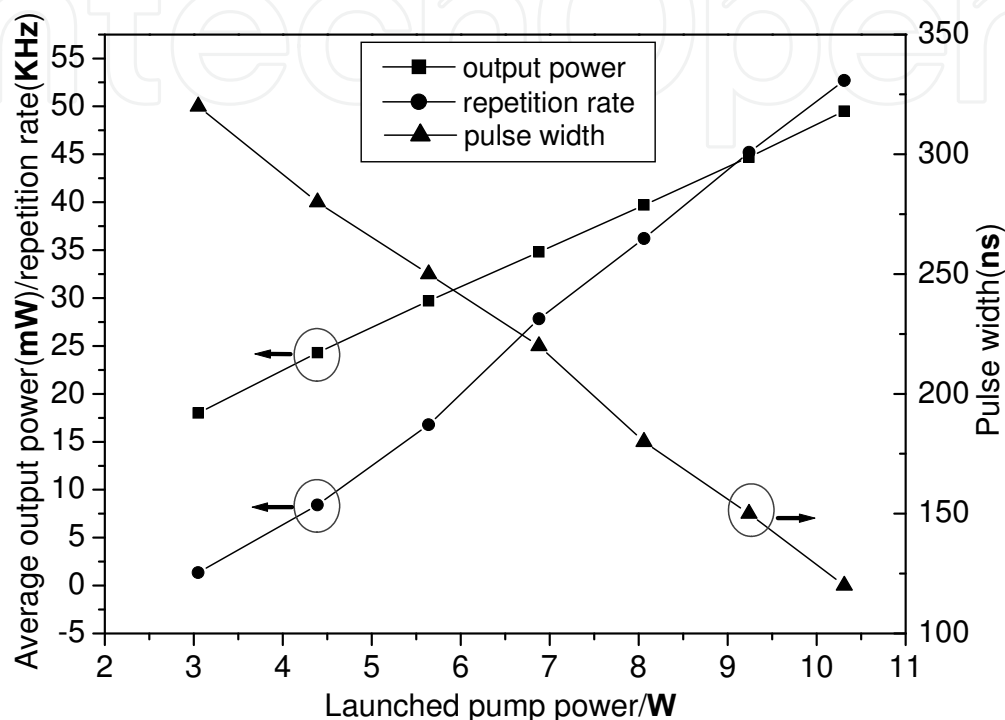


Fig. 52. Average output power, pulse repetition rate and pulse width as a function of launched pump power for a 5 cm-length fiber.

When the polycrystalline Cr<sup>2+</sup>:ZnSe microchips are replaced by a partially reflecting mirror, the short fiber lasers are operated in the CW regime. The performance of CW operation of short Tm<sup>3+</sup>-doped fiber lasers has been described in the previous publication [33]. The maximum output power of a 5-cm long fiber laser is ~290 mW, corresponding to a slope efficiency of 2.9%. The Q-switched fiber lasers can extract about 17% energy of the CW operation.

Pulse width of 120 ns is obtained from the 5-cm long fiber laser, which presents the shortest pulse duration achieved from passive Q-switched Tm<sup>3+</sup>-doped fiber lasers. It is expected that sub-hundred-nanosecond pulses can be accessible by shortening the fiber length to ~1 cm. The pulse repetition rate increases linearly and reaches the maximum value of 53 kHz with the pump power of 10.3 W.

Peak power shown in Fig. 53 is obtained by dividing the pulse energy by the pulse width [84]. As the pump power is increased, both the pulse energy and peak power decrease. The decrease of pulse energy and peak power can be accounted by the faster increase of repetition rate than that of the output power (see Fig. 52). The maximum pulse energy and peak power are ~14  $\mu$ J and 45 W, respectively, which decreases to ~1  $\mu$ J and ~8 W at higher power level.

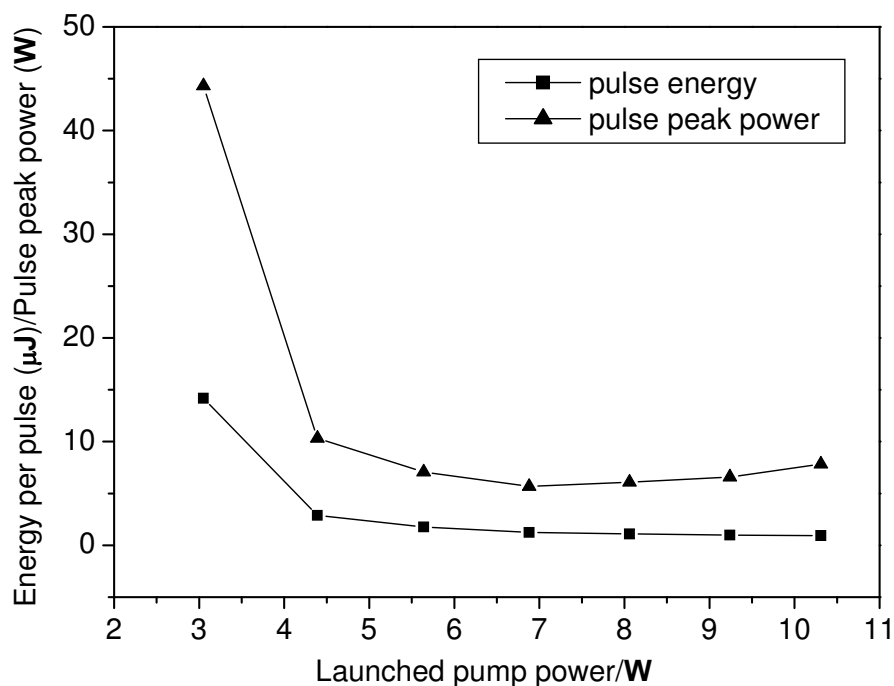


Fig. 53. Energy per pulse and pulse peak power as a function of launched pump power for the 5 cm-length fiber.

With 8-W launched pump power, a typical pulse train and individual pulse obtained from the 50-cm long fiber laser are shown in Fig. 54. As shown in Fig. 54(a), the intensity stability of the Q-switched pulse train (84 kHz) is over 90%, and the pulse spacing stability is near 90%. The single laser pulse in Fig. 56(b) shows a smooth and typical pulse shape with the pulse duration of  $\sim 450$  ns. Mode-locking phenomenon, investigated by T. A. King et al [87] in passive Q-switching long  $\text{Tm}^{3+}$ -doped fibers, has not been observed in our short  $\text{Tm}^{3+}$ -doped fibers.

Average output power, repetition rate and pulse width, obtained at pump level of 10.3 W, as a function of fiber length are shown in Fig. 55 [90]. As a result of longer cavity round-trip time, the pulse duration becomes broader by using the longer fiber. When the fiber is longer than 20 cm, the pulse duration is broadened to around 300 ns. The pulse repetition rate increases linearly with fiber length at first, and then shows a sharp augmentation when the fiber longer than 50 cm. The highest average output power and repetition rate generated from a 50 cm-long fiber laser, are  $\sim 200$  mW and 530 kHz, respectively.

Pulse energy and peak power obtained for various fiber lengths at pump power of 3 and 10.3 W, are shown in Fig. 56 [90]. As the fiber length is changed from 5 to 50 cm, the pulse energy displays a moderate decrease with increasing fiber length. On the other hand, the peak power reduces by one order of magnitude. The decrease of peak power comes mainly from the broadening of the pulse width as shown in Fig. 55. When the fiber length changed from 5 to 20 cm, the pulse width increases much faster, leading to a remarkable decrease of the peak power.

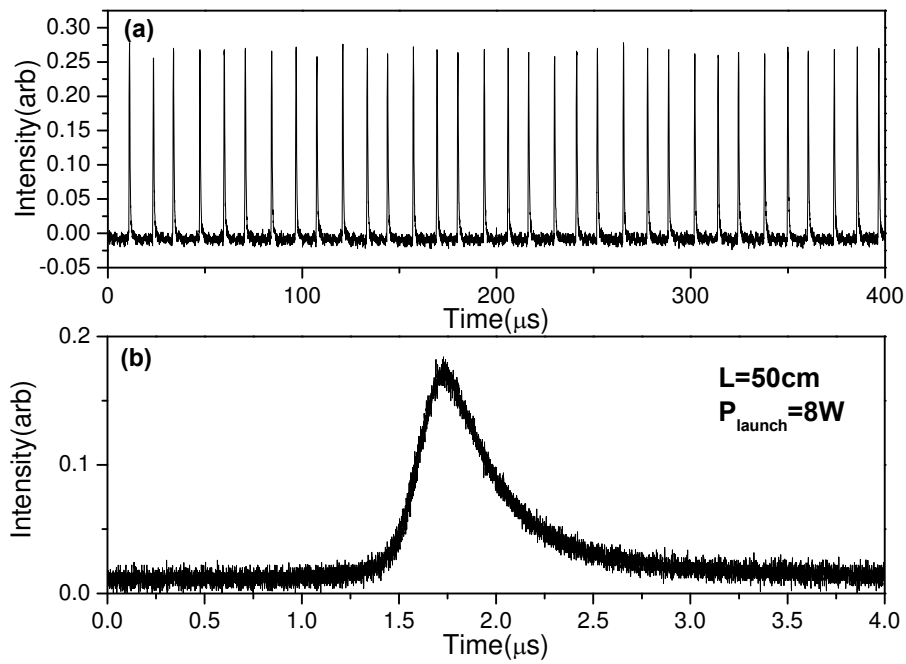


Fig. 54. The pulse train and a single pulse for a 50 cm-length fiber at 8 watts of launched pump power.

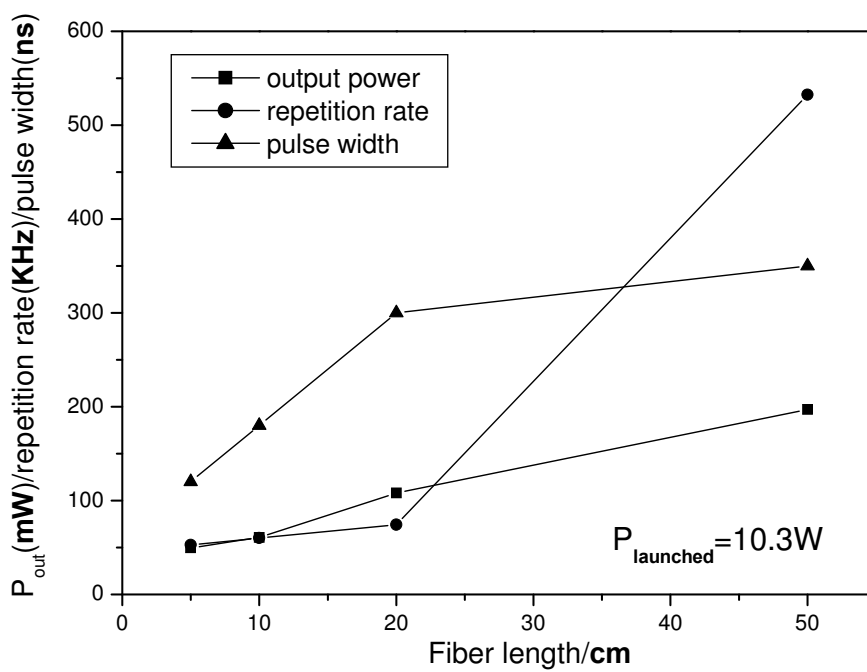


Fig. 55. Maximum average output power, repetition rate, and minimum pulse width as a function of fiber length at 10.3 W of launched pump power.

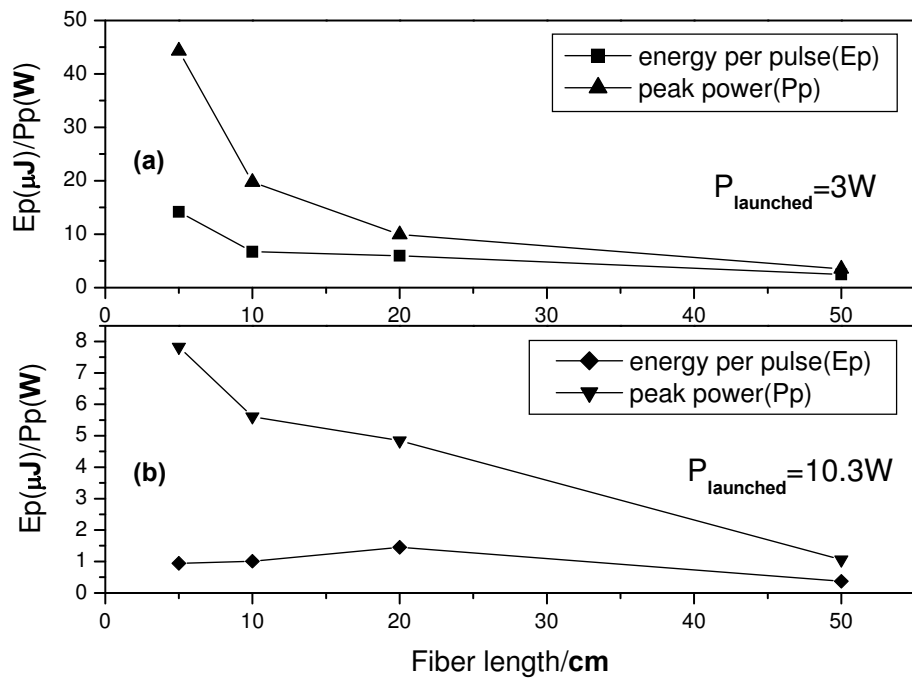


Fig. 56. Pulse energy and pulse peak power as a function of fiber length at launched pump power of 3 W (a) and 10.3 W (b).

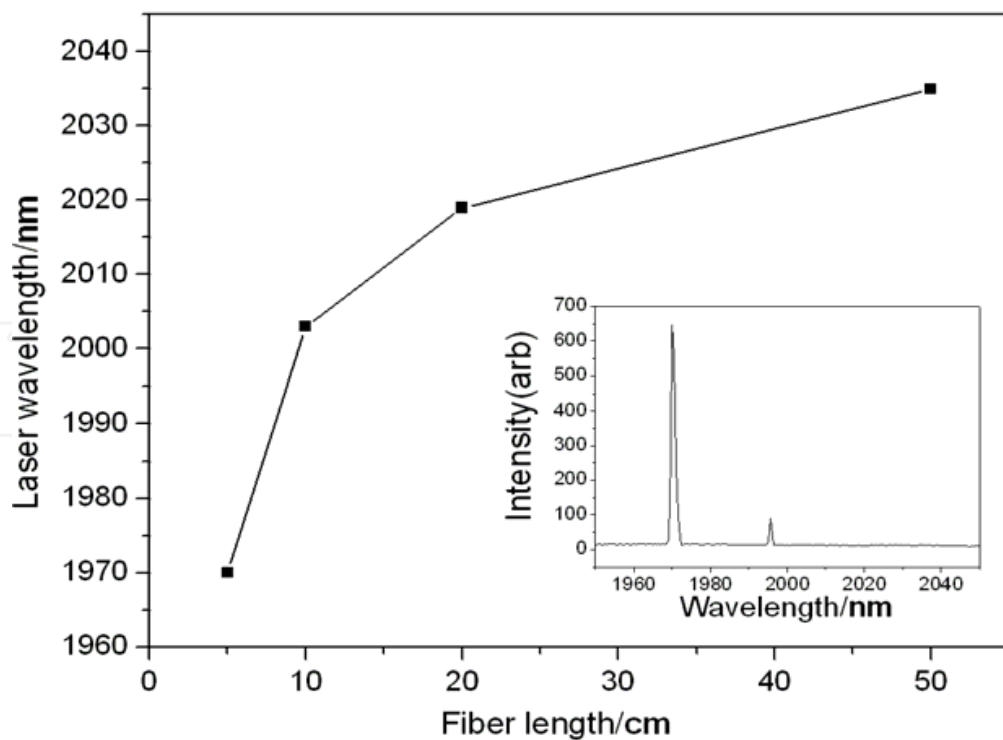


Fig. 57. Laser wavelength as a function of fiber length; inset is the laser spectrum obtained with the 5 cm-length fiber at 8 W of pump power.

Laser wavelength of the fiber laser as a function of fiber length is shown in Fig. 57 [90]. When the fiber length alters from 5 to 50 cm, the laser wavelength shows a parabolic increase from 1970 to 2035 nm. The elongation of wavelength is a result of the re-absorption of laser light in the Tm<sup>3+</sup>-doped fibers. From the inset of Fig. 57, the fiber laser was operated in multiple modes with the bandwidth (FWHM) of around 2 nm for the main peak.

#### 4. Conclusion

Polycrystalline Cr<sup>2+</sup>:ZnSe microchips can be used to passively Q-switch the thulium-doped silica fibers effectively. With this technique, pulse duration as short as 120 ns and repetition rate as high as 530 kHz can be achieved from several-centimeter-length Tm<sup>3+</sup> fibers. The moderate pulse energy and peak power (14 μJ and 45 W) can be further improved by increasing the thulium doping concentration or adopting high-gain, high absorption glass fibers. The combination of polycrystalline microchips, short-length fibers and LDA pump source provides a simple and reliable laser device. Besides, the easy-growth feature of polycrystalline Cr<sup>2+</sup>:ZnSe adds the laser system outstanding advantages of convenience and economy. Due to its wide absorption spectrum from ~1.5 to 2.1 μm, polycrystalline Cr<sup>2+</sup>:ZnSe can also be used to passively Q-switch Er<sup>3+</sup> lasers and Tm<sup>3+</sup>:Ho<sup>3+</sup>-doped lasers. Such short pulse width, 2-μm lasers have wide applications in trace gas detecting and communications.

#### 5. Tm<sup>3+</sup>-doped fiber laser pumped Cr<sup>2+</sup>:ZnSe solid-state laser

##### *Introduction*

The application requirement for room-temperature tunable mid-IR sources like, e.g. spectroscopic, medical, and remote sensing has provoked increased interest for long-wavelength, i.e. above 2 μm, tunable directly diode-pumped solid-state lasers.

Divalent transition-metal doped II-VI chalcogenides laser materials have such interesting features as: room-temperature operation between 2 and 5 μm, broad tunability, negligibly low excited state absorption, high emission cross section, possibility of direct diode pumping and CW operation. Infrared transition metal ion-doped solid-state lasers, have become the critical components in optical frequency standards, space-based remote sensing systems, and have potential application in femtochemistry and attosecond science[91-94].

For achieving laser output over 2 μm, Cr<sup>2+</sup>:ZnSe crystal is a good candidate. The low maximum phonon frequency in ZnSe (~250 cm<sup>-1</sup>) leads to a low nonradiative decay rate and high fluorescence quantum yield (close to unity) [95]. This provides Cr:ZnSe with the highest gain among vibronic lasers and enables efficient room-temperature operation. The remarkable characteristics of the ultrabroadband (~1000 nm) Cr<sup>2+</sup>:ZnSe crystal, such as the high emission cross section of the order of 10<sup>-18</sup> cm<sup>2</sup> [96], the negligibly low excited state absorption (ESA) [97], the fairly good chemical and mechanical stability and the thermal conductivity nearly as high as in sapphire, gives this material enormous potential as a laser medium for diode-pumped tunable MIR lasers.

Remarkable progress has been achieved in Cr<sup>2+</sup>-doped zinc chalcogenides, and in particular of Cr:ZnSe as broadly tunable continuous wave (CW) laser operating around 2.5 μm. Diode-pumped room-temperature CW Cr<sup>2+</sup>:ZnSe laser was first demonstrated by Sorokin et al. in 2002 [93]. Tuning below 2 μm was first demonstrated by Umit and Alphan in 2006 [98].

Record of the highest average pulse power of 18.5W was achieved by CTI in 2004 [99]. Sorokina et al have achieved a wavelength tuning range over 1100 nm and ps-level laser pulses in Cr<sup>2+</sup>:ZnSe lasers [100-101]. Among all solid-state laser materials, the gain spectrum of Cr<sup>2+</sup>:ZnSe is the broadest. This feature of the Cr<sup>2+</sup>:ZnSe laser make it possible to produce 1~2 optical-cycle ultra-short laser pulses, which will find great potential applications in the femtosecond laser regime.

### 5.1 Watt-level CW ceramic Cr<sup>2+</sup>:ZnSe laser pumped by Tm<sup>3+</sup> fiber laser

In this section, watt-level CW laser, based on 1.7-mm ceramic Cr<sup>2+</sup>:ZnSe disk in the mid-infrared range around 2.4 μm is introduced.

#### Material Characterization

The Cr<sup>2+</sup>:ZnSe disk is doped by means of PVT. The pure ZnSe poly-crystal and Cr powder was mixed in a vacuum tube under temperature of 950°C. After diffusion for 200 hours, Cr<sup>2+</sup> ion-doping concentration reached 10<sup>19</sup>/cm<sup>3</sup>. The disk has a diameter of 15mm and a thickness of 1.7mm. The diagram of energy levels of Cr<sup>2+</sup> in Cr:ZnSe crystal is shown in Fig. 58 [102]. The energy levels associated with laser operation are the <sup>5</sup>T<sub>2</sub> ground state and the <sup>5</sup>E excited state. Transitions to/from the other nearby excited states, the <sup>3</sup>T<sub>1</sub> and <sup>3</sup>T<sub>2</sub> states, are spin forbidden and are weak compared to the transition from <sup>5</sup>T<sub>2</sub> to <sup>5</sup>E [103]. There is a possibility of excited state absorption (ESA) due to the <sup>5</sup>E-<sup>3</sup>T<sub>1</sub> transition, but it was shown to have a small cross section in Cr<sup>2+</sup>:ZnSe. The wavelength of the strongest line comes from the <sup>5</sup>E-<sup>3</sup>T<sub>1</sub> transition. The II-VI materials themselves are fully transparent over the wavelength range of interest. Altogether this provides Cr<sup>2+</sup>:ZnSe the highest gain among vibronic lasers and enables efficient broadband room-temperature operation[101,104].

The absorption spectra of Cr:ZnSe, shown in Fig. 59 [105], is centered at 1776nm and has a bandwidth of 400 nm, which makes a wide pumping range.

A double-clad Tm<sup>3+</sup>-doped silica fiber laser for excitation, an Omni-λ500 spectrometer and PD (InAs Photodiode) detector for wavelength measurements, the super fluorescence

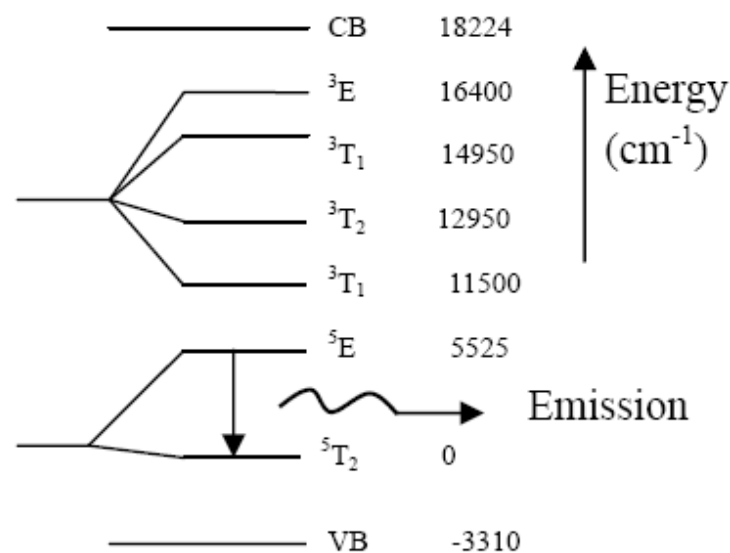


Fig. 58. Cr<sup>2+</sup> Energy levels in Cr<sup>2+</sup>:ZnSe as described by Grebe et al.

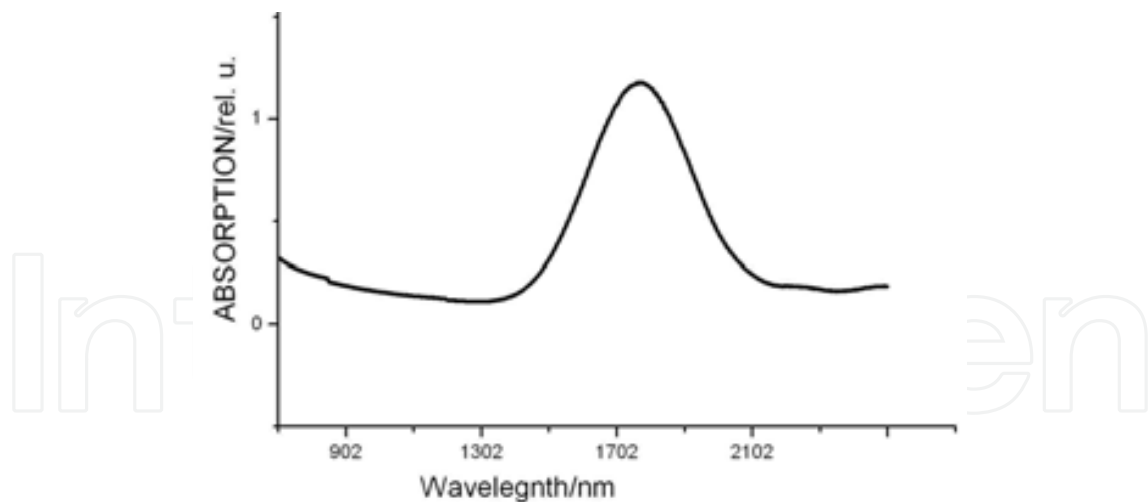


Fig. 59. Cr:ZnSe disk absorption spectra

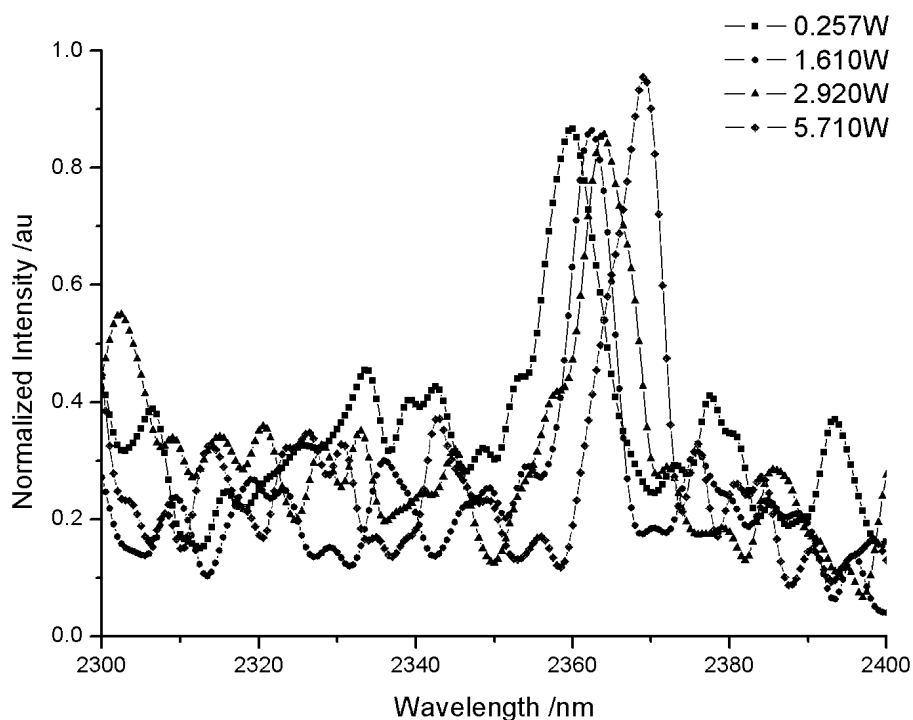


Fig. 60. Super fluorescence spectra of Cr<sup>2+</sup>:ZnSe pumped by different power

spectra of Cr:ZnSe pumped by different power is shown in Fig. 60 [105]. The peak emission increases from 2.360 $\mu$ m to 2.369 $\mu$ m with increase of pump power and the bandwidth of super fluorescence was about 20 nm which decreased by several nanometers when pump intensity increased. Rotating the angle of incidence ( $0^\circ$  for pump beam launched on the crystal surface vertically), the intensity and peak emission wavelength of super fluorescence varied significantly, shown in Fig. 61.

#### Experimental setups

Cr<sup>2+</sup>:ZnSe disk has been coated with tens of microns thick PR (Partial-Reflective) film on one surface, with measured transmission of 5% at 2.4 $\mu$ m, and AR (Anti-Reflective) film at both 1.9 $\mu$ m and 2.4 $\mu$ m on the other. The PR film has a transmittance of lower than 3% at 1.9 $\mu$ m.

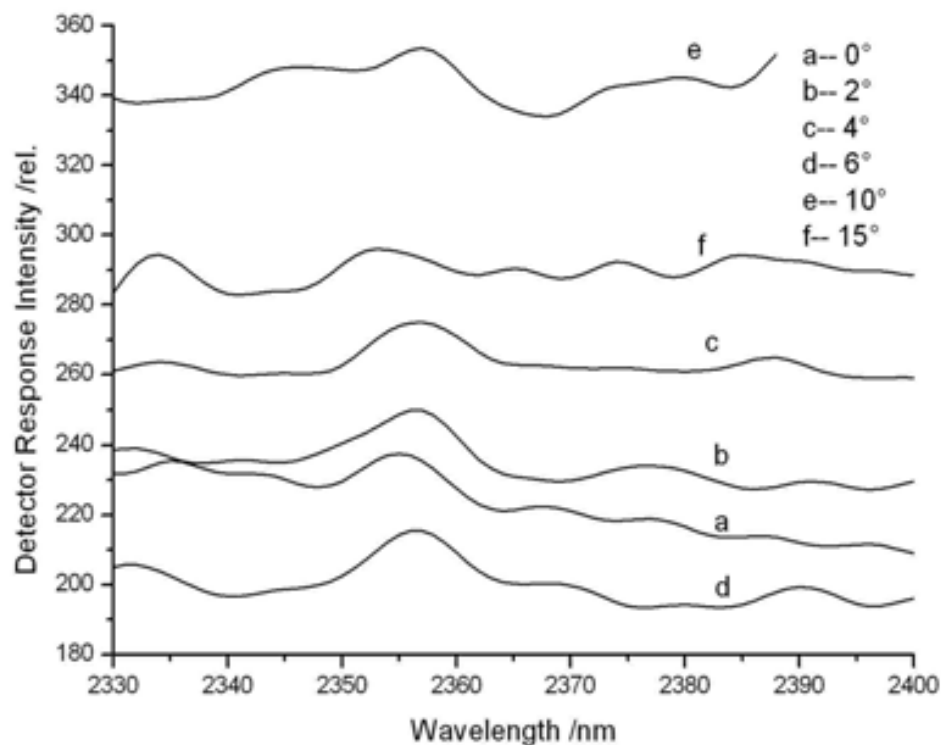


Fig. 61. Super fluorescence spectra of  $\text{Cr}^{2+}:\text{ZnSe}$  pumped in different angles

The laser was pumped by a double-clad  $\text{Tm}^{3+}$ -doped silica fiber laser. The pump beam was focused on the disk into a 0.5-mm-diameter spot.

The laser setup (Fig. 62) consists of the coated  $\text{Cr}^{2+}:\text{ZnSe}$  disk, whose surface coated with a PR film, was used as the output window, a concave HR mirror with a radius of curvature of 500mm as the rear mirror. The  $\text{Tm}^{3+}$ -doped silica fiber laser beam was directly delivered onto the disk with the angle no more than  $10^\circ$  to the optical axis. The fiber of the  $\text{Tm}^{3+}$ -doped fiber laser had a core diameter of  $30\mu\text{m}$  and pure silica inner-cladding of size  $250\mu\text{m}$  with a low refractive index ( $n=1.375$ ) polymer outercladding of size  $400\mu\text{m}$ , and was pumped at one end by beam-shaped diode-bars at 790nm delivering a maximum combined pump power of  $\sim 80\text{W}$ . The  $\text{Tm}^{3+}$ -doped fiber laser produced a maximum output of  $\sim 8\text{W}$  and the peak wavelength was 2050nm. The ZnSe disk was mounted on a copper holder for cooling. The laser operated at room temperature in continuous wave regime, producing maximum  $\sim 110\text{mW}$  of output power at 5% output coupling. Another laser arrangement was set by inserting two focusing lens of 13mm and 22.6mm focal length and a reflective mirror to improve the beam overlap on the ZnSe disk surface, shown in Fig. 63 [105]. In the second arrangement of laser setup, the laser performance was effectively improved.

#### Experimental results

The resonator is shown in Fig. 62. The plat-concave cavity length is  $\sim 100\text{mm}$ , with no extra etalons. The cw laser output characters are given in Fig. 64. With 5% output coupler, the threshold power was  $\sim 600\text{mW}$  of the incident power. In this arrangement of laser, the pump fiber was directly headed to the surface of  $\text{Cr}:\text{ZnSe}$  disc with no focusing. So, the pump laser

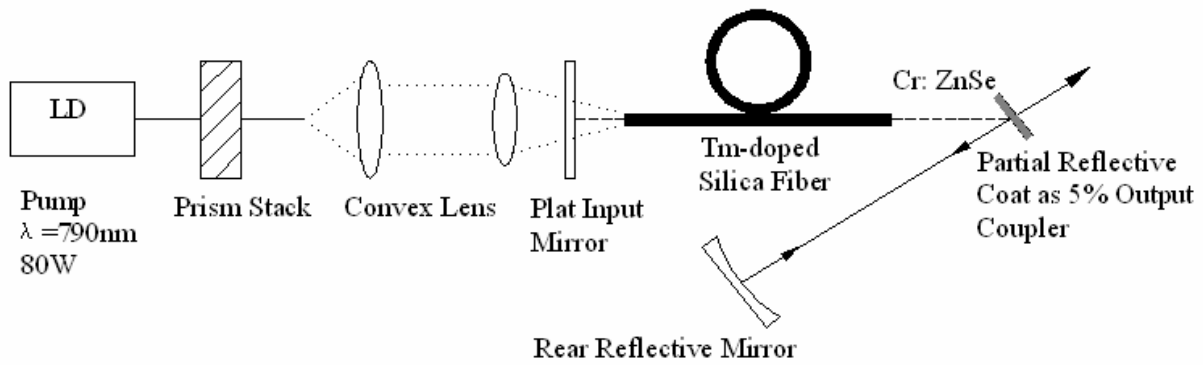


Fig. 62. Schematic diagram of the ceramic Cr:ZnSe laser setup

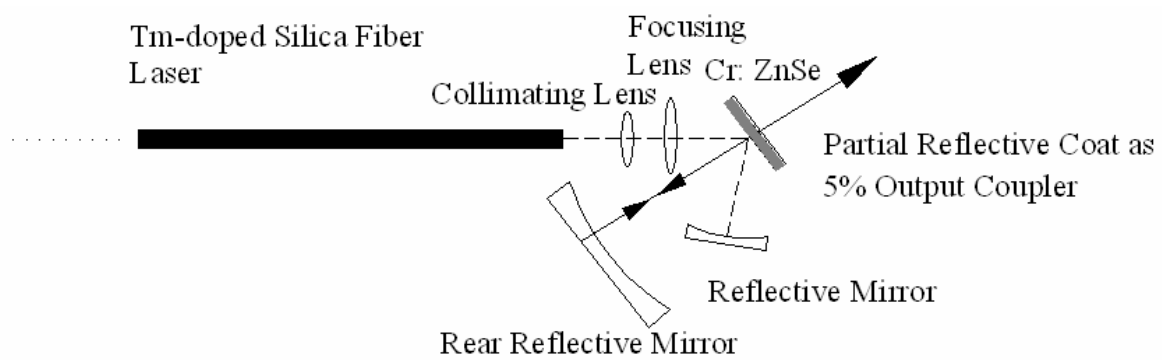


Fig. 63. The second arrangement of Cr:ZnSe laser setup

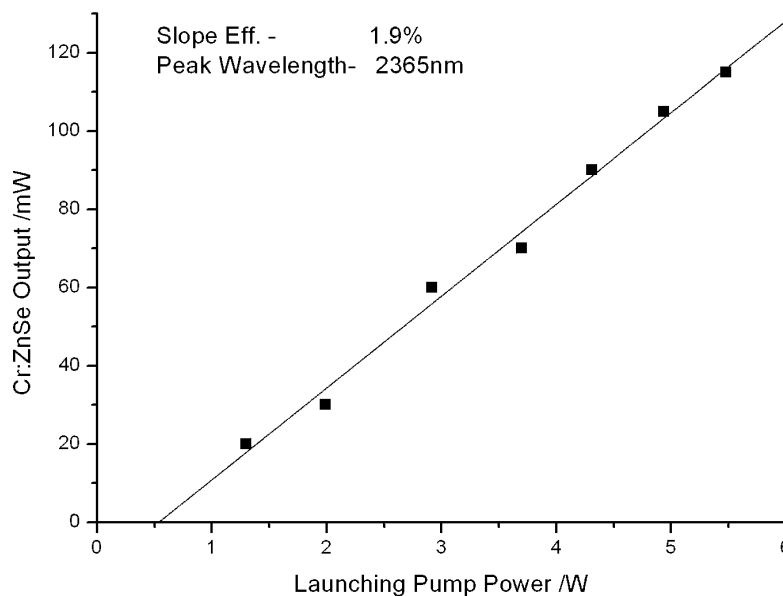


Fig. 64. Output power versus launching power of the Cr<sup>2+</sup>:ZnSe laser in the first arrangement

spot was as big as 3 mm in diameter which is as big as the laser output window. Highest output laser power was ~110mW with 4.4W of the launching power, corresponding to a

conversion efficiency of 1.9%, which is quite low and is mostly due to the loss of the pump power. To raise the slope efficiency, the pump laser beam should be focused to a much smaller spot at the entrance surface of active medium--Cr:ZnSe. And an extra rear reflective mirror should be placed to reduce the loss of the pump power.

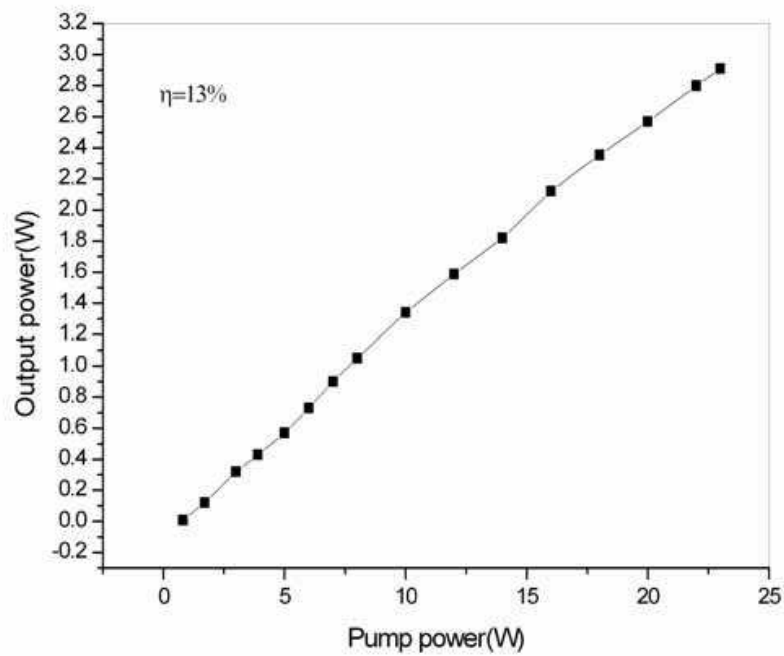


Fig. 65. Output power versus launching power of the Cr<sup>2+</sup>:ZnSe laser in the second arrangement

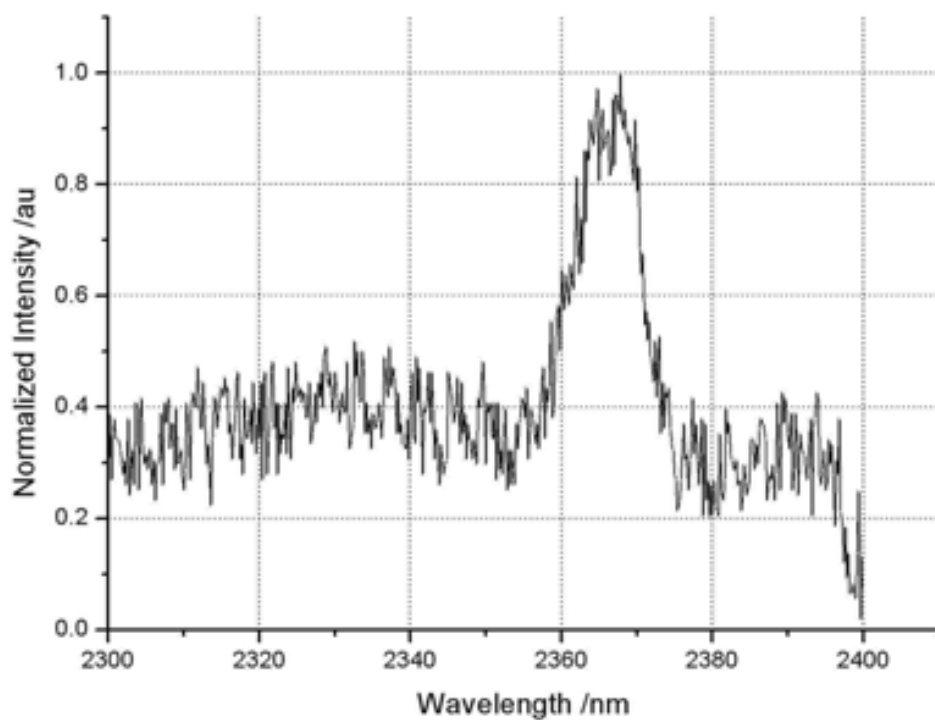


Fig. 66. Emission spectra of the Cr<sup>2+</sup>:ZnSe laser

In the second arrangement of the laser, the collimated pump beam was focused on the disc into a 0.5-mm-diameter spot by an uncoated 22.6mm lens, and the cavity length was decreased to 26mm. The laser output characteristic and spectrum are shown in Fig. 65 and Fig. 66. As shown in Fig. 66, maximum output power of 2.91 W was achieved with a slope efficiency of 13% with respect to the launching pump power. The efficiency is far lower than the limit of ~56% of the modeling result. It is mostly caused by the coatings at the surfaces of ZnSe disk, which were optimized at 2.4 μm and have very narrow bandwidth. At the peak wavelength of our laser around 2.367 μm, the reflectivity and transmittance were lower than the optimal values. Another result of this narrow-band coating is the relative narrow laser linewidth. As shown in Fig. 66 [105], the measured laser linewidth was only 10 nm, which was much narrower than that reported by other authors [91, 94 and 99]. Tightly focusing pump beam into the ZnSe disk can improve the laser output power. However, it poses a hazard of damage on the surface coatings. Further work of optimizing beam delivery, focusing optics and recoating ZnSe surface relative to the peak wavelength of laser will surely decrease the threshold and increase the output power.

## 5.2 Wavelength tunability of Cr<sup>2+</sup>:ZnSe laser

The Cr<sup>2+</sup>:ZnSe laser has good wavelength tunability. In our experiment, the band width of the laser light from the Cr<sup>2+</sup>:ZnSe laser is about 10 nm. Therefore, we studied the tunability character of the Cr<sup>2+</sup>:ZnSe laser by adopting the angle-tuning technique.

In the experiment, the incident angle of the pump beam on the ZnSe crystal will change with rotating this crystal. The anti-reflection film coated on the crystal acts as a partial-reflection mirror due to its non-hundred-percent transmittance. Therefore, the two surfaces of the ZnSe crystal form a quasi Fabry-Poret etalon, which has a selection effect on laser modes and exert the wavelength-tuning function. In the Fabry-Poret cavity, light experiences multi-pass reflection between the two parallel surfaces M<sub>1</sub> and M<sub>2</sub>, leading to interference. Light beams leaving the M<sub>2</sub> with the same phase will interfere coherently. The wavelength walking through the etalon after the multi-pass reflection will possess a phase delay as

$$\delta = \frac{2\pi}{\lambda} 2nd \cos \Theta, \quad (13)$$

where,  $nd$  is the optical length of the crystal,  $\Theta = \Theta' / n$  is the refractive angle,  $\lambda$  is the light wavelength. The transmittance of the crystal-etalon is

$$T = \left[ 1 + \frac{4r}{(1-r)^2} \sin^2 \left( \frac{\delta}{2} \right) \right]^{-1}, \quad (14)$$

where,  $r$  is the reflectance of the crystal surface. When the optical length difference of the transmitted light beams is multi times of  $\lambda$ , the transmittance will be maximum [106]:

$$T_{\max} = 1, \\ 2nd \cos \Theta = m\lambda, \quad m = 1, 2, 3 \dots$$

As shown in Fig. 67 [107], when the ZnSe crystal is rotated, the incident angle of the pump beam will change (the incident angle is referred to the angle between the normal of the crystal surface and the axis of the cavity). Consequently, the resonant wavelength will change correspondingly, leading to output laser wavelength tuned over 100 nm range (2272→2383nm). Besides, under different rotating angles of the crystal, the overlap between the pump beam and the laser beam will be different, leading to different laser threshold for different wavelength output. When the incident angle is  $0^\circ$ , the pump beam is normal to the crystal surface, the pump and laser beam modes have a good overlap. At this case, the output power is the highest, and the laser spectrum has only one peak band. When the incident angle is increased to  $2^\circ$  (by tilting the crystal), laser wavelength red-shifts a little. As the incident angle is enhanced to  $4^\circ$ , the modes overlap become worse, so the sidebands appear in the spectrum. Further increasing the incident angle ( $10^\circ \rightarrow 15^\circ$ ), the selectivity of the cavity decreases seriously, leading to occurrence of 2, 3, and 5 spectral peaks. Besides, the band width of the laser spectrum is broadened. Detailed experimental results are shown in table 3 [107].

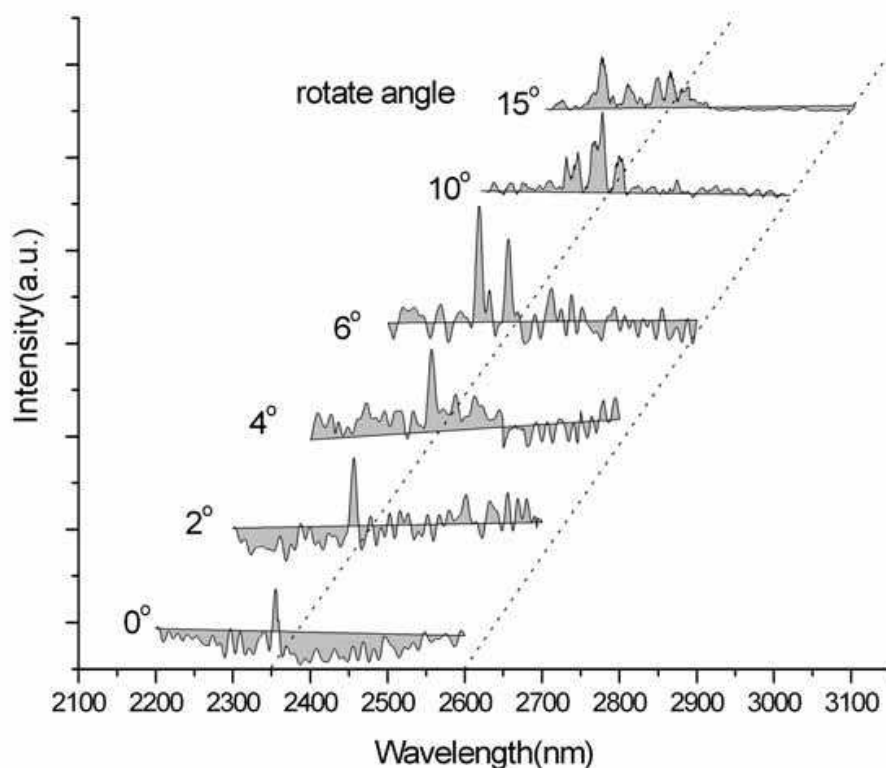


Fig. 67. laser wavelength change with different input angles of the pump light.

| Rotating angle | Spectral peak position                  | FWHM  |
|----------------|---|-------|
| $0^\circ$      | 2355nm                                  | ~10nm |
| $2^\circ$      | 2356nm                                  | ~13nm |
| $4^\circ$      | 2357nm (small sidebands)                | ~11nm |
| $6^\circ$      | 2318nm (two peaks)                      | ~10nm |
| $10^\circ$     | 2319nm (three peaks)                    | ~18nm |
| $15^\circ$     | 2272,2306,2345,2360,2383nm (five peaks) | ~15nm |

Table 3.  $\text{Cr}^{2+}:\text{ZnSe}$  angle-tuning spectra

## 6. Conclusion and prospect of 2 $\mu\text{m}$ Tm<sup>3+</sup>-doped fiber laser

Based on the high-degree development of high-brightness laser diodes and optimizing of Tm<sup>3+</sup> fiber fabrication technique, and further understanding about the spectral properties of Tm<sup>3+</sup> ions, Output power and performance of the Tm<sup>3+</sup>-doped fiber laser can be improved to a higher level. Due to its so many specific advantages, the Tm<sup>3+</sup>-doped fiber laser has great potential in the development toward high-power output, wide wavelength tunability, narrow pulse duration, and high peak power. With further enhancement of the performance and quality of the Tm<sup>3+</sup>-doped fiber laser, this kind of  $\sim 2\text{-}\mu\text{m}$  laser device will have wide applications in medicine, machining, environment detecting, LIDAR, optical-parametric-oscillation (OPO) pump sources, and so on.

There are several directions for the development of Tm<sup>3+</sup>-doped fiber laser in the future.

- High power regime;
- Pulsed mid-infrared laser output, high-peak power, including femto-second laser pulse operation;
- Single frequency (narrow linewidth) and single mode operation;
- Wide tunable mid-infrared laser output (including multi-color wavelength laser output simultaneously).

## 7. References

- [1] P. Myslinski, X. Pan, C. Barnard, J. Chrostowski, B. T. Sullivan, and J. F. Bayon, "Q-switched thulium-doped fiber laser," *Opt. Eng.* 32 (9), 2025-2030 (1993).
- [2] L. Esterowitz, "Diode-pumped holmium, thulium, and erbium lasers between 2 and 3  $\mu\text{m}$  operating CW at room-temperature," *Opt. Eng.*, 29 (6): 676-680 (1990).
- [3] R. C. Stoneman and L. Esterowitz, "Efficient, broadly tunable, laser-pumped Tm-YAG and Tm-YSGG CW lasers," *Opt. Lett.*, 15 (9): 486-488 (1990).
- [4] S. W. Henderson, P. J. M. Suni, C. P. Hale, S. M. Hannon, J. R. Magee, D. L. Bruns, and E. H. Yuen, "Coherent laser-radar at 2  $\mu\text{m}$  using solid-state lasers," *IEEE Trans. Geosci. Remote Sens.*, 31 (1): 4-15 (1993).
- [5] I.T. Sorokina, K.L. Vodopyanov (Eds.): *Solid-State Mid-Infrared Laser Sources*, Topics Appl. Phys. 89, 219-255 (2003).
- [6] Hanna, D. C., R. M. Percival, R. G. Smart, A. C. Tropper, "Efficient and tunable operation of a Tm-doped fibre laser," *Opt. Commun.* 75: 283-286 (1990).
- [7] S. Agger, J.H. Povlsen and P. Varming, "Single-frequency thulium-doped distributed-feedback fiber laser," *Optics Letters*, 29(13): 1503-1505 (2004).
- [8] H.W. Gandy, R.J. Ginther and J.F. Weller, Stimulated emission of Tm<sup>3+</sup> radiation in silicate glass, *J. Appl. Phys.* 38: 3030-3031 (1967).]
- [9] R.G. Smart, J.N. Carter, A.C. Tropper and D.C. Hanna, "continuous-wave oscillation of Tm-doped fluorozirconate fibre laser at around 1.47 $\mu\text{m}$ , 1.9 and 2.3  $\mu\text{m}$  when pumped at 790nm", *Opt. Commun.* 82: 563-570 (1991).
- [10] Jihong Geng, Jianfeng Wu, and Shibin Jiang, "Efficient operation of diode-pumped single-frequency thulium-doped fiber lasers near 2  $\mu\text{m}$ ," *Opt. Lett.*, 32 (4): 355-357 (2007).

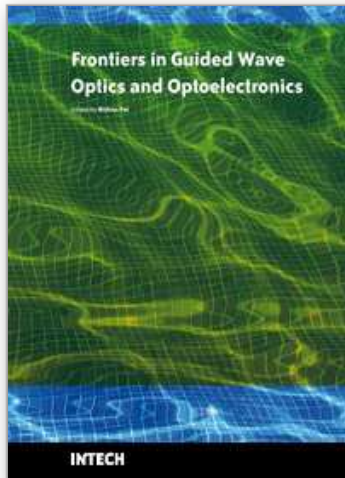
- [11] N. Y. Voo, J. K. Sahu, and M. Ibsen, "345-mW 1836-nm Single-Frequency DFB Fiber Laser MOPA," *IEEE Photon. Technol. Lett.* 17, 2550 (2005).
- [12] Jianqiu Xu, Mahendra Prabhu, Jianren Lu, Ken-ichi Ueda, and Da Xing, "Efficient double-clad thulium-doped fiber laser with a ring cavity," *Applied Optics*, 2001, 40(12): 1983-1988.
- [13] Stuart D. Jackson and Terence A. King, "Theoretical Modeling of Tm-Doped Silica Fiber Lasers, *J. Lightwave Technology*", 17(5): 948-956 (1999).
- [14] Yuen H. Tsang, Daniel J. Coleman, Terence A. King, "High power 1.9  $\mu\text{m}$  Tm<sup>3+</sup>-silica fibre laser pumped at 1.09  $\mu\text{m}$  by a Yb<sup>3+</sup>-silica fibre laser," *Optics Communications* 231 (2004).
- [15] D. C. Hanna, M. J. McCarthy, I. R. Perry, P. J. Suni, "Efficient high-power continuous-wave operation of monomode Tm-doped fibre laser at 2  $\mu\text{m}$  pumped by Nd YAG laser at 1.064  $\mu\text{m}$ ," *Electron. Lett.*, (1989) 25 (20): 1365-1366.
- [16] P.S. Golding, S.D. Jackson, P.-K. Tsai, B.C. Dickinson, T.A. King, "Efficient high power operation of a Tm-doped silica fiber laser pumped at 1.319  $\mu\text{m}$ ," *Optics Communications* 175: 179-183 (2000).
- [17] M. Meleshkevich, N. Platonov, D. Gapontsev, A. Drozhzhin, V. Sergeev, and V. Gapontsev, "415W Single-mode CW Thulium fiber laser in allfiber format," in *Proc. Eur. Conf. Lasers Electro-Opt., 2007 Int. quantum Electron. Conf. (CLEOE-IQEC 2007)*, Munich, Germany, Jun. 17-22, p. 1.
- [18] D.C. Hanna, I.M. Jauncey, R.M. Percival, I. R. Perry, R.G. Smart, P. J. Suni, J. E. Townsend, A. C. Tropper: Continuous-wave oscillation of a monomode thulium-doped fibre laser, *Electron. Lett.* 24, 1222 (1988).
- [19] W. L. Barnes, J.E. Townsend: Highly tunable and efficient diode pumped operation of Tm<sup>3+</sup> doped fibre lasers, *Electron. Lett.* 26, 746 (1990).
- [20] J. N. Carter, R.G. Smart, D.C. Hanna, A.C. Tropper: CW diode-pumped operation of 1.97  $\mu\text{m}$  thulium-doped fluorozirconate fibre laser, *Electron. Lett.* 26, 599 (1990).
- [21] Jackson, S.D., and King, T.A.: 'High-power diode-cladding-pumped Tm-doped silica fiber laser', *Opt. Lett.*, 1998, 23, pp. 1462-1464.]
- [22] R.A. Hayward, W.A. Clarkson, P.W. Turner, J. Nilsson, A.B. Grudinin and D.C. Hanna, Efficient cladding-pumped Tm-doped silica fibre laser with high power singlemode output at 2 $\mu\text{m}$ , *Electron. Lett.*, 36 (8): 711-712 (2000)
- [23] G. Frith, D.G. Lancaster and S.D. Jackson, "85W Tm<sup>3+</sup>-doped silica fibre laser," *Electron. Lett.*, 41, 687-688 (2005).
- [24] Y. Jeong, P. Dupriez, J. K. Sahu, J. Nilsson, D. Shen, and W. A. Clarkson, "Thulium-ytterbium co-doped fiber laser with 75 W of output power at 2  $\mu\text{m}$ ," *SPIE* (2004) 5620: 28-35]
- [25] Evgueni Slobodtchikov, Peter F. Moulton, Gavin Frith, "Efficient, High-Power, Tm-doped Silica Fiber Laser," 2007ASSP-MF2.
- [26] P. F. Moulton, G. A. Rines, E. V. Slobodtchikov, K. F. Wall, G. Frith, B. Samson, and A. L. G. Carter, "Tm-Doped Fiber Lasers: Fundamentals and Power Scaling," *IEEE J. Sel. Topics in Quantum Electronics*, 15 (1): 85-92 (2009).
- [27] G. D. Goodno, L. D. Book, and J. E. Rothenberg, "low-phase-noise single-frequency single mode 608 W thulium fiber amplifier," *Opt. Lett.* 34 (8): 1204-1206 (2009)

- [28] Orazio Svelto, "principles of Lasers", P142, 4<sup>th</sup> edit. 1998, Plenum Press, New York.
- [29] A. E. Siegman, LASERS, 1986, P492, P1017, Miller/Scheier Associates, Palo Alto, CA.
- [30] Jianfeng Wu, Shibin Jiang, Tao Luo, Jihong Geng, N. Peyghambarian, and Norman P. Barnes. "Efficient Thulium-Doped 2- $\mu$ m Germanate Fiber Laser," *IEEE Photon. Technol. Lett.* 18 (2): 334-336 (2006).
- [31] Jihong Geng, Jianfeng Wu, and Shibin Jiang, "Efficient operation of diode-pumped single-frequency thulium-doped fiber lasers near 2  $\mu$ m," *Opt. Lett.*, 32 (4): 355-357 (2007).
- [32] N. Y. Voo, J. K. Sahu, and M. Ibsen, "345-mW 1836-nm Single-Frequency DFB Fiber Laser MOPA," *IEEE Photon. Technol. Lett.* 17, 2550 (2005).
- [33] Yulong Tang, Yong Yang, Xiaojin Cheng and Jianqiu Xu. Short Tm<sup>3+</sup>-doped fiber lasers with watt-level output near 2  $\mu$ m [J]. *Chinese Opt. Lett.*, 2008, 6 (1): 44-46.
- [34] S. D. Jackson and S. Mossman, "Efficiency dependence on the Tm<sup>3+</sup> and Al<sup>3+</sup> concentrations for Tm<sup>3+</sup>-doped silica double-clad fiber lasers," *Appl. Opt.*, 42, no. 15, pp. 2702-2707, 2003.
- [35] Orazio Svelto, "principles of Lasers", P5, 4<sup>th</sup> edit. 1998, Plenum Press, New York.
- [36] S.D. Jackson and S. Mossman, "Efficiency dependence on the Tm<sup>3+</sup> Al<sup>3+</sup> concentrations for Tm<sup>3+</sup> -doped silica double-clad fiber lasers," *Appl. Opt.*, vol. 42, no. 15, pp. 2702-2707, 2003.
- [37] S. D. Jackson, "Cross relaxation and energy transfer upconversion processes relevant to the functioning of 2  $\mu$ m, Tm<sup>3+</sup> -doped silica fiber lasers," *Opt. Commun.*, vol. 230, pp. 197-203, 2004.
- [38] Ping Yan, Shupeng Yin, and Mali Gong. 175-W continuous-wave master oscillator power amplifier structure ytterbium-doped all-f iber laser [J]. *Chinese Opt. Lett.*, 2008, 6 (8): 580-582.
- [39] Dong Xue, Qihong Lou, Jun Zhou, Lingfeng Kong, Jinyan Li, and Shiyu Li. A 110-W fiber laser with homemade double-clad fiber [J]. *Chinese Opt. Lett.*, 2005, 3 (6): 345-347.
- [40] S. D. Jackson and T. A. King. High-power diode-cladding-pumped Tm-doped silica fiber laser. *Opt. Lett.*, 1998, 28(18): 1462-1464.
- [41] S. D. Jackson and T. A. King. Dynamics of the output of heavily Tm-doped double-clad silica fiber lasers [J]. *J. Opt. Soc. Am. B*, 1999, 16(12): 2178-2188.
- [42] Walter Koechner, "solid-state laser engineering," 5<sup>th</sup> edit. p95, Springer series, 1999.
- [43] A. V. Smith, B. T. Do, G. R. Hadley and R. L. Farrow. Optical Damage Limits to Pulse Energy From Fibers [J]. *IEEE J. Selected Topics in Quantum Electron.*, 2009, 15(1): 153-158.
- [44] W. H. Lowdermilk and D. Milam. Laser-Induced Surface and Coating Damage [J]. *IEEE J. Quantum Electron.*, 1981, QE-17(9): 1888-1903.
- [45] S. Yoo, C. Basu, A. J. Boyland, C. Sones, J. Nilsson, J. K. Sahu and D. Payne. Photo darkening in Yb-doped aluminosilicate fibers induced by 488 nm irradiation [J]. *Opt. Lett.*, 2007, 32(12): 1626-1628.
- [46] <http://www.slideshare.net/nufchas/power-scaling-790nmpumped-tmdoped-devices-from-191-to-213-m> .

- [47] Yulong Tang, Yong Yang, and Jianqiu Xu. High Power Tm<sup>3+</sup>-Doped Fiber Lasers Tuned by a Variable Reflective Output Coupler [J]. *Research Letters in Optics*, 2008, 2008: 1-3.
- [48] X. Zou, and H. Toratani, "Spectroscopic properties and energy transfers in Tm<sup>3+</sup> singly- and Tm<sup>3+</sup>/Ho<sup>3+</sup> doubly-doped glasses," *Journal of non-crystalline solids* 195, 113-124 (1996).
- [49] G. P. Agrawal (1995). *Nonlinear Fiber Optics*, Academic, San Diego, CA.
- [50] W. Torruellas, Y. Chen, B. McIntosh, J. Farroni, K. Tankala, S. Webster, D. Hagan, M. J. Soileau, M. Messerly and J. Dawson. High peak power Ytterbium doped fiber amplifiers [J]. *Proc. of SPIE* 2006, 6102:61020N-1-61020N-7.
- [51] Jianqiu Xu, Yulong Tang, Yong Yang, and Yin Hang. High power tunable Tm<sup>3+</sup>-fiber lasers and its application in pumping Cr<sup>2+</sup>:ZnSe lasers [C]. *CLEO/QELS 2008*, Paper JTua3.
- [52] Xin Ye, Tao Fang, Zhimin Wang, Shixun Dai, Jianqiu Xu. Nd:glass belt lasers with improved beam quality [J]. *Chinese Opt. Lett.*, 2005, 5 (9): 527-529.
- [53] Allain, J.Y., M.Monerie, H.Poignant. "Tunable CW lasing around 0.82 1.48 1.88 and 2.35  $\mu\text{m}$  in thulium-doped fluorozirconate fibre", *Electronics Letters*, 25 (24): 1660-1662 (1989).
- [54] S. D. Jackson and T. A. King, "High-power diode-cladding-pumped Tm-doped silica fiber laser", *Optics Letters*, 23 (18): 1462-1464 (1998).
- [55] T. Yamamoto, Y. Miyajima and T. Komukai, "1.9  $\mu\text{m}$  Tm<sup>3+</sup>-doped silica fibre laser pumped at 1.57  $\mu\text{m}$ ", *Electron. Lett.* 30 (3), 220-221 (1994).
- [56] D. C. Hanna, R. M. Percival, R. G. Smart, and A. C. Tropper, "Efficient and tunable operation of a Tm<sup>3+</sup>-doped fiber laser", *Opt. Commun.* 75 (3-4), 283-286 (1990).
- [57] C. Ghisler, W. Luthy and H. P. Weber, "Tuning of a Tm<sup>3+</sup> Ho<sup>3+</sup> Silica Fiber Laser at 2 $\mu\text{m}$ ", *IEEE J. Quantum Electron.*, 31 (11): 1877-1879 (1995).
- [58] R. L. Shubochkin, V. A. Kozlov, A. L. G. Carter, and T. F. Morse, "Tunable Thulium-Doped All-Fiber Laser", *IEEE Photon. Tech. Lett.* 10 (7), 944-945 (1998).]
- [59] D. Y. Shen, J. K. Sahu, and W. A. Clarkson, "High-power widely tunable Tm<sup>3+</sup>: fiber lasers pumped by an Er, Yb co-doped fibre laser at 1.6  $\mu\text{m}$ ," *Opt. Express* 14 (13), 6084-6090 (2006).
- [60] W. L. Barnes, J. E. Townsend, "Highly tunable and efficient diode pumped operation of Tm<sup>3+</sup> doped fibre lasers", *Electron. Lett.* 26 (11), 746-747 (1990).
- [61] W. A. Clarkson, N. P. Barnes, P. W. Turner, J. Nilsson, and D. C. Hanna, "High-power cladding-pumped Tm<sup>3+</sup>-doped silica fiber laser with wavelength tuning from 1860 to 2090 nm," *Opt. Lett.* 27 (22), 1989-1991 (2002).
- [62] Ashraf F. El-Sherif, Terence A. King, "Dynamics and self-pulsing effects in Tm<sup>3+</sup>-doped silica fibre lasers," *Opt. Commun.* 208, 381-389(2002).
- [63] F.Z. Qamar and T.A. King, "Self-induced pulsations, Q-witching and mode-locking in Tm-silica fibre lasers", *J. Mod. Opt.* 52 (7), 1031-1043 (2005).
- [64] T. Erneux, "Q-switching bifurcation in a laser with a saturable absorber," *J. Opt. Soc. Am. B* 5 (5), 1063-1069 (1988).
- [65] P. Le Boudec, M. Le Flohic, P. L. Francois, F. Sanchez, and G. Stephan, "Self-pulsing in Er<sup>3+</sup>-doped fibre laser," *Opt. Quantum Electron.* 25, 359-367 (1993).

- [66] R. Leners, P. L. Francois, and G. Stephan, "Simultaneous effects of gain and loss anisotropies on the thresholds of a bipolarization fiber laser," *Opt. Lett.* 19 (4), 275-277 (1994).
- [67] P. Le Boudec, C. Jaouen, P. L. Francois, and J.-F. Bayon, F. Sanchez, P. Besnard, and G. Stephan, "Antiphase dynamics and chaos in self-pulsing erbium-doped fiber lasers," *Opt. Lett.* 18 (22), 1890-1892 (1993).
- [68] P. L. Boudec, P. L. Francois, E. Delevaque, J. F. Bayon, F. Sanchez, G. M. Stephan, "Influence of ion pairs on the dynamical behaviour of Er<sup>3+</sup>-doped fibre lasers," *Opt. Quantum Electron.* 25, 501-507 (1993).
- [69] S. Colin, E. Contesse, P. Le Boudec, G. Stephan, F. Sanchez, "Evidence of a saturable-absorption effect in heavily erbium-doped fibers," *Opt. Lett.* 21 (24), 1987-1989 (1996).
- [70] A. Hideur, T. Chartier, C. Ozkul, F. Sanchez, "Dynamics and stabilization of a high power side-pumped Yb-doped double-clad fiber laser," *Opt. Commun.* 186, 311-317 (2000).
- [71] F.Z. Qamar and T.A. King, "Self- mode-locking effects in heavily doped single-clad Tm<sup>3+</sup>-doped silica fibre lasers", *J. Mod. Opt.* 52 (8), 1053-1063 (2005).
- [72] Yulong Tang, Jianqiu Xu, "Self-induced pulsing in Tm<sup>3+</sup>-doped fiber lasers with different output couplings," *Photonics and OptoElectronics Meetings (POEM2008)*, Nov. 2008, Wuhan, China.
- [73] Michel J. F. Digonnet, "Rare-Earth-Doped Fiber Lasers and Amplifiers," second ed. New York, Basel, 382 (2001).
- [74] F. Sanchez, P.L. Boudec, P.L. Francois and G. Stephan, "Effects of ion pairs on the dynamics of erbium-doped fiber lasers," *Phys. Rev. A* 48 (3), 2220-2229 (1993).
- [75] W. Koechner, "Solid-State Laser Engineering", Fifth Edition, springer-Verlag Berlin Heidelberg New York, pp.17-27, 1999.
- [76] Gunnar Rustad and Knut Stenersen, "Modeling of Laser-Pumped Tm and Ho Lasers Accounting for Upconversion and Ground-State Depletion", *IEEE Journal of Quantum Electronics*, vol. 32, no. 9, pp. 1645-1656, September 1996.
- [77] Igor Razdobreev and Alexander Shestakov, "Self-pulsing of a monolithic Tm-doped YAlO<sub>3</sub> microlaser", *Physical Review A*, vol. 73, no. 5, pp. 053815 (1-5), 2006.
- [78] S.D. Jackson and T.A. King, "Theoretical modeling of Tm-doped silica fiber lasers," *J. Lightwave Tech.* vol. 17, no. 5, 948-956, 1999.
- [79] B. M. Walsh, N. P. Barnes, "Comparison of Tm:ZBLAN and Tm: silica fiber lasers; Spectroscopy and tunable pulsed laser operation around 1.9 μm," *Appl. Phys. B*, vol. 78, 325-333 (2004).
- [80] Yulong Tang, Jianqiu Xu, "Effects of Excited-state Absorption on Self-pulsing in Tm<sup>3+</sup>-doped Fiber Lasers," *IEEE J. of Quant. Electronics*, (2009) being submitted.
- [81] Yulong Tang, Jianqiu Xu, "Theoretical study on self-pulsing in Tm<sup>3+</sup>-doped fiber lasers," *Optics communications*, (2009) being submitted.
- [82] B. C. Dickinson, S. D. Jackson, and T. A. King, *Opt. Commun.* 182 (2000) 199.
- [83] Y. J. Zhang, B. Q. Yao, Y. L. Ju, and Y. Zh. Wang, *Opt. Express* 13 (2005) 1085.
- [84] A. F. El-Sherif, T. A. King, *Opt. Commun.* 218 (2003) 337.

- [85] A. F. El-Sherif, T. A. King, *Opt. Lett.* 28 (2003) 22.
- [86] R. C. Sharp, D. E. Spock, N. Pan, and J. Elliot, *Opt. Lett.* 21 (1996) 881.
- [87] F. Z. Qamar, T. A. King, *Opt. Commun.* 248 (2005) 501.
- [88] S. D. Jackson, *Appl. Opt.* 46 (2007) 3311.
- [89] V.I. Levchenko, V.N. Yakimovich, L.I. Postnova, V.I. Konstantinov, V.P. Mikhailov, N.V. Kuleshov, *J. Crystal Growth*, 198/199 (1999) 980.
- [90] Yulong Tang, Yong Yang, Jianqiu Xu and Yin Hang, "Passive Q-switching of short-length  $Tm^{3+}$ -doped silica fiber lasers by polycrystalline  $Cr^{2+}:ZnSe$  microchips," *Optics Communications* 281 (2008) 5588-5591.
- [91] R. H. Page, K. I. Schaffers, L. D. DeLoach, G. D. Wilke, F. D. Patel, J. B. Tassano Jr., S. A. Payne, W. F. Krupke, K.-T. Chen, and A. Burger, *IEEE JOURNAL OF QUANTUM ELECTRONICS*, 33, 11 (1997).
- [92] G. J. Wagner, T. J. Carrig, R. H. Jarman, R. H. Page, K. I. Schaffers, J.-O. Ndad, X. Ma, and A. Burger, *Trends in Optics and Photonics, ADVANCED SOLID-STATE LASERS* 26, 8 (1999).
- [93] E. Sorokin and I. T. Sorokina, *APPLIED PHYSICS LETTERS* 80, 3 (2002).
- [94] E. Sorokin, S. Naumov, and I. T. Sorokina, *IEEE JOURNAL OF SELECTED TOPICS IN QUANTUM ELECTRONICS* 11, 23 (2005).
- [95] I.T. Sorokina, K.L. Vodopyanov (Eds.): *Solid-State Mid-Infrared Laser Sources*, *Topics Appl. Phys.* 89, p271 (2003).
- [96] L.D. DeLoach, R.H. Page, G.D. Wilke, S.A. Payne, W.P. Krupke: *Transition metal-doped zinc chalcogenides: spectroscopy and laser demonstration of a new class of gain media*, *IEEE J. Quantum Electron.* 32, 885-895 (1996)
- [97] A.V. Podlipensky, V. G. Shcherbitsky, N.V. Kuleshov, V. I. Levchenko, V. N. Yakimovich, M. Mond, E. Heumann, G. Huber, H. Kretschmann, S. Kuck: *Efficient laser operation and continuous-wave diode pumping of  $Cr^{2+}:ZnSe$  single crystals*, *Appl. Phys. B.* 72, 253-255 (2001).
- [98] U. Demirbas and A. Sennaroglu, *OPTICS LETTERS* 31, 3 (2006).
- [99]. T. J. Carrig, G. J. Wagner, W. J. Alford, and A. Zakel, *Proceedings of SPIE* 5460, 9 (2004).
- [100] I. T. Sorokina, E. Sorokin, A. D. Lieto, M. Tonelli, R. H. Page, and K. I. Schaffers, *JOURNAL OF OPTICAL SOCIETY OF AMERICA* 18, 5 (2001).
- [101] I. T. Sorokina, *OPTICAL MATERIALS* 26, 18 (2004).
- [102] G. Grebe, G. Roussos, and H.-J. Schultz, *JOURNAL OF PHYSICS C: SOLID STATE PHYSICS*, 6 (1976).
- [103] G. Goetz, H. Zimmerman, and H.-J. Schultz, *Zeitschrift für Physik B*, 18 (1993).
- [104] J. B. McKay, Thesis, THE AIR FORCE AIR UNIVERSITY, 2003.
- [105] YANG Yong, TANG Yu-Long, XU Jian-Qiu and HANG Yin, "Tm-Doped Fibre Laser Pumped  $Cr^{2+}:ZnSe$  Poly-Crystal Laser," *CHIN.PHYS.LETT.* Vol. 25, No. 1 (2008) 116.
- [106] W. Koechner, *Solid-State Laser Engineering*, Vol. 1, 6 ed. (Springer, 2006).
- [107] Yong Yang, Yulong Tang, Jianqiu Xu and Yin Hang, "Study on Laser Output and Tuning Ability of  $Cr^{2+}:ZnSe$ ," *Chinese Lasers*, 35 (10): 1495~1499 (2008) (Chinese).



## **Frontiers in Guided Wave Optics and Optoelectronics**

Edited by Bishnu Pal

ISBN 978-953-7619-82-4

Hard cover, 674 pages

**Publisher** InTech

**Published online** 01, February, 2010

**Published in print edition** February, 2010

As the editor, I feel extremely happy to present to the readers such a rich collection of chapters authored/co-authored by a large number of experts from around the world covering the broad field of guided wave optics and optoelectronics. Most of the chapters are state-of-the-art on respective topics or areas that are emerging. Several authors narrated technological challenges in a lucid manner, which was possible because of individual expertise of the authors in their own subject specialties. I have no doubt that this book will be useful to graduate students, teachers, researchers, and practicing engineers and technologists and that they would love to have it on their book shelves for ready reference at any time.

### **How to reference**

In order to correctly reference this scholarly work, feel free to copy and paste the following:

Yulong Tang and Jianqiu Xu (2010). High Power Tunable Tm<sup>3+</sup>-fiber Lasers and Its Application in Pumping Cr<sup>2+</sup>:ZnSe Lasers, *Frontiers in Guided Wave Optics and Optoelectronics*, Bishnu Pal (Ed.), ISBN: 978-953-7619-82-4, InTech, Available from: <http://www.intechopen.com/books/frontiers-in-guided-wave-optics-and-optoelectronics/high-power-tunable-tm3-fiber-lasers-and-its-application-in-pumping-cr2-znse-lasers>

# **INTECH**

open science | open minds

### **InTech Europe**

University Campus STeP Ri  
Slavka Krautzeka 83/A  
51000 Rijeka, Croatia  
Phone: +385 (51) 770 447  
Fax: +385 (51) 686 166  
[www.intechopen.com](http://www.intechopen.com)

### **InTech China**

Unit 405, Office Block, Hotel Equatorial Shanghai  
No.65, Yan An Road (West), Shanghai, 200040, China  
中国上海市延安西路65号上海国际贵都大饭店办公楼405单元  
Phone: +86-21-62489820  
Fax: +86-21-62489821

© 2010 The Author(s). Licensee IntechOpen. This chapter is distributed under the terms of the [Creative Commons Attribution-NonCommercial-ShareAlike-3.0 License](#), which permits use, distribution and reproduction for non-commercial purposes, provided the original is properly cited and derivative works building on this content are distributed under the same license.

IntechOpen

IntechOpen